NASA CR-134818
PWA-5201

DEVELOPMENT OF ADVANCED FUEL CELL SYSTEM

(Phase III)

by

L. M. Handley
A. P. Meyer
W. F. Bell

30 January 1975

PRATT & WHITNEY AIRCRAFT

Prepared for

NATIONAL AERONAUTICS AND SPACE ADMINISTRATION

NASA Lewis Research Center
Contract NAS3-15339
Dr. L. H. Thaller, Project Manager

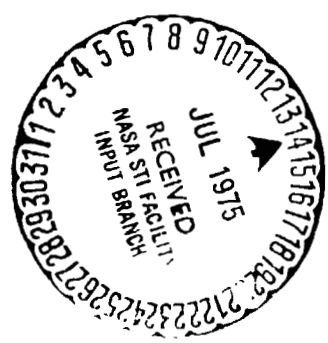

NASA CR-134818
PWA-5201

FINAL REPORT

DEVELOPMENT OF ADVANCED FUEL CELL SYSTEM

(Phase III)

by

L. M. Handley
A. P. Meyer
W. F. Bell

30 January 1975

PRATT & WHITNEY AIRCRAFT
South Windsor Engineering Facility
Box 109, Governors Highway
South Windsor, Connecticut 06074

Prepared for

NATIONAL AERONAUTICS AND SPACE ADMINISTRATION

CONTRACT NAS3-15339

NASA Lewis Research Center
Cleveland, Ohio
Dr. L. H. Thaller, Project Manager
Power Procurement Section

NOTE – On January 1, 1975, the fuel cell operations of Pratt & Whitney Aircraft Division, United Aircraft Corporation became part of the newly formed Power Utility Division, United Aircraft Corporation. On May 1, 1975, the name of Power Utility Division, United Aircraft Corporation was changed to Power Systems Division, United Technologies Corporation.

FOREWORD

This report describes the several research and development tasks performed during Phase III of an advanced fuel cell technology program.

The work was performed under a NASA Contract NAS3-15339 from 1 October 1973 through 31 October 1974. The NASA Program Manager for this contract was Dr. Lawrence H. Thaller. The contributions of Dr. Thaller and other members of the Direct Energy Conversion Laboratory staff at the NASA Lewis Research Center are gratefully acknowledged.

Principal Pratt & Whitney Aircraft personnel who directed the tasks performed in this program were:

J. K. Stedman
L. M. Handley
A. P. Meyer
W. F. Bell
M. S. Freed
R. C. Nickols, Jr.
R. W. Vine

CONTENTS

ILLUSTRATIONS

ILLUSTRATIONS (CONT'D)

ILLUSTRATIONS (CONT'D)

TABLES

ABSTRACT

A multiple task research and development program was performed to improve the weight, life and performance characteristics of hydrogen-oxygen alkaline fuel cells for advanced power systems. During Phase III, covered by this report, gradual wetting of the anode structure and subsequent long-term performance loss was determined to be caused by deposition of a silicon-containing material on the anode. This deposit was attributed to degradation of the asbestos matrix, and attention was therefore placed on development of a substitute matrix of potassium titanate, with considerable success. Testing confirmed the suitability to this program of a supported catalyst anode of low platinum loading. An 80 percent gold - 20 percent platinum catalyst cathode was developed which has the same performance and stability as the standard 90 percent gold - 10 percent platinum cathode but at half the loading. A hybrid polysulfone/epoxy-glass fiber frame was developed which combines the resistance to the cell environment of pure polysulfone with the fabricating ease of epoxy glass fiber laminate. These new cell components were evaluated in six different configurations of full-size cells and 12 tests. At the conclusion of Phase III, one cell operating at 100 amps/ft^2 completed 10,020 hours of testing and another cell operating at 200 amps/ft^2 completed 6680 hours. A study identified the ways in which the baseline Engineering Model System would be modified to accommodate the requirements of the Space Tug application.

I. SUMMARY

This document reports the activity and results of Phase III of a long range research program to improve the life, weight, and performance of alkaline fuel cells. The specific tasks are focused on meeting technology goals defined by the Engineering Model System (EMS), an advanced, long life, lightweight, powerplant concept. The program is evolutionary in nature. Work is being carried out at the laboratory level, in subscale cells and in full scale cell assemblies. As fundamental improvements are defined in the laboratory, e.g., better catalysts and materials, they are committed to evaluation in the working environment of subscale fuel cells. If their merit is demonstrated at this level, they are committed to the full-scale cell tests for a final evaluation. The work completed during this phase of the program built on the accomplishments of the Phase I and II effort. Each of the tasks and the results achieved are summarized below and are reported in detail in the sections which follow.

A. Materials Research

1.0 Electrodes

Task Description - This task focused on investigation and evaluation of electrode catalysts and structures. The overall task objective was to attain higher performance/lower catalyst loading and improved long term stability.

Results - During earlier phases of this program, it was determined that increased wetting (flooding) of anode structures with time was a mode of performance decay. Early in Phase III, developments aimed at minimizing this effect were investigated, but none was an unqualified success. However, as a result of post-test examination of a cell run for 7,560 hours, it was determined that the gradual flooding phenomenon was associated with the deposition, onto the gas-side of the anode, of a silicon-containing material attributed to degradation of the asbestos matrix. The emphasis on anode structure development was switched to an evaluation of cells with matrices of potassium titanate, a non-silicate material. Also during Phase III, additional testing confirmed the suitability to this program of a supported catalyst anode of low platinum loading, originally developed in P&WA R&D programs.

Development of the 80 percent gold - 20 percent platinum (80Au-20Pt) catalyst cathode continued. Catalyst preparation techniques were improved to obtain higher surface areas and other desirable physical properties consistently. Methods to fabricate electrodes incorporating this catalyst into improved structures were investigated. Electrodes of this type were tested as cathodes in laboratory-size endurance cells and in full-scale cells. Results indicate this cathode has performance equivalent to the standard 90Au-10Pt catalyst cathode with one-half the catalyst loading of the standard cathode. The 80Au-20Pt cathode also shows a rate of performance decay because of catalyst recrystallization equivalent to that of the 90Au-10Pt cathode, which is entirely satisfactory.

2.0 Matrices

Test Description - Phase II efforts focused on developing methods for fabricating Fybex matrices with improved mechanical properties. These efforts were thwarted, however, by changes made in the manufacturing process by the supplier of the raw material. These changes altered the Zeta potential of the Fybex fibers and in turn the mech[illegible] properties of the matrix. To solve this problem, procedures were developed for [illegible] matrices which were unaffected by the change in Zeta potential. In ad[illegible]ion, seve[illegible] other new materials were evaluated to determine their suitability as an alkaline fuel cell matrix.

Results - Two approaches for fabricating Fybex matrices were evaluated: silk screen printing and vacuum filtration. Vacuum filtration was the more successful. Using a mixture of 96 percent Fybex - 4 percent TFE, satisfactory bubble pressures of 30 to 33 psi (20.7 to 22.8 n/cm^2) were achieved with 1.6 mils (0.039 mm) of solid material, half the solids content of a standard asbestos matrix. Gas chromatography analysis showed this type of matrix contained no materials which oxidized at temperatures as high as 400°F (204°C). Brucite magnesium hydroxide, "Litofol S" asbestos, silicon nitride, and polybenzimadazole were also evaluated as matrix materials. The first three were rejected because of insufficient corrosion resistance at 250°F; the last was dropped because of the e[illegible]ense required to obtain the material in a suitable form.

3.0 Lightweight Electrolyte Reservoir Plate

Task Description - The heaviest single component in the EMS cell is the nickel electrolyte reservoir plate (ERP). Substituting a nonmetallic material for this porous structure would result in sizeable system weight saving. The effort begun in Phase I to produce a structure with high porosity made of low density materials was continued.

Results - Methods for fabrication of lightweight nickel-plated porous polysulfone ERP's developed during Phase II were used to produce ERP's for nine full-size cells tested or delivered during Phase III. As a result of the satisfactory test experience in full-size cells, the lightweight ERP is now considered part of the baseline cell configuration.

4.0 Unitization Research

Task Description - The main thrust of the fabrication and unitization effort in Phase III was evaluation of a new hybrid polysulfone/epoxy-glass fiber frame.

Results - Ten full-size cells using the new frame were constructed and tested. Measurements of carbonate levels in the electrolyte after operating periods of various lengths indicate this frame is substantially more resistant to the cell environment than the previous standard epoxy-glass fiber frame. The new hybrid frame is almost as good as pure polysulfone and is considerably easier to fabricate.

5.0 Non-Operating Cells

Task Description - A full size non-operating cell with an epoxy-glass fiber frame was exposed to hydrogen for 100 hours at 212°F (100°C) and 16 psia (11 n/cm^2). The purpose of the test was to evaluate the amount of electrolyte conversion to carbonate to determine if epoxy-glass fiber is suitable as a frame material for the ERP and the passive water removal matrix.

Results - The epoxy-glass fiber frame was found to be completely satisfactory in the hydrogen atmosphere and is now considered the standard frame for the passive water removal matrix.

B. Cell Development

Task Description - Several single cell tasks provide the means for evaluating the performance and endurance characteristics of evolutionary EMS cell designs. The investigations performed in this area are: evaluation of alternative cell designs, testing to measure the compatibility of alternative cell frame materials and construction techniques in the actual cell environment, and development of cell fabrication procedures to translate the most compatible materials available into practical cell configurations. Single cell hardware was also fabricated and delivered to the NASA LeRC.

Results - Six different NASA-approved cell designs were evaluated in tests of 12 cells. Two additional cells were delivered to NASA. Over 73,000 hours of fuel cell operating time have been accumulated on 35 different cells since the inception of the program. Cell endurance capability has improved markedly. At the conclusion of Phase III one cell operated at 100 amps/ft^2 (107.6 ma/cm^2) had completed 10,020 hours ng and another operating at 200 amps/ft^2 (215.2 ma/cm^2) had completed 6680 s.

Three important new cell components were introduced into full-size cells during Phase III. These are the 80Au-20Pt cathode, the low-loaded supported catalyst anode, and the hybrid polysulfone/epoxy-glass fiber frame.

The hybrid frame is now accepted as the standard. On the basis of the testing to date, the new electrodes seem to be at least as stable with time as the 90Au-10Pt cathode and the PPF anode, and they offer the potential for substantially lower cost.

C. System Design Analysis

Task Description - As a result of increasing NASA interest in a fuel cell power supply for the Space Tug, a study was performed to determine how the conceptual design of the Engineering Model System (EMS) would be changed to accommodate the requirements of the Tug, particularly the lower power and voltage.

Results - The EMS schematic is modified by substituting a pumped liquid cooling loop for the original evaporative cooling system and (if water recovery is needed) by incorporating a static condenser/separator to condense product water vapor and remove it for storage. Passive water removal in the stack is retained.

The EMS stack configuration is modified by changing the number of 0.1146-ft^2 (106.4-cm^2) cells per plaque from six to two and by reducing the number of plaques from 88 to either 17 or 34 depending on the desired Tug power level. Use of the two-cell plaque keeps the multicell plaque option open for future higher power, higher voltage requirements.

Estimated weight of a complete 3-kw cell stack (34 plaques) is 17 pounds (8 kilograms), which is consistent with a Tug powerplant minimum weight of 33 pounds (15 kilograms), assuming no water recovery. Stack dimensions (including end plates) are 7.2 inches thick x 5.6 inches wide x 14.5 inches long (18.3 x 14.2 x 36.8 cm).

II. INTRODUCTION

The Lewis Research Center of the National Aeronautics and Space Administration is conducting a fuel cell system technology advancement program oriented toward advanced space applications. The emphasis in this program is on applied fuel cell research and development to build a new technology base from which advanced fuel cell systems can be developed. The work is being guided by an advanced fuel cell system, the specifications for which require a system weight of 20 lb/kw and an operating life of 10,000 hours.

The technology being developed has broad applicability for space and undersea power systems touching as it does on the fundamentals of fuel cell science and art (electrode catalysts and structures, matrix materials, compatibility of structural materials, lightweight cell components, and fabrication techniques).

The several work areas of the program and the emphasis in each were planned to meet the objectives stated by NASA LeRC; the key elements of these objectives are:

> "Goals – The NASA Lewis Research Center is embarking on an advanced fuel cell program . . . The overall goal is to advance the technology to provide a low cost, long life fuel cell system to meet Shuttle requirements . . .
>
> Phasing - A multi-phase development program is anticipated. The first phases cover two aspects of the total program.
>
> 1) The initiation of an on-going technology program to achieve necessary improvements in the fuel cells and ancillary components.
>
> 2) A preliminary design for an Engineering Model System that will incorporate the best current ideas for meeting the program goals."

The program consists of contractor performed work and complementary work performed at the Lewis Research Center. Phase I, II, and III of the program have been completed. In each phase several interrelated program tasks have been performed aimed at meeting requirements of the next generation of fuel cell systems, as well as providing supporting technology for on-going, mission-oriented fuel cell system programs. In programs that are specifically mission-oriented, very often scheduling constraints require that technology shortcomings be circumvented by design rather than being addressed directly. Advanced technology programs, on the other hand, permit more effort to be applied for solving basic problems. The potential benefits of such a program are two-fold. First, a superior system can emerge at a technological level where a potential user can compare it to an exisiting inventory system. Second, and of equal importance, technology generated during such a program can be utilized by on-going mission-oriented programs.

The guidelines for the work accomplished in Phase III are contained in the Introduction to Exhibit A of the contract:

"This third year of the NASA Lewis advanced technology fuel cell program is directed primarily toward the advanced materials area. Unlike earlier efforts where many new materials were screened for environmental compatibility, this year's effort will be directed at the successful application of some of these materials into test hardware. Again the system design and ancillary components areas will continue at a low level. The prime objective of this effort will be to design and begin testing of cell components which are expected to meet or exceed the 10,000 hour life goal at 20 pounds per kilowatt at 180°F. The secondary objective will be to look toward the goal of operation at 250°F.

"As in the previous phases of this program, the approach is that of an evolutionary technological advancement in the area of system hardware, coupled with a multi-faceted advanced materials program in the area of cell electrodes, cell matrices, and methods of construction."

This report describes the several research and development tasks performed by P&WA during the third phase of this advanced fuel cell program. The program tasks performed during Phase III were organized into three areas:

A. Materials Research

- Electrodes
- Matrices
- Lightweight Electrolyte Reservoir Plate
- Unitization
- Non-Operating Cells

B. Cell Development

C. System Design Analysis

The goals for each task area were defined by the NASA LeRC. The Engineering Model System, the advanced powerplant concept, was defined during Phase I.

A summary of the results achieved during Phase III relative to these goals is presented in Section I Summary. The following sections present detailed discussions of the work performed in individual task areas.

III. MATERIALS RESEARCH

A. Electrodes

1.0 Approach

The original objective of the Phase I electrode technology advancement effort was to improve the performance and stability of the alkaline electrolyte fuel cell, principally by the development of new cathode catalysts. As the work progressed, data were generated which indicated that structural development of both electrodes would improve stability of cells operating at powerplant conditions. Several catalysts showed potential for improving performance and stability in both anodes and cathodes. These alloys were further evaluated and developed during Phases II and III.

2.0 Anode Development

During earlier phases of this program, it was determined that increased wetting (flooding) of anode structures with time was a mode of performance decay. Early in Phase III, developments aimed at minimizing this effect were investigated but none was an unqualified success. However, as a result of post-test examination of Single Cell No. 25, it was determined that the gradual flooding phenomenon was associated with the deposition, onto the gas-side of the anode, of a silicon-containing deposit attributed to asbestos matrix degradation. The emphasis on anode structure development was switched to an evaluation of cells with matrices of potassium titanate, a non-silicate material. Also during Phase III, additional testing confirmed the suitability to this program of a supported catalyst anode of low platinum loading, originally developed in P&WA R&D programs.

At the beginning of Phase III, the approach to improve anode performance and stability included the investigation of high-sinter-temperatu PPF (platinum-palladium anodes. Standard PPF electrodes are sintered at 590°F (310°C), but a sintering temperature of 635°F (335°C) was found to increase the hydrophobicity of the catalyst-Teflon structure. This approach had been successful for anodes used in the Air Force-sponsored High Power Density (HPD) Fuel Cell Program where electrolyte-filling procedures, startup procedures, and operating conditions are different. However, an endurance test of a laboratory 2 x 2-inch (5.08 x 5.08 cm) cell using this anode (Cell No. M-0208) was unsuccessful, as shown in Figure 1. This result was attributed to less-than-optimum filling with electrolyte of the catalyst-Teflon structure. Measured catalytic activity of the anode from the cell was only 8 ma/cm^2 at 1.0 volt on oxygen in the half-cell diagnostic test, compared with 15 to 16 ma/cm^2 at the same conditions for typical 590°F (310°C) sintered anodes. Our experience with low-loaded (3 mg/cm^2) PPF anodes in previously reported laboratory cells (See Phase II Final Report, PWA-4984) showed that anode poisoning can have a detrimental effect on cell performance if only a small portion of the catalyst is wetted with electrolyte. Attempts to improve the degree of filling were also unsuccessful. Short cell tests using cycling between hydrogen and oxygen evolution, testing under high current density and high polarization conditions which might induce electrolyte transport, and vacuum filling were tried. All of these attempts resulted in activity levels less than those measured in post-test evaluations of anodes tested in the HPD program. In addition, a laboratory cell was

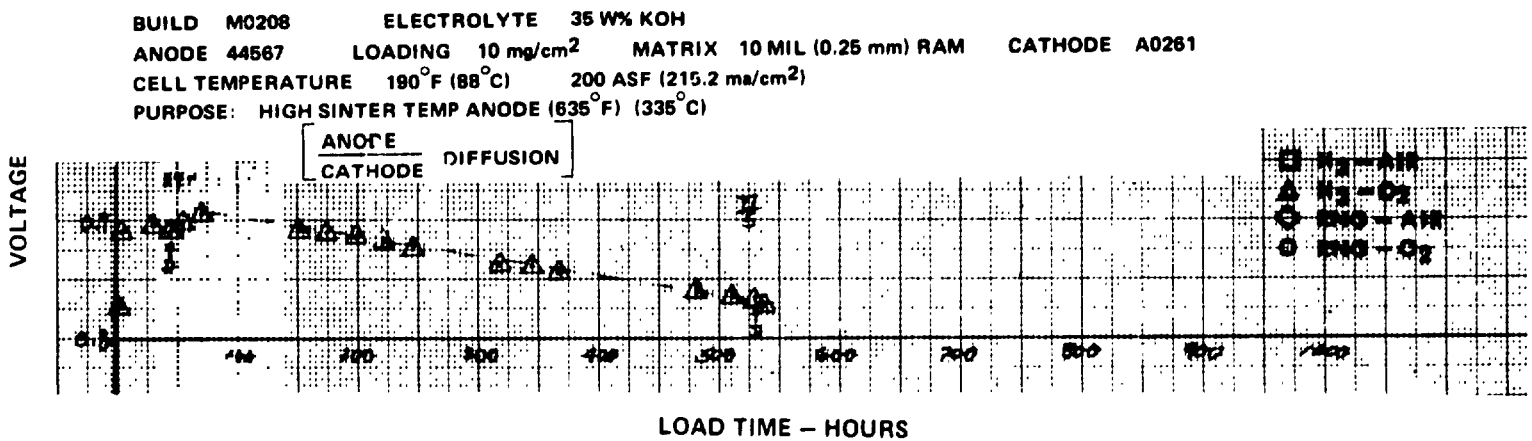

Figure 1 - Performance History of Cell No. M-0208 with High-Sinter-Temperature Anode

started with a 635°F (335°C) sintered anode using the procedure for startup of the HPD cells; i.e., startup under nitrogen to a temperature of 250°F (121°C) and open circuit operation for one hour before switching to normal laboratory conditions [190°F (87.8°C) at 200 ASF (215.2 ma/cm^2) with pure hydrogen and oxygen]. Initial cell performance was good but the anode was not totally filled and did not continue to fill with time or with a repeat of the startup procedure. Full-size single cells were also used to investigate this approach, with little success; see Section IV of this report.

In another attempt to achieve better anode stability, a PPF anode was prepared by sintering at 590°F (310°C) with 35 percent Teflon (compared with 20 percent in the standard PPF anode). However, half-cell testing indicated poor Teflon distribution. In order to improve Teflon distribution, methods of flocculating the catalyst and Teflon into optimum-size agglomerates using appropriate colloidal chemistry principles were investigated. First attempts used platinum black catalyst ultrasonically dispersed in aqueous media with wetting agents to which Teflon dispersions were added. Then the catalyst and Teflon were co-flocculated using pH adjustments and ions which would counteract the dispersing agents. The first attempts produced anodes with low Teflon contents which were not stable to flooding. A second attempt in which the dispersions were flocculated separately achieved higher Teflon loadings and gave good performance with stable anode polarization; see Figure 2. However, a test stand malfunction terminated the test before a conclusive evaluation of this "flocced" anode structure could be determined.

At this point in the program, Single Cell No. 25, which incorporated PPF electrodes as both anode and cathode and a reconstituted asbestos matrix, completed a 7400-hour test and was disassembled and examined. Most of the performance change during the test was attributed to anode flooding, since a film of electrolyte was observed on the reactant gas side of the anode following test. However, electrolyte take-up determinations and visual observations indicated that the bulk of the electrode was not completely flooded, but that a gray-colored deposit on the gas side of the electrode was associated with the flooded layer. Analysis of this gray-colored deposit showed silicon to be a major constituent. Since that time, additional long-term cells containing asbestos matrices have shown this gray-colored wettable deposit in varying amounts. It is believed that this material is a degradation product from the asbestos matrix and that its presence is a contributary cause for the significant anode performance degradation observed in long-term cells. In view of this important discovery, the program to develop hydrophobic electrode structures which would be more stable to electrolyte flooding was redirected to development of a silicate-free matrix which could be combined with conventional or advanced catalyst anodes.

Efforts under the matrix development subtask had resulted in successful fabrication of a high-bubble-pressure Fybex D - Teflon matrix. A 2 x 2-inch (5.08 x 5.08 cm) cell incorporating this matrix was fabricated for laboratory checkout prior to endurance testing. This cell also incorporated a standard PPF and a 90 Au-10Pt cathode. Instead of the usual asbestos matrix, both the anode and the cathode were coated on the electrolyte side with an 8-mil (0.2 mm) thick layer of the Fybex-Teflon matrix material to give a total thickness of 16 mils (0.4 mm). Initial voltage was 894 mv at 200 ASF (215.2 ma/cm^2) at a temperature of 190°F (87.8°C). The Internal Resistance (IR) at 200 ASF (215.2 ma/cm^2) was

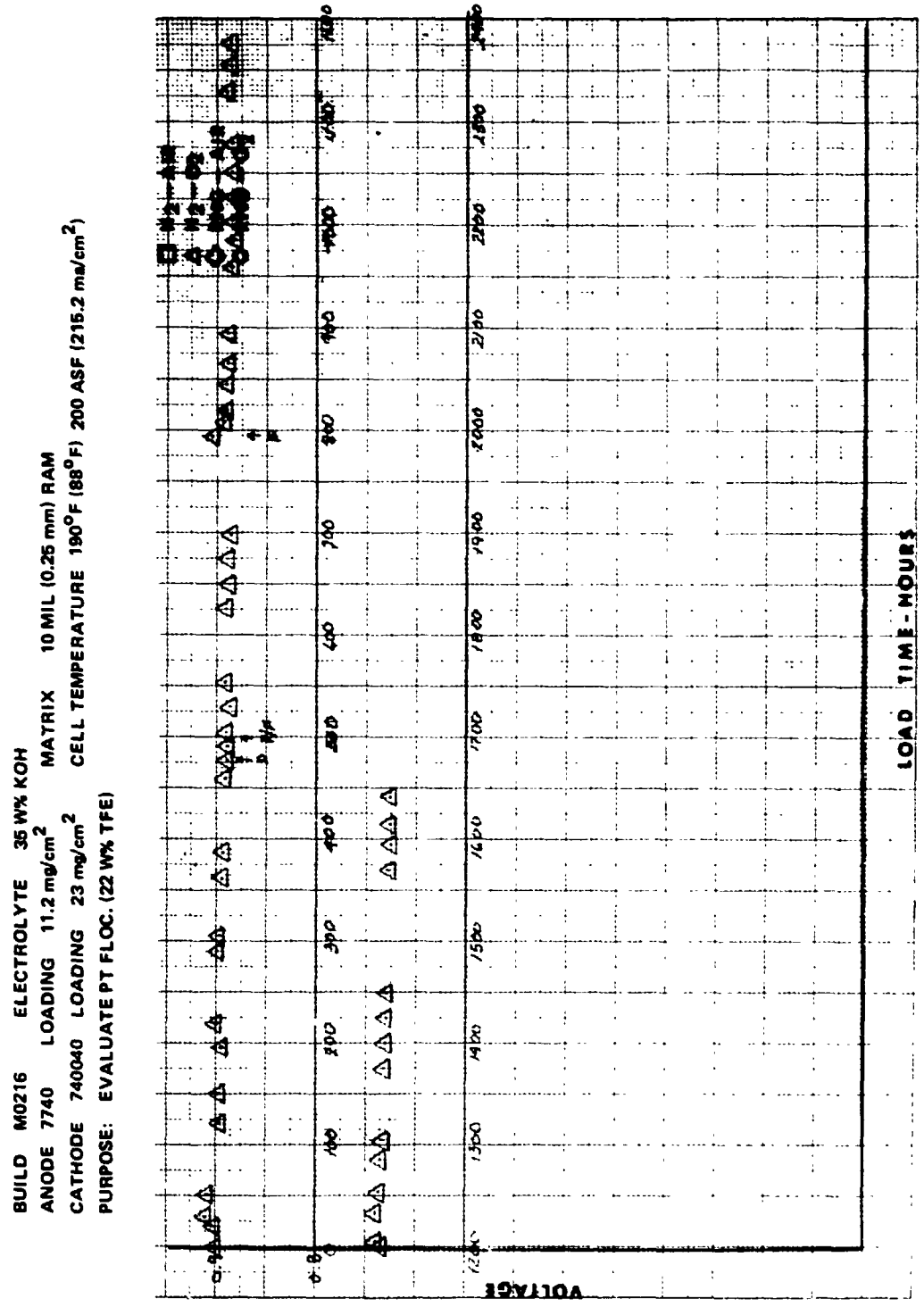

Figure 2 – Performance History of Cell No. M-0216 with Flocced Catalyst Anode

10 mv, which compares favorably with the 12 to 15 mv values normally measured on 10-mil (0.26 mm) thick reconstituted asbestos in the 2 x 2-inch (5.08 x 5.08 cm) test hardware. This cell was then tested as an endurance cell at 16 psia (11 n/cm^2) and 250°F (121°C) with 48 percent KOH electrolyte at 100 ASF (107.6 ma/cm^2). Figure 3 shows the performance history of this cell. Diagnostics performed at 580 hours showed most of the decay to be due to decreased cathode activity. Diagnostics at 1290 hours showed a total loss of 20 mv due to decreased cathode activity and a slight loss in the diffusion-controlled region. A small amount of shorting or crossover became apparent at this time. This cell completed 2325 hours on test and was shut down when definite crossover was experienced. Post-test examination of the cell showed that crossover was located in a gasket area rather than through the matrix. Total decay for this cell was 28 mv or 12 μv/hour which is typical of good cells tested at lower temperature.

In another test of the Fybex-Teflon matrix, a 2 x 2-inch (5.08 x 5.08 cm) cell incorporating this matrix, standard PPF anode, and 90 Au-10 Pt cathode was tested at standard laboratory endurance conditions [16 psia (11 n/cm^2), 190°F (87.8°C) and 200 ASF (215.2 ma/cm^2)]. The performance history is presented in Figure 4. This cell completed 2300 hours and was shut down when a test stand malfunction allowed excessive polarization of the anode. Overall decay rate was 13.0 μv/hr but only 6.5 μv/hr could be attributed to anode losses. Longer test durations are needed to determine conclusively the advantages of the Fybex matrix over the asbestos matrix, since the gradual anode flooding now attributed to matrix degradation is seen best in longer duration tests.

A laboratory test was also performed on a cell which incorporated 90Au-10Pt catalyst on both anode and cathode. This test was performed to establish if this anode would have more resistance to electrolyte flooding than the standard PPF anode, particularly in view of the fact that this electrode when tested as a cathode does show wetting stability. This test was terminated at 1590 hours when decay accelerated because of excessive carbonate formation. The test was not re-run since emphasis on the anode structure developments had been shifted to the potassium titanate matrix.

One of the objectives of the electrode development task during Phase III was to evaluate a supported catalyst anode developed under other R&D programs and to incorporate this anode configuration into the single cell endurance program. This electrode contains only one-twentieth of the precious metal content of a standard PPF anode. Electrodes of this type were fabricated in the laboratory and were tested as the anodes of Cell Nos. 35 and 36. Cell No. 35 is noteworthy since it showed good performance and the lowest overall decay rate of any cell tested to date in this program. Electrodes of this type fabricated in the shop were tested as the anodes of Cell Nos. 38, 39, 39A, 40 and 41. Results indicated some variation in hydrophobicity of these anodes, and development efforts were started to make the anodes more reproducible. Initial tests indicate differences among lots of the supported catalyst in regard to certain ions introduced during the catalyst preparation process. Techniques to wash the catalyst free of these contaminating ions are being incorporated into the processing. Future supported catalyst anodes should be uniformly easy to fill with electrolyte.

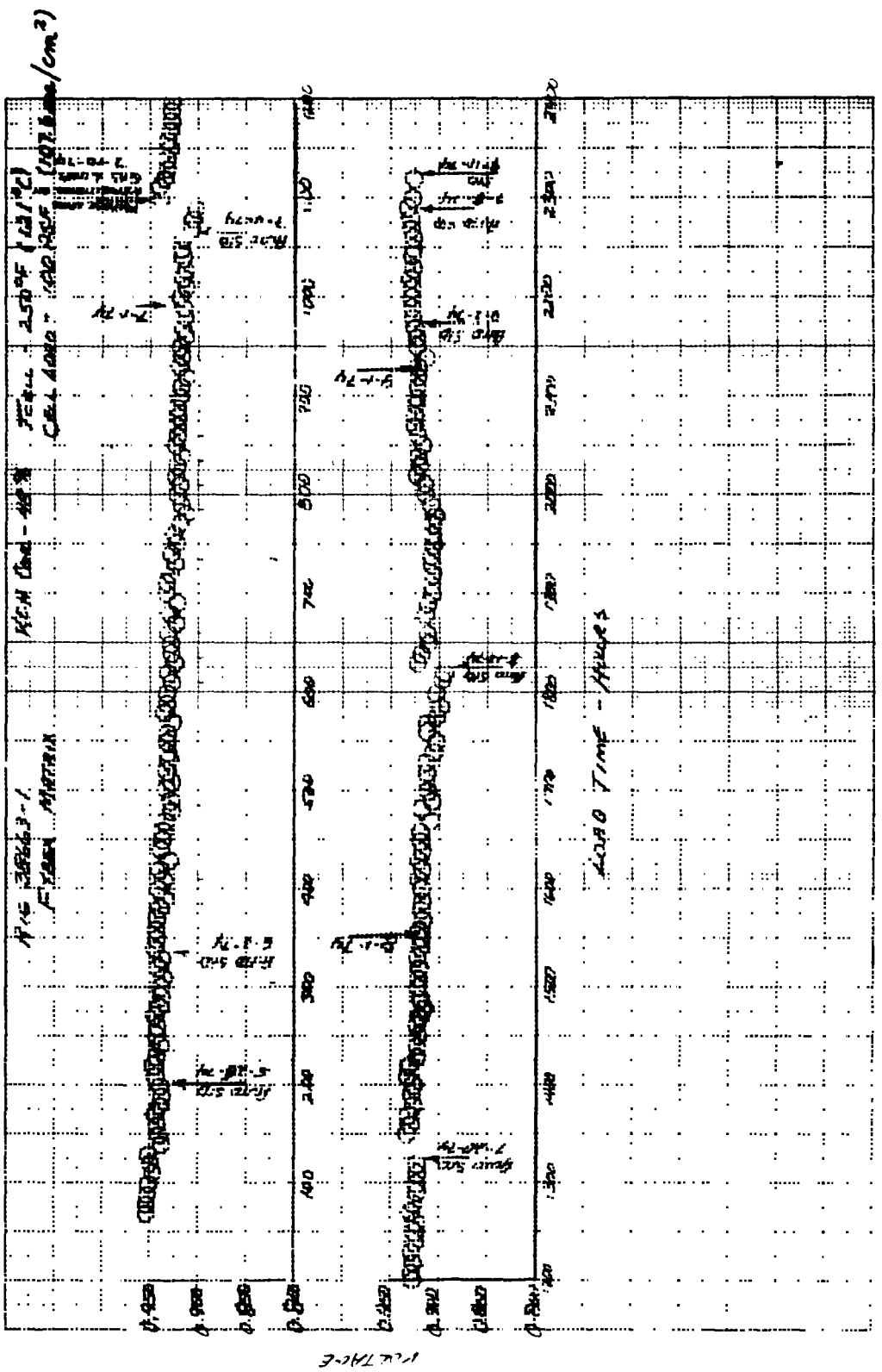

Figure 3 – Performance History of Endurance Cell with Fybex Matrix at 250°F (121°C)

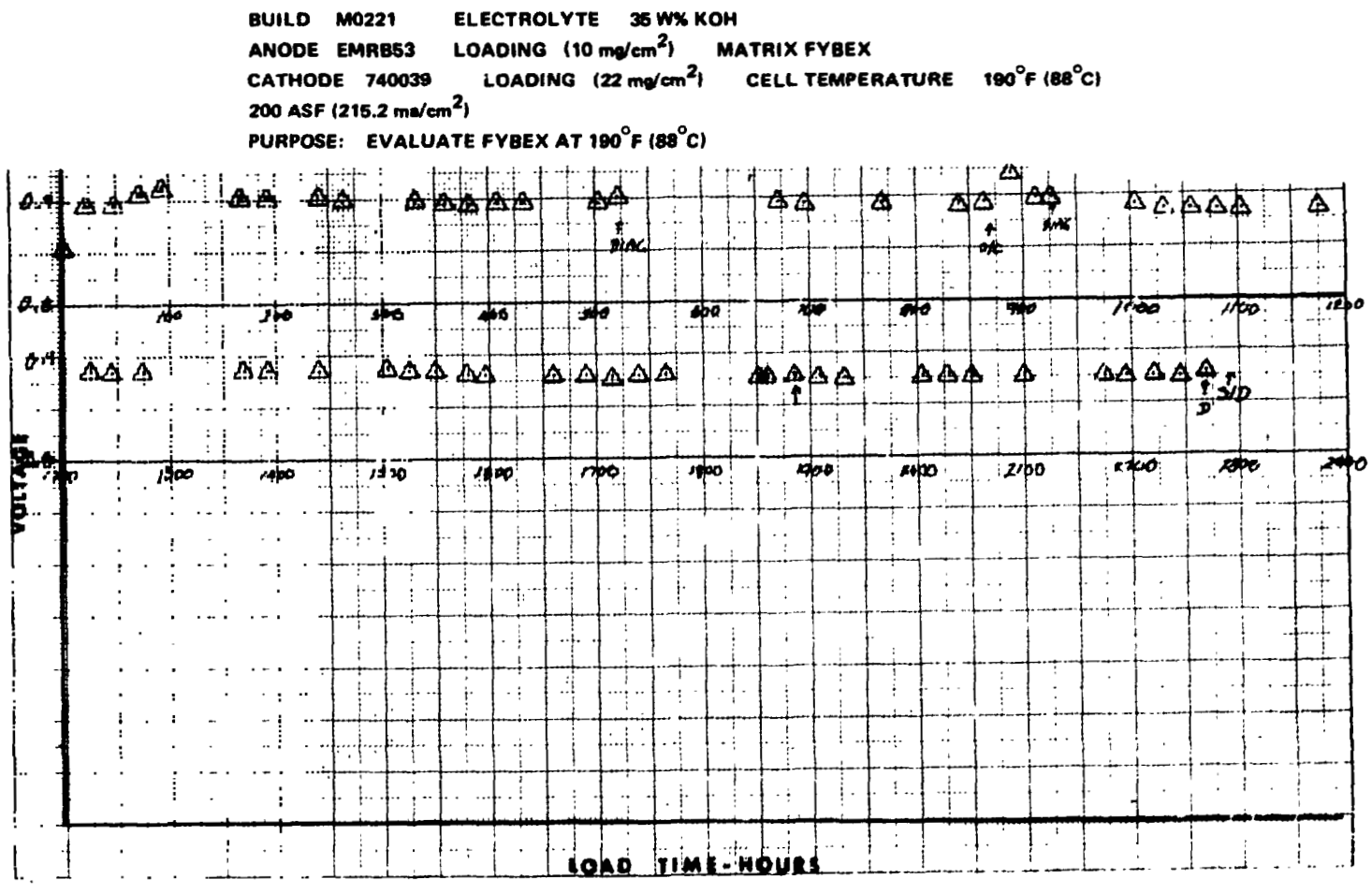

Figure 4 – Performance History of Cell No. M-0221 with Fybex Matrix at 190°F (88°C)

3.0 Cathode Development

During this program phase, development of the 80Au-20Pt catalyst cathode was continued. Catalyst preparation techniques were improved to obtain surface areas of 30 m^2/g and other desirable physical properties consistently. Methods to fabricate electrodes incorporating this catalyst into improved structures were investigated. Electrodes of this type were tested as cathodes in laboratory-size endurance cells and in full-scale (1.375 x 12-inch) (3.5 x 30.5 cm) strip cells. Results to date indicate that this cathode with 10 mg/cm^2 catalyst loading has performance equivalent to the standard 90Au-10Pt catalyst cathode with 20 mg/cm^2 catalyst loading. The 80Au-20Pt cathode also shows a rate of performance decay because of catalyst recrystallization equivalent to that of the 90Au-10Pt cathode, which is entirely satisfactory. Details of the tests and analyses are described below.

During Phase II, preliminary testing of cathodes incorporating 80Au-20Pt catalyst indicated that this catalyst composition was a promising candidate for improved stability. During Phase III, additional development of the 80Au-20Pt catalyst was pursued. The technique for preparation of this catalyst composition was modified to produce catalyst with approximately 30 square meters per gram (m^2/g) surface area, with all of the platinum alloyed in solid solution with the gold, and with "bulk" (apparent specific volume) approximately 1.35 cubic centimeters per gram (cc/g). These physical properties allow loadings of 10 mg/cm^2 while still maintaining the total activity of a 20 to 25 mg/cm^2 90Au-10Pt catalyst cathode. Furthermore, the high degree of alloying holds promise that the decay due to recrystallization of the catalyst, with its attendant activity loss, will be minimized. However, the bulk is still lower than desirable if the catalyst layer thickness, porosity, etc. are to be optimized.

Methods of fabrication of the 80Au-20Pt catalyst into suitable electrode structures were investigated. Since the catalyst loading was decreased, the catalyst bulk had to be increased to maintain the total catalyst layer thickness and thus to prevent holes or bare spots in the catalyst layer. During the same period, laboratory experiments were conducted using various blending techniques to decrease gross porosity and to mix the catalyst and Teflon particles which make up the catalyst layer. Mechanical blending and ultrasonic blending were investigated to disperse catalyst particles and these dispersions were then flocculated into agglomerates with Teflon dispersions using procedures developed in company-funded programs. As Phase III ended, full-size electrodes with adequate structure were prepared for evaluation testing in single cells. However, further optimization of structure and fabrication procedures are desirable.

Endurance tests of laboratory 2 x 2-inch (5.08 x 5.08 cm) cells with 80Au-20Pt cathodes continued. Cell No. M-0217 incorporated an 80Au-20Pt catalyst cathode, a PPF anode, and reconstituted asbestos matrix. It had attained 425 hours with fairly stable performance when the reactant gas saturator malfunctioned during a weekend, and reactant gas crossover developed. A test of another specimen of this cathode was started as Cell No. M-0219 and was still being tested at the end of Phase III. A plot of the performance of this cell as a function of time is shown in Figure 5. Figure 6 shows that the activation level and decay rate for this cathode are similar to those of 90Au-10Pt catalyst cathodes. Since

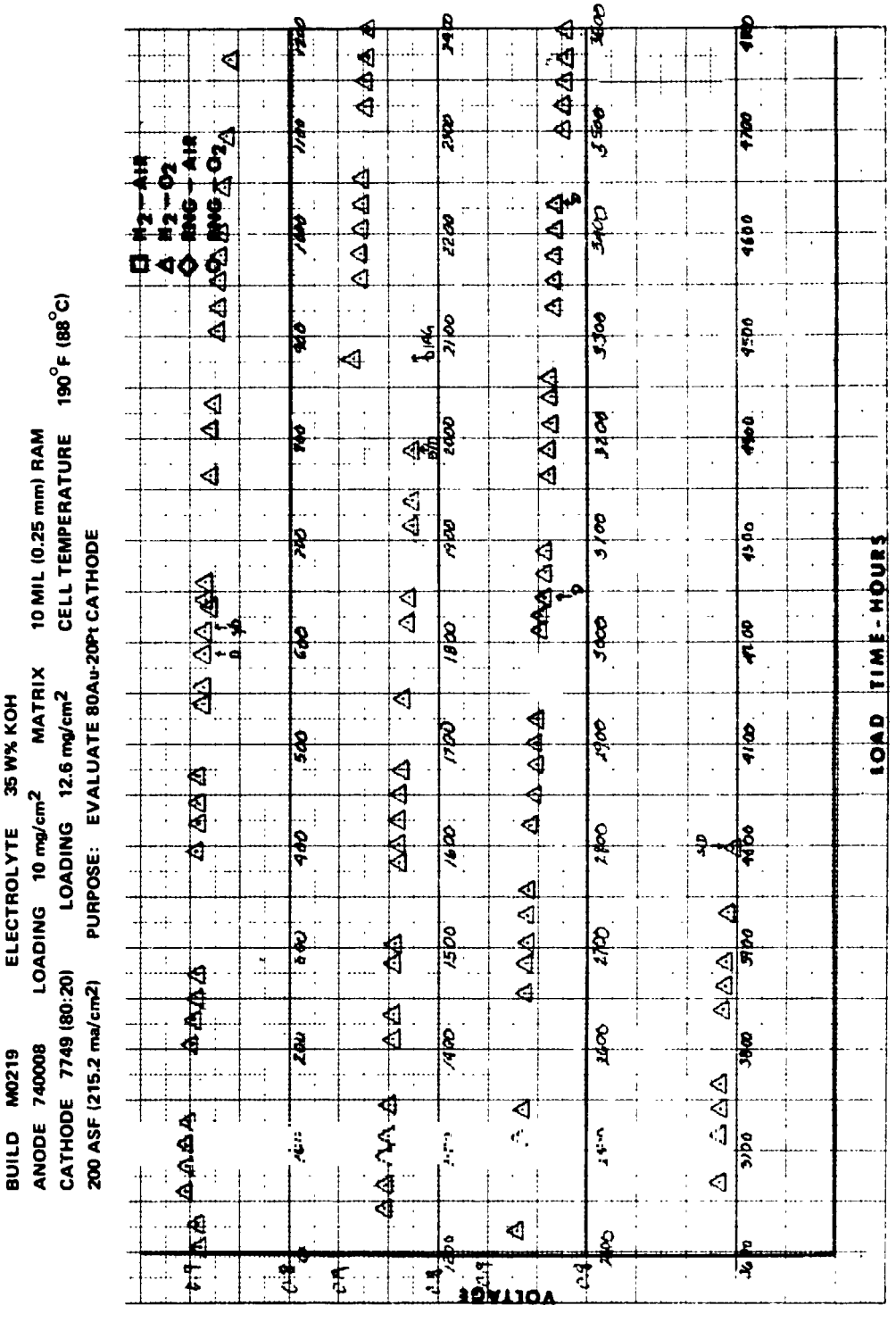

Figure 5 – Performance History of Cell No. M-0219 with 80Au-20Pt Cathode

ORIGINAL PAGE IS
OF POOR QUALITY

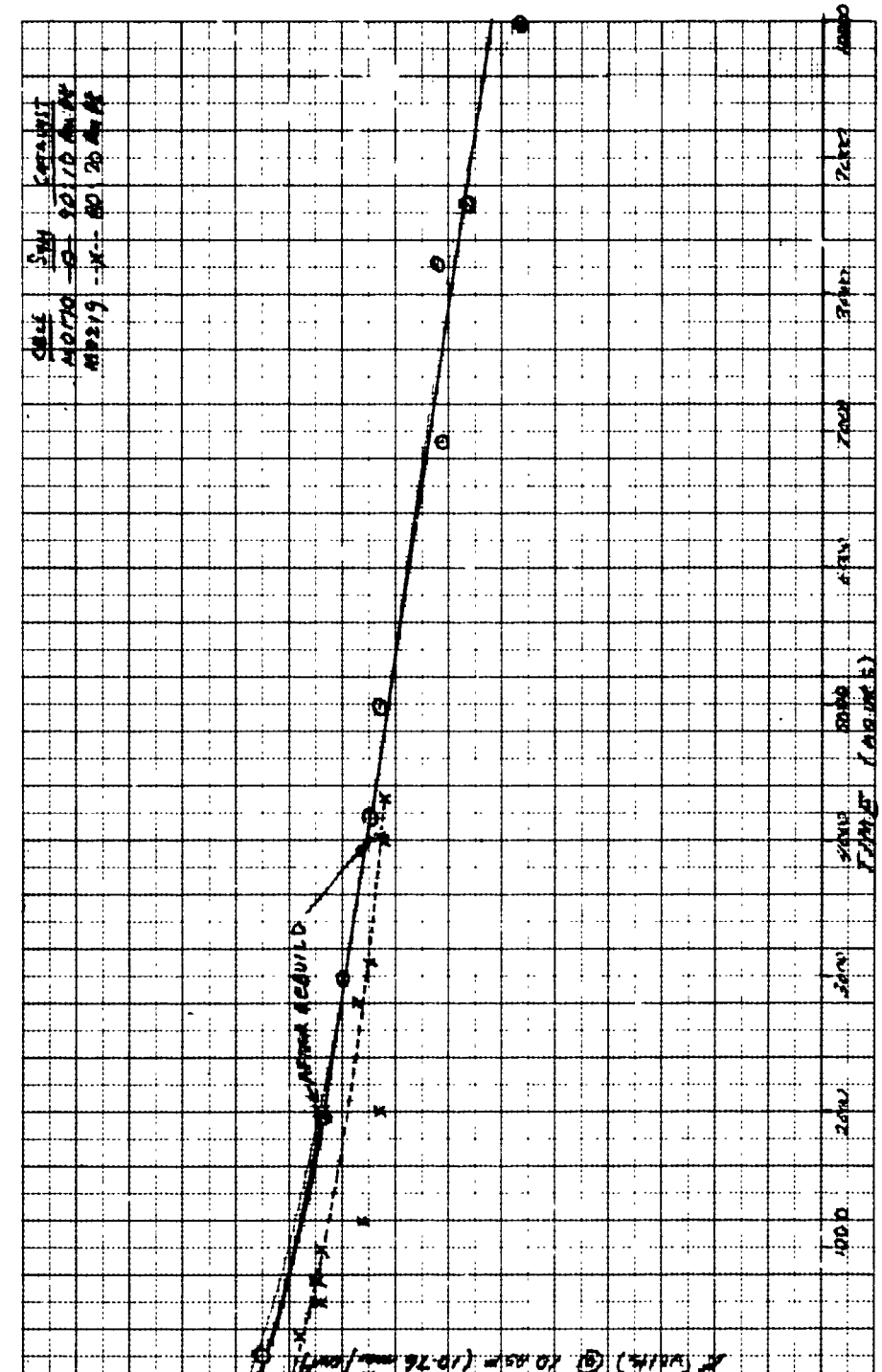

Figure 6 – Comparison of Cathode Activation Loss Rates – 80Au-20Pt vs. 90Au-10Pt

the 80Au-20Pt catalyst has higher initial activity because of its greater surface area, the activity after testing remains higher than that of the 90Au-10Pt catalyst cathodes.

Full-size, single-cell testing included the 80Au-20Pt catalyst cathode in Cell Nos. 40 and 41; these tests are described in Section IV of this report.

Under the company-supported research efforts, a long-term 90Au-10Pt cathode laboratory cell test reached 10,002 hours and was shut down for post-test evaluation. Cell voltage at shutdown was 835 mv at 100 ASF (107.6 ma/cm^2). Figure 7 presents the performance history of the cell. Figure 8 shows the cathode half-cell test results at 0, 5000, 6400 and 10,000 hours. Most of the activation loss occurred during the first 5000 hours.

4.0 Post-Test Evaluation of Full-Size Electrodes

As part of the Phase III program, full-scale 0.1146 ft^2 (10[illegible] cells were endurance tested to evaluate catalyst compositions and electrode structures' [illegible]bility to design conditions. The endurance tests are described in Section IV of this repo[illegible]. Post-test analyses of three of these cells are described in this section. The evaluations included half-cell testing of electrode sections and chemical and microstructural analyses, including X-ray examination techniques to determine crystallite size. In some cases the estimates of losses based on these results disagree with the loss estimates obtained from diagnostic tests performed on the cell as a unit; these discrepancies have not been resolved, although some can be explained by differences between half-cell and full-cell performance levels.

Cell No. 25 consisted of standard PPF electrodes as both anode and cathodes, reconstituted abestos matrix (RAM), and a Ni-plate polysulfone electrolyte reservoir plate (ERP). The cell was tested for 7560 hours at 100 ASF (107.6 ma/cm^2). Post-test chemical and X-ray analyses. showed that the cathode had experienced the typical loss of Pt and Pd and their transport to the matrix and anode. The loss of surface area calculated from the observed increase in cathode crystallite size would be expected to have a greater effect than the 23-mv loss of activity noted during diagnostics. Anode catalyst crystallite size had also increased, but the gain in total amount of catalyst at the anode, because of transport from the cathode, compensated for the loss of active area. Both anode and cathode initially contained 9 mg Pt/cm^2 and 1 mg Pd/cm^2. Post-test chemical analyses showed 3.2 mg Pt/cm^2 and 0.006 mg Pd/cm^2 left in the cathode; with 1.39 mg Pt/cm^2 and 0.68 mg Pd/cm^2 in the matrix; and 14.2 mg Pt/cm^2 and 1.40 mg Pd/cm^2 in the anode.

However, a significant portion of the decay was attributed to anode flooding, based on the following observations. Diagnostic data taken during test and after disassembly gave an IR-free cell loss of 189 mv. When corrected for carbonates (17 mv) and loss of cathode catalyst active area (23 mv), the total diffusion loss for both electrodes was 149 mv. Post-test half-cell tests indicated that the whole of this loss was attributable to the anode and that the cathode showed no diffusional losses. When the cell was disassembled following test, a film of electrolyte was observed on the gas-side of the anode. A grey-colored deposit was also observed on the gas-side of the anode, analysis of which showed silicon as the major constituent. This grey-colored material was wettable and was not soluble in acid or

BUILD M0170 ELECTROLYTE 35 W% KOH
ANODE PT. SUP. LOADING 0.5 mg/cm^2 MATRIX 10 MIL (0.25 mm) RAM
CATHODE 90Au-10Pt LOADING 18 mg/cm^2
CELL TEMPERATURE 190°F (88°C) 200 ASF (215.2 ma/cm^2)
PURPOSE: EVALUATION OF SUPPORTED ANODE (0.5 mg/cm^2)

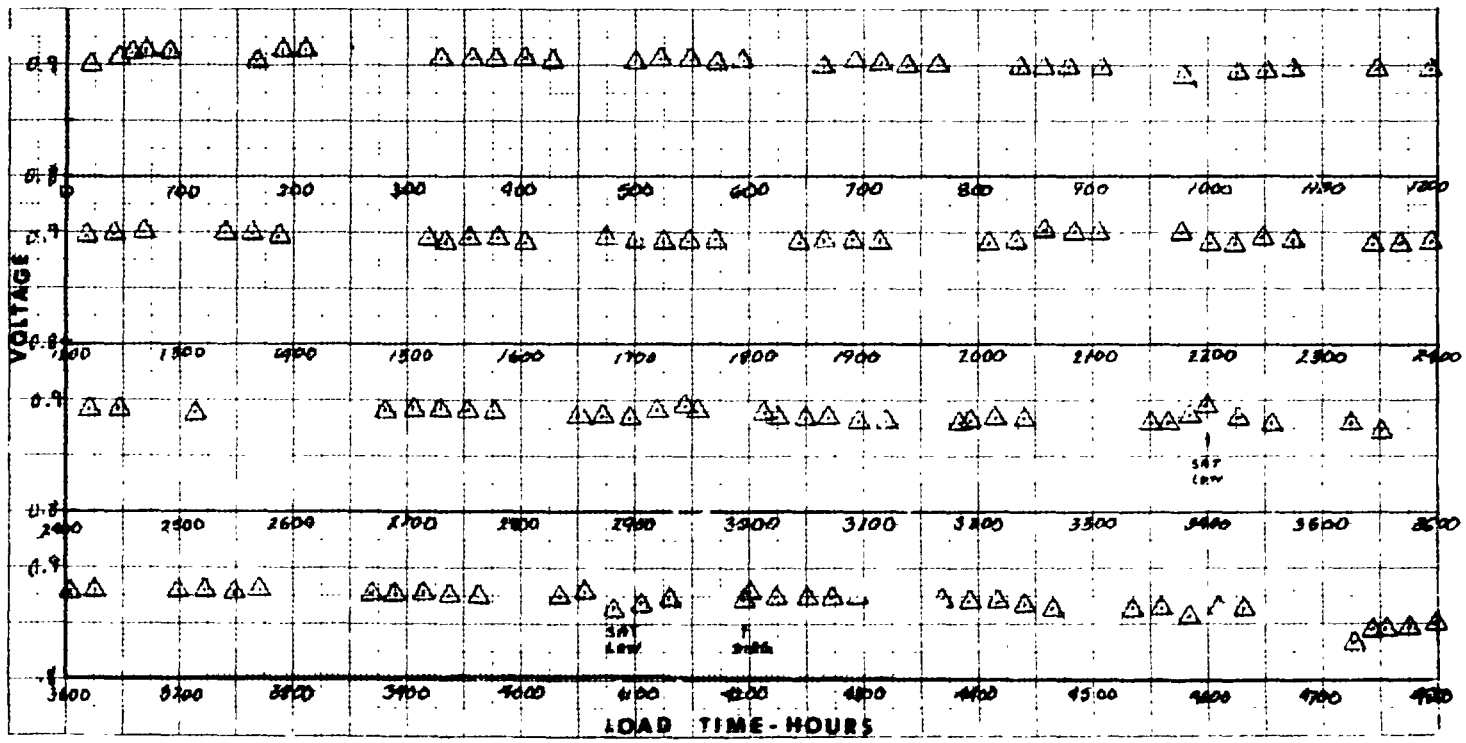

Figure 7 -- 10,000-Hour Performance History of Laboratory Cell No. M-0170 with 90Au-10Pt Cathode

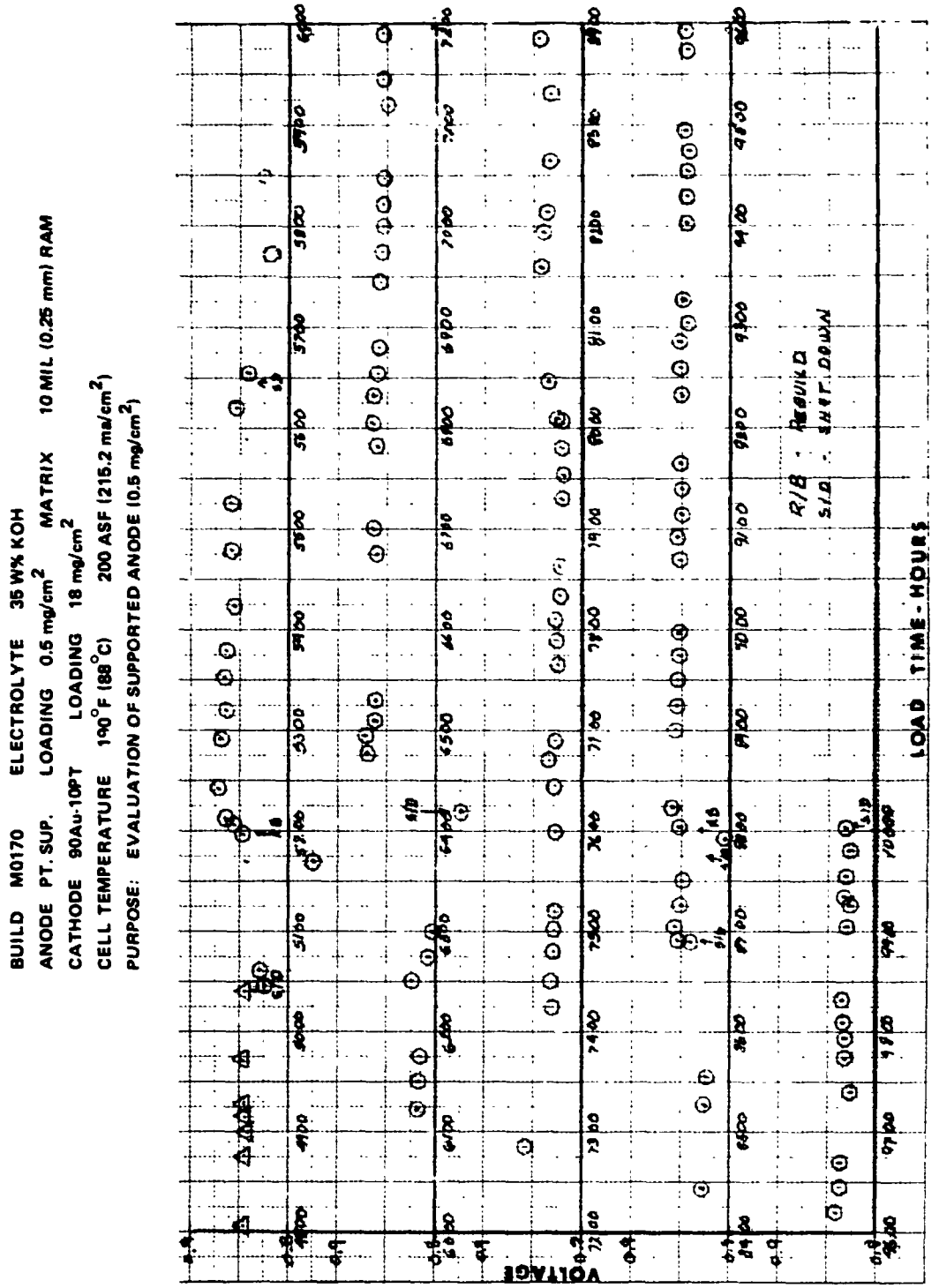

Figure 7 (Cont'd) – 10,000-Hour Performance History of Laboratory Cell No. M-0170 with 90Au-10Pt Cathode

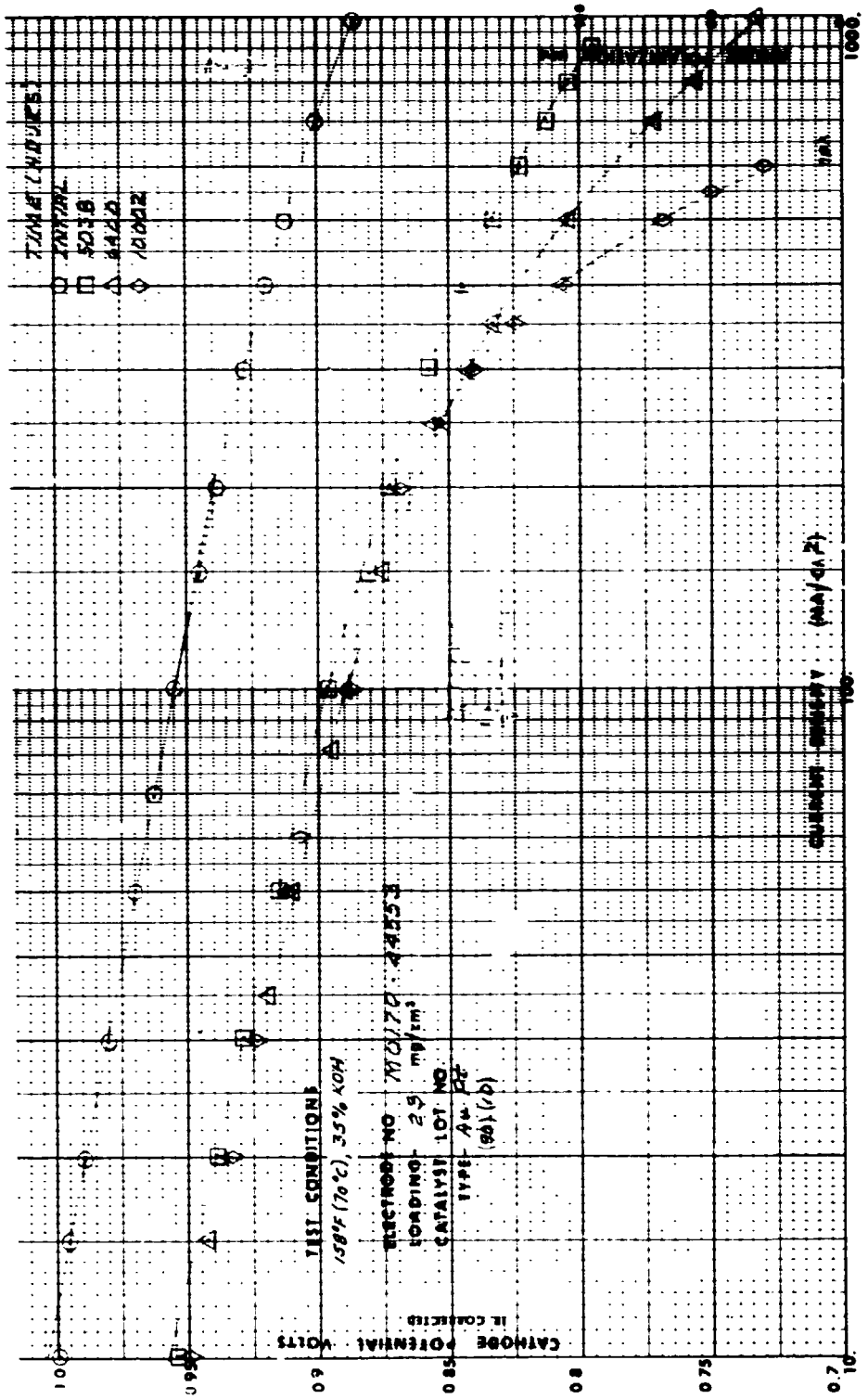

Figure 8 – Half-Cell Test Results for Cell No. M-0170 Cathode at 0, 5000, 6400 and 10,000 Hours

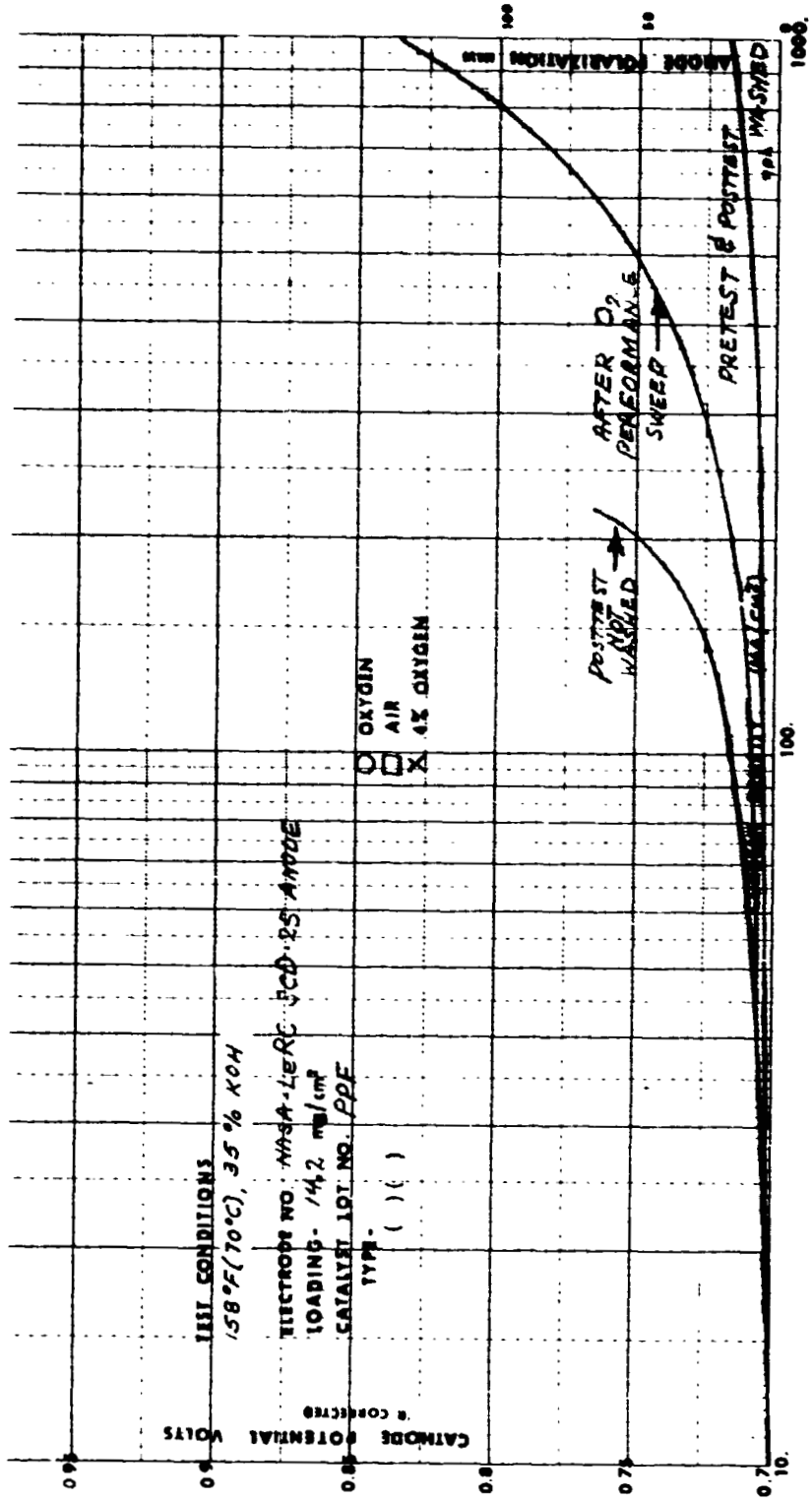

Figure 9 – After Test Evaluation of Anode From Cell No. 25

base, or in organic solvents. When the anode was washed in water to remove electrolyte and dried, good performance was temporarily restored in half-cell tests (Figure 9) but flooding was soon observed. Resintering the anode at higher temperature did not prevent gas-side flooding. Electrolyte take-up determinations and visual observations in the half cell indicated that the bulk of the electrode was not completely flooded, but that the flooded zone corresponded to the grey-colored deposit. Since silicon is a major constituent of both the deposit and the asbestos matrix, the deposit is believed to be a degradation product from the asbestos matrix. Its presence was taken as the reason for the significant anode performance degradation observed in long-term cells, and led to the change in emphasis in the anode development program previously described. Post-test examination of long-term cells from company-funded programs have also shown the grey-colored deposits in varying amounts.

Cell No. 30 consisted of a standard PPF anode, a 90Au-10Pt catalyst cathode, RAM, and a porous nickel ERP unitized into a polysulfone frame. This cell was tested for 10,021 hours at 100 ASF (107.6 ma/cm^2) and demonstrated the performance and long life of the Au-Pt catalyst cathode. Carbonate conversion was limited by use of the polysulfone UEA frame. Details of the operating history are discussed in Section IV of this report. Total cell voltage loss was 190 mv, or 19 μv/hour. Post-test analyses showed that these losses were divided as follows: Total anode losses, 95 to 99 mv; anode loss due to carbonates, 27 mv; anode diffusion losses, 70 mv. Total cathode losses, 83 to 97 mv; cathode activation losses, 65 mv; and cathode diffusional losses, 18 mv. The anode diffusional losses were attributed in the most part to localized flooding caused by silicon-containing deposits in turn caused by matrix degradation and transport.

Cell No. 32 consisted of a 635°F (335°C) sintered PPF anode, a Au-Pt cathode, RAM, and a porous nickel ERP. This cell was tested for 395 hours at 100 ASF (107.6 ma/cm^2). Post-test inspection revealed that the cathode was assembled with the gas-side against the matrix and post-test evaluations indicated that the anode was only approximately one-third filled with electrolyte. Post-test examination of Cell No. 31, which also contained a 635°F (335°C) sintered PPF anode and was tested for 3000 hours, also showed lack of complete electrolyte fill. These cells had been tested before the examination of Cell No. 25, when the emphasis was on more hydrophobic anode structures.

B. Matrices

During the Phase I program, NASA LeRC and P&WA began evaluation of potassium titanate as an alkaline fuel cell matrix material. The material evaluated was manufactured by E. I. Dupont de Nemours & Company under the trade name Fybex. Early tests at the LeRC and P&WA showed Fybex to be compatible with KOH and to exhibit good bubble pressures, up to 20 psid (13.8 n/cm^2).

Phase II efforts focused on developing methods for fabricating Fybex matrices with improved mechanical properties. These efforts were thwarted, however, by changes made by the supplier, Dupont, in the process for manufacturing the raw material. These changes altered the Zeta potential of the Fybex fibers and in turn the mechanical properties P&WA could achieve

in fabricating a matrix. To solve this problem two approaches were considered: (1) specially process the Fybex to reobtain the Zeta potentials of the original pilot lots of material, or (2) develop procedures for fabricating matrices which were unaffected by the change in Zeta potential. The latter approach was selected for the Phase III matrix program. In addition, several other new materials were evaluated to determine their suitability as an alkaline fuel cell matrix.

1.0 Potassium Titanate Matrix Development

At the outset of Phase III, two forms of potassium titanate, Fybex D and Tipersul, were obtained from DuPont. However, Fybex was the only form available in quantity, and DuPont announced that Tipersul would no longer be manufactured. Therefore, it was decided to concentrate the development effort on Fybex D. Table I lists the properties of this material. Data supplied by DuPont and by the United Aircraft Research Laboratory are presented.

TABLE I

CHARACTERISTICS OF FYBEX D (RAW MATERIAL)

Data Source	Properties
DuPont's literature	$K_2Ti_8O_{17}$; 0.10 to 0.15μ fiber diameter
UARL's X-Ray Diffraction and Electron Microscope	$K_2Ti_6O_{13}$
Scanning Electron Microscope	4.2μ average fiber length (2 to 22μ range)
Emission Spectroscopy	0.5 w% Ca, 0.2 w% Cu, 0.1 w% Si, all others less than 0.04 w%.

The disagreement between DuPont's literature and UARL's analyses is academic since the intent was to establish a baseline for subsequent analysis of Fybex which has been exposed to potassium hydroxide electrolyte.

Two approaches for fabricating the Fybex matrices were evaluated: (1) silk screen printing and (2) vacuum filtration. The silk screen printing evaluations began with Fybex compositions, bonded with TFE 3170, screen printed onto PPF anodes and Au-Pt cathodes. Printing technique variations included the printing of multiple matrix layers and the use of different mesh and thickness electrode screens; composition variations included unmilled versus milled Fybex, different printing ink stabilizers, additions of Calgon water softener to act as a Fybex dispersant and variable binder content. Maximum bubble pressures ranging from 7 to 10 psi (4.8 to 6.9 n/cm^2) were achieved by printing approximately one-half of the matrix on each

electrode and sintering at 530°F (276°C) for 15 minutes. The best combination consisted of 4 weight percent TFE 3170, unmilled Fybex, Polyox (polyethylene oxide), printing ink stabilizer and 9 weight percent Calgon based upon Fybex content. Such structures typically contained a total of one to two mils (0.025 to 0.051 mm) of solid material compared to the three mils (0.076 mm) of solids present in 10 mil (0.25 mm) thick Reconstituted Asbestos Matrices (RAM). Matrices fabricated in this manner did not contain any materials which oxidized up to 400°F (204°C), and at temperatures above 400°F (204°C) they produced less carbon monoxide and carbon dioxide than Johns-Manville fuel cell grade asbestos. These results were obtained by differential scanning calorimetry and gas chromatography, respectively. Table II contains the gas chromatography analysis results.

TABLE II

GAS CHROMATOGRAPHY ANALYSIS(1)

Matrix Material	ppm CO_2	ppm CO	ppm CH_4
Fybex + 4 w% TFE 3170(2)	200	0	0
JM Asbestos	1000	500	0

Notes: (1) 70% He + 30% O_2 atmosphere at 35 psi (24.2 n/cm^2) and 250°F (121°C) for 100 hours.

(2) 8.7 w% Calgon + 0.5 w% Polyox based upon Fybex content; sintered at 530°F (276°C) for 15 minutes.

Additional screen printing trials with unmilled or fluid-energy-milled zirconia plus two weight percent TFE 3170 resulted in bubble pressures of less than 2.5 psi (1.7 n/cm^2); bubble pressures from 1.4 to 1.8 psi (0.9 to 1.2 n/cm^2) were measured for screen printed carbon (0.02 to 0.5 μ particles) plus four weight percent TFE 3170 structures.

The inability to fabricate high bubble pressure, screen printed matrices, and the results of an analytical study to define the characteristics of high bubble pressure matrices (see Appendix) led to the conclusion that screen printed structures would have lower bubble pressures than filtered matrix structures. As a result, the fabrication effort was returned to filtration. To begin, a 96 weight percent Fybex/4 weight percent TFE 3170 water base composition was filtered directly onto electrodes. This was followed by drying and sintering of the matrix. Bubble pressures between 30 and 33 psi (20.7 and 228 n/cm^2) were achieved with 1.6 mils (0.04 mm) of solid material, half on each electrode. This is approximately half the solids content of a standard 10-mil (0.25 mm) thick, 70 percent porous RAM. A comparison of bubble pressures and porosimetry measured for screen printed and filtered matrix structures

is listed in Table III. Equations relating bubble pressure to matrix mean pore size, the particle size required to yield a certain pore size in a matrix and the particle size required to yield a certain bubble pressure were derived and can be found in the Appendix.

Similar results were obtained when zirconia matrices were fabricated by these two methods. One filtering trial using zirconia plus two weight percent TFE 3170 produced a structure with a 6 psi (4.1 n/cm^2) bubble pressure; screen printed compositions had bubble pressures less than 2.5 psi (1.7 n/cm^2); see Table III. These matrices had lower bubble pressures than the Fybex because of the larger particle size of the basic zirconia material.

TABLE III

BUBBLE PRESSURE AND POROSIMETRY COMPARISON

Matrix Material	Screen Printed	Filtered
Fybex + 4% TFE	7 to 10 psi (1) (4.8 to 6.9 n/cm^2)	30 to 33 psi (2) (20.7 to 22.8 n/cm^2)
Unmilled Zirconia (7.7μ) + 2% TFE	2.5	6.0
Milled Zirconia (2.4μ) + 2% TFE	$<$ 1.3	–

Notes: (1) Mean pore size ~ 1.0μ; 80% Pore size range ~ 0.1 to 100μ; Geometric porosity ~ 86%.

(2) Mean pore size ~ 1.1μ; 80% Pore size range ~ 0.3 to 32μ; Geometric porosity $\geq$ 95%.

Several 2 x 2-inch (5.08 x 5.08 cm) anodes and cathodes were coated with filtered Fybex/4 weight percent TFE 3170 matrix structures for cell testing. Table IV contains a list of the cells built of these electrodes and tested to date. They are compared to a typical cell containing a 10 mil (0.25 mm) thick RAM. Performances at 190°F (88°C) are comparable; however, the higher performance of the filtered Fybex matrix cell at 250°F (121°C) is apparent. The tests of these cells are reviewed in greater detail in Section III A of this report.

Attempts to make fibrillated Teflon bonded Fybex structures by rolling were also made. These were unsuccessful. Fybex compositions containing 10, 20 and 30 weight percent TFE 3170 or 20 weight percent TFE 6 were rolled and the Teflon fibrillated, but such structures lacked physical integrity.

TABLE IV

CELL TEST COMPARISONS

	Cell Type		
	Laboratory	Laboratory	Research & Technology Cell
Matrix	10 mil (0.25 mm) RAM	Filtered Fybex	Filtered Fybex
Active Area	2 x 2-inch (5.08 x 5.08 cm)	2 x 2-inch (5.08 x 5.08 cm)	2 x 2-inch (5.08 x 5.08 cm)
Electrodes:			
Anode	PPF	PPF	PPF
Cathode	90Au-10Pt	90Au-10Pt	90Au-10Pt
ERP	100 mil (0.25 cm) Ni	100 mil (0.25 cm) Ni	100 mil (0.25 cm) Ni
Test Conditions:			
Temperature	190°F (88°C)	190°F (88°C)	190°F/250°F (88°C/121°C)
Electrolyte	35% KOH	35% KOH	35% KOH/42% KOH
Initial Performance:			
mv @ 200 ASF ($215.2\ ma/cm^2$)	906	907	894/924
IR, mv @ 200 ASF ($215.2\ ma/cm^2$)	15	9	17 (1)

NOTES: (1) IR @ 100 ASF ($107.6\ ma/cm^2$)

2.0 Evaluation of Other Matrix Materials

Several other materials were evaluated for matrix fabrication. Each of these is discussed below.

a. Brucite Magnesium Hydroxide

During Phase I of the contract, effort was expended on developing brucite matrix structures, and NASA LeRC requested that P&WA determine whether or not this activity should be continued. Johns-Manville was contacted and indicated that they currently do not produce brucite, probably never will, and that to supply 100 pounds (45.4 kilograms) of the material

"would be a major undertaking". This information combined with the limited success of previous fabrication trials and corrosion test results prompted the decision to suspend brucite matrix development.

b. "Litofol S" Asbestos

Six "Litofol S" asbestos paper structures manufactured by Rex Asbestwerke in West Germany and supplied to P&WA by NASA JSC were tested and exhibited excellent matrix structures. For example, the Rex asbestos appears to be superior to J-M reconstituted asbestos from the standpoint of porosity and bubble pressure:

Type of Asbestos	Sample Thickness	Porosity	Bubble Pressure
Rex Litofol S	15-20 mils (0.38-0.51 mm)	88%	60-92 psi (41-63 n/cm^2)
J-M Fuel Cell Grade, Reconstituted	20 mils (0.51 mm)	75%	54-68 psi (37-47 n/cm^2)

However, asbestos degrades noticeably at temperatures of 250°F or above, and the Rex matrix is no exception. The material experienced an excessive weight loss while being corrosion tested, and was deemed unacceptable for use in potassium hydroxide electrolyte at 250°F (121°C). Corrosion test results and Scanning Electron Microscope (SEM) photomicrographs of the material are presented in Table V and Figure 10 respectively.

c. Silicon Nitride

Beta silicon nitride bonded with 10 weight percent TFE 3170 was also corrosion tested. Although SEM photomicrographs of the corrosion tested material did not reveal any visual degradation (Figure 11), the sample lost 11 weight percent while submerged in 42 percent KOH at 250°F (121°C) for 1000 hours (Table V), and it was considered unacceptable.

d. Polybenzimadazole

Polybenzimadazole (PBI), a ladder polymer material supplied by Celanese Corporation, has been analyzed in a P&WA R&D program. The fibrous material experienced a weight loss of only 1.2 percent while immersed in 42 percent potassium hydroxide at 250°F (121°C) for 5000 hours (Table V). SEM photomicrographs showed that no changes in fiber diameter or surface morphology occurred during corrosion testing; see Figure 12. Gas chromatography has shown that PBI contains relatively small amounts of carbon monoxide and carbon dioxide producing material compared to JM fuel cell grade asbestos, and preheating the fibers at 400°F (204°C) for one hour produced an even cleaner product (Table VI). Initial samples received were in the form of woven textiles; however, non-woven fibers have since been supplied by Celanese. Current technology permits fabrication of PBI fibers with a minimum average diameter of approximately 15 microns, eliminating the possibility of fabricating high bubble pressure

matrices. Celanese would require outside funding to determine the feasibility of fabricating PBI fibers with diameters similar to asbestos fibers. This investigation may be considered in the future.

C. Lightweight Electrolyte Reservoir Plate

During Phase II, methods for fabrication of lightweight electrolyte reservoir plates were developed. These procedures produced a basic nickel-plated porous polysulfone configuration. Full-size ERP's were fabricated and were successfully tested in Cell No. 25.

These methods were used for the production of the plastic ERP's in Cell Nos. 25, 33, 34, 37, 38, 39, 39A, 40, and 41 tested or delivered during Phase III. Figure 14 is a schematic of the Electrolyte Reservoir Plate (ERP), showing its relationship to the cell and its functions. Table VII lists required ERP characteristics. These data are presented for reference.

TABLE V

CORROSION TESTED(1) MATRIX MATERIALS

Sample	Time-Hours	Weight Change-percent	SEM Analysis
Rex "Litofol S"	250	-30.2	Noticeable corrosion
Asbestos	1000	-66.8	Substantial corrosion (Fig. 10)
90 w% Silicon Nitride (2) + 10 w% TFE 3170	250	- 3.6	No visual degradation
	1000	-11.3	No visual degradation (Fig. 11)
PBI	200	+ 0.7	No visual degradation
	500	- 1.6	No visual degradation
	5000	- 1.2	No visual degradation (Fig. 12)
75 w% Fybex + 25 w% FEP(3)	250	- 1.1	No visual degradation
	1000	0	No visual degradation (Fig. 13)

NOTES: (1) 250°F(121°C) 42% KOH
(2) Beta Si_3N_4 manufactured by Cerac, Inc.
(3) Pressed pellet structure.

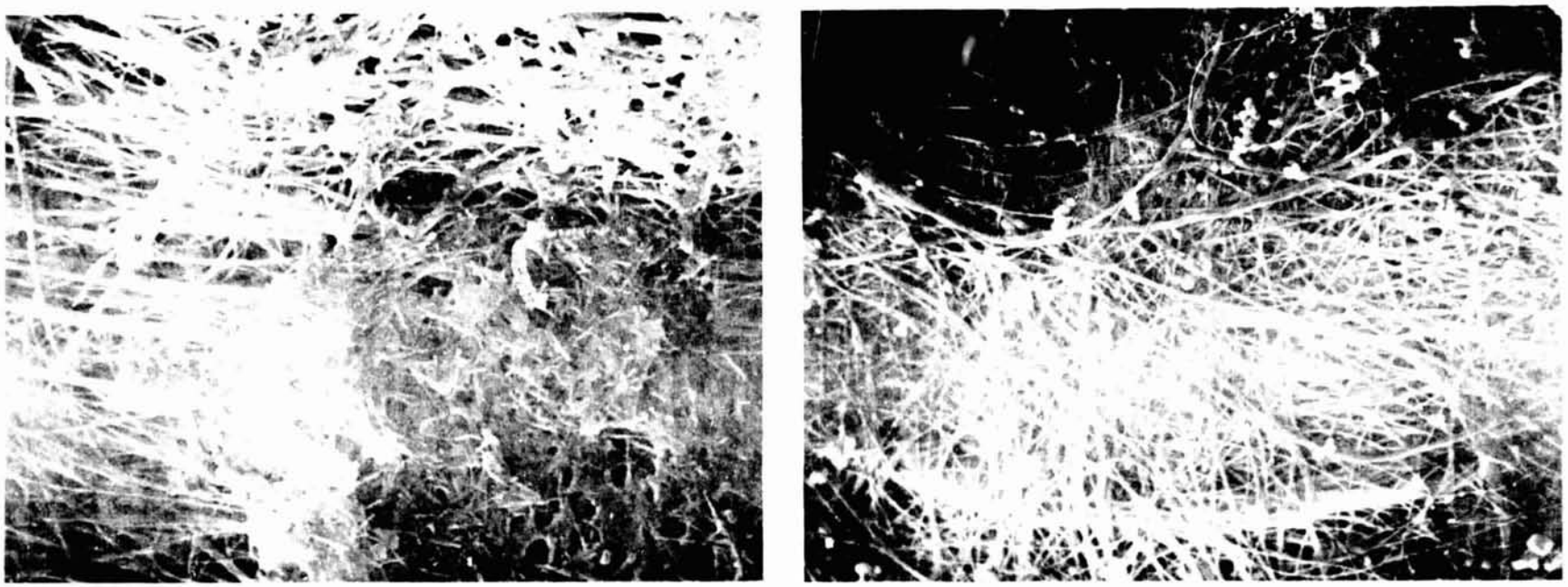

BEFORE EXPOSURE

AFTER 1000 HOURS

MAG: 5000X

Figure 10 – Scanning Electron Micrographs of Rex "Litofol S" Asbestos

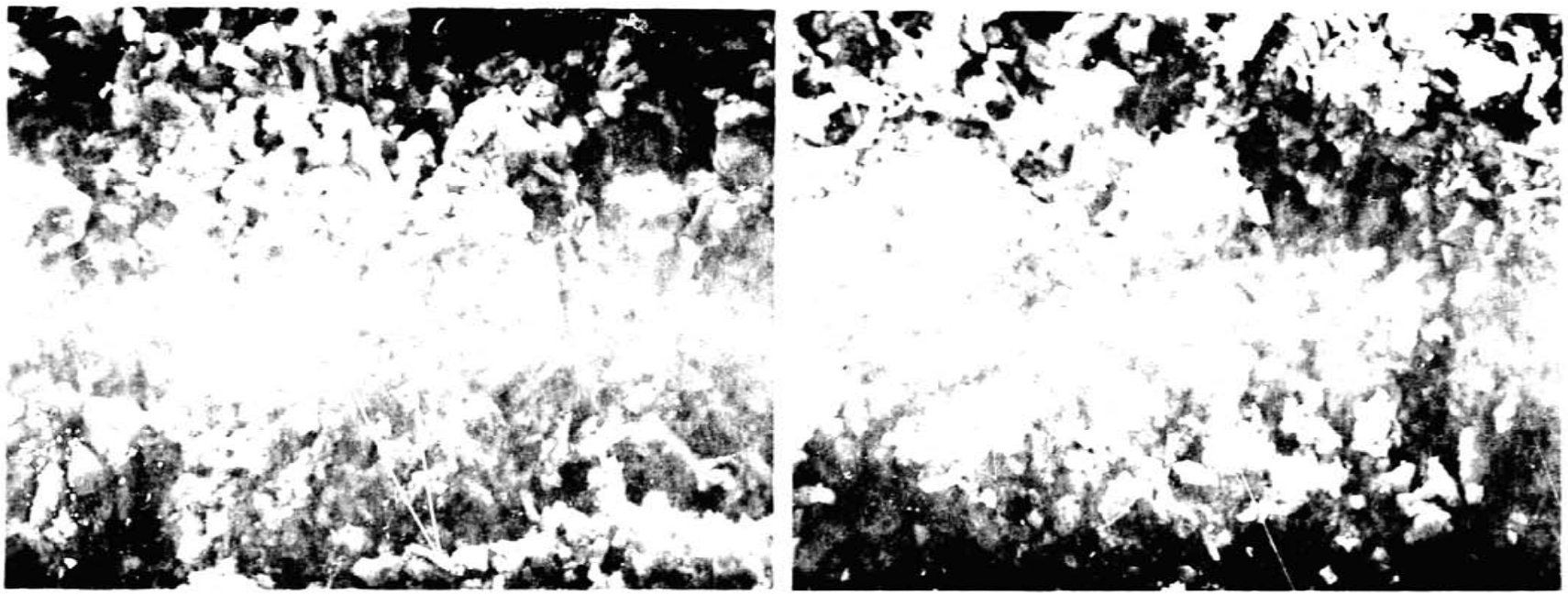

BEFORE EXPOSURE

AFTER 1000 HOURS

MAG: 2000X

Figure 11 – Scanning Electron Micrographs of 90% Silicon Nitride Plus 10% TFE 3170

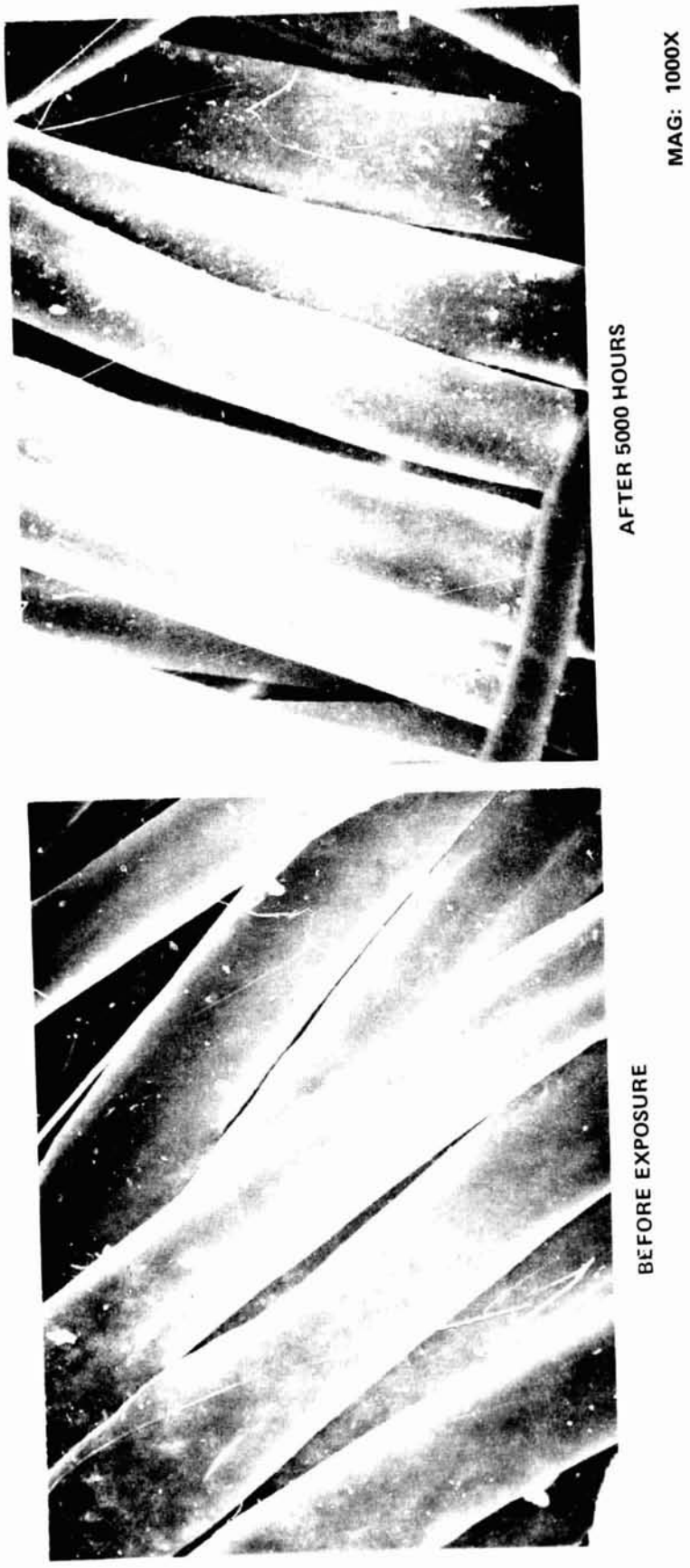

Figure 12 – Scanning Electron Micrographs of Polybenzimadazole

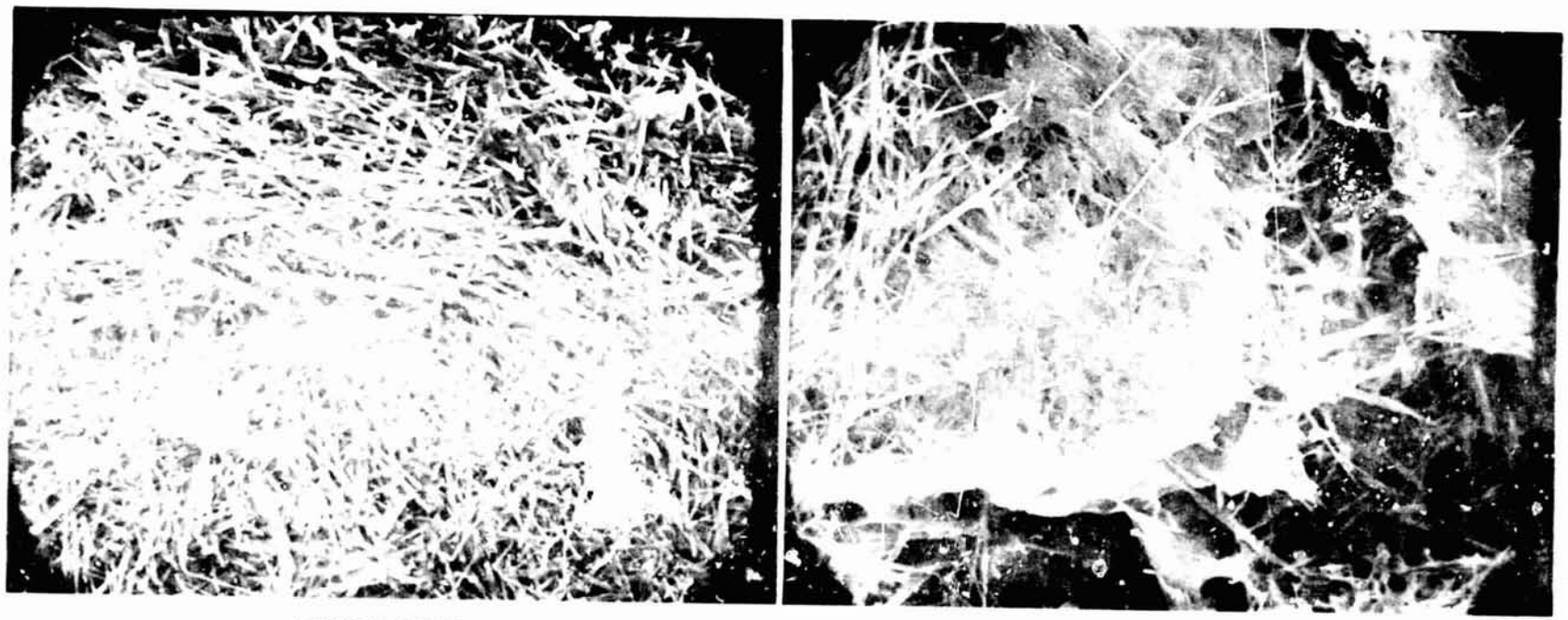

BEFORE EXPOSURE

AFTER 1000 HOURS

MAG: 2000X

Figure 13 – Scanning Electronmicrgraphs of 75% Fybex Plus 25% FEP 120

TABLE VI

GAS CHROMATOGRAPHY[1] ANALYSIS OF PBI

	JM Asbestos[2]	PBI	Heat Treated[3] PBI
CO_2	1000 ppm	2000 ppm	800 ppm
CO	50	130	60
CH_4	None	None	None

NOTES: (1) NASA-LeRC technique, i.e. 100 hours at 250°F (121°C) in 35 psi (24 n/cm^2) environment consisting of 70% He and 30% O_2.

(2) Johns-Manville fuel cell grade asbestos.

(3) 400°F (204°C), one hour.

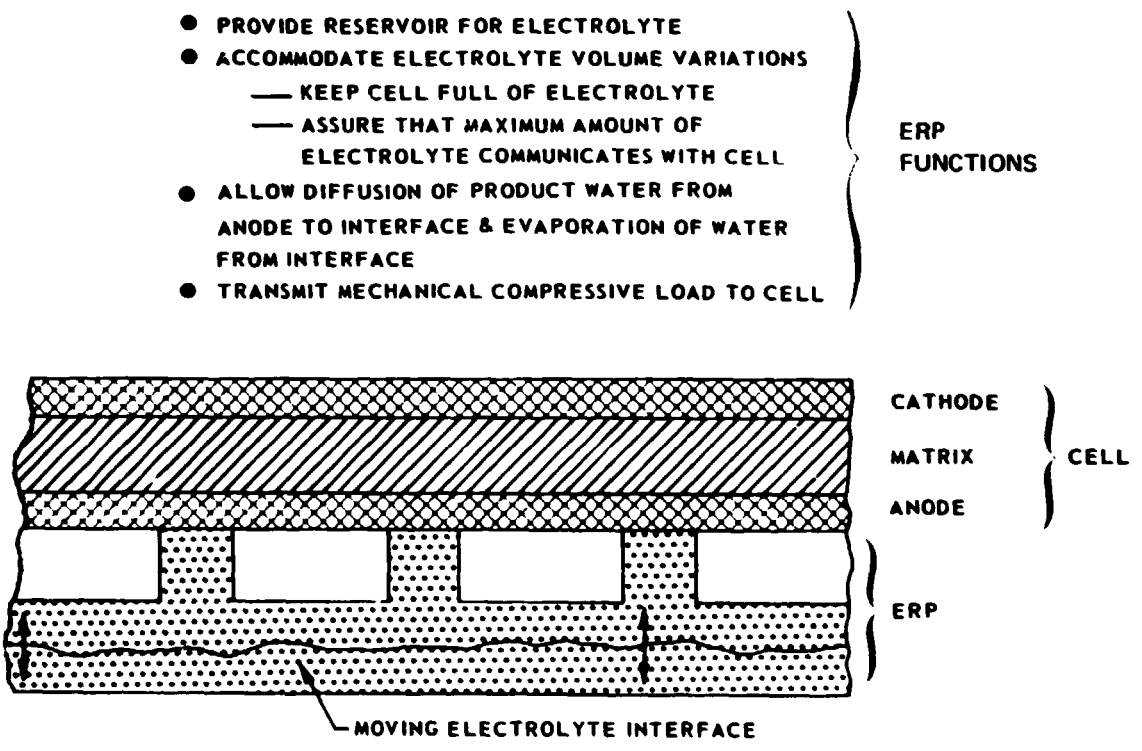

Figure 14 – Electrolyte Reservior Plate Functions

TABLE VII

LIGHTWEIGHT ERP REQUIREMENTS

Pore size	3 to 8 microns
Porosity	As high as practical
Electrolyte flow	Readily wet by electrolyte - minimum hysteresis - ΔP vs ΔV
Compressive strength	200 psi (138 n/cm^2) minimum
Environment	200°F (93.3°C) 10,000 hrs in 25 to 45 weight percent aqueous KOH and hydrogen
Configuration	Flat plate, 10 to 30 mil (0.25 to 0.76 mm) thick, reactant flow passages in one face

Investigation of ERP's was continued during this period under the Air Force High Power Density Fuel Cell Program (Contract No. F33615-72-C-1371). This work revealed that the nickel plating on the porous polysulfone plates could oxidize over long periods of time when stored as a manufactured part ready for incorporation into a cell. This results in the ERP becoming hydrophobic. Consequently, procedures to reduce the nickel prior to incorporating the ERP's into a cell were developed. Storage when in a cell does not result in ERP plating oxidation because the ERP is located on the anode in a reducing hydrogen environment. The operating characteristics of ERP's that had oxidized, and were then subsequently reduced, were found to be the same as unoxidized ERP's.

D. Unitization

The EMS weight and life goals imposed stringent requirements on cell fabrication technology. Thin cells were required to minimize weight and must be fabricated to close tolerances. A cell frame thickness variation of a few thousandths of an inch which would be acceptable in conventional thicker cells but would represent a significant percentage of total cell dimension for lightweight cells. This could result in degraded cell performance because of poor contact between cell components, and sealing of adjacent subassemblies could be unreliable. The reactant differential pressure (bubble pressure) capability of the matrix-to-frame joint in the water transport plate and the fuel cell subassemblies must be reliable. The materials used to make this joint and to form the cell frame must be highly resistant to attack by reactants, water and electrolyte. Finally, assembly and bonding processes used must be compatible with normal manufacturing equipment and result in reasonable costs.

Much of the unitization work in Phases I and II involved identifying materials compatible with the fuel cell environment and learning to fabricate these materials into cells with acceptable dimensional and bubble pressure characteristics. The most compatible of these materials could not be fabricated into cell frames using adhesive bonded joints. To permit their use, thermal laminating was explored as a method for bonding and fabricating them into cell frames. A major problem was encountered using this fabrication method. The temperatures needed for laminating caused a differential thermal expansion between the cell electrodes and frame. The result was that the dimensional characteristics of these cells were poor because of screen wrinkling. Materials which could be laminated at lower temperatures were less compatible with the ful cell environment.

At the end of Phase II, P&WA conceived a cell design which overcame these corrosion and fabricating problems. This was a hybrid frame, composed of polysulfone and glass fiber-epoxy. In this method polysulfone, which had demonstrated excellent compatibility with the fuel cell environment, was utilized as a frame around the asbestos matrix, see Figure 15. Then glass fiber-epoxy was used to form a frame that surrounds the polysulfone. The function of the polysulfone is to minimize contact between the electrolyte and the glass fiber-epoxy. The amount of polysulfone is minimized because of the large thermal expansion coefficient difference between it and the electrode screens. Glass fiber-epoxy is utilized to counteract the polysulfone expansion problems and act as a stiffener. P&WA sponsored a program with the TME Corporation of Salem, New Hampshire to develop a frame of this design. TME Corporation is a specialist in fabrication of laminated polymer assemblies. When TME achieved success, several cells of this design were fabricated for testing and the techniques for their manufacture were transferred to P&WA's advanced cell fabricating operation.

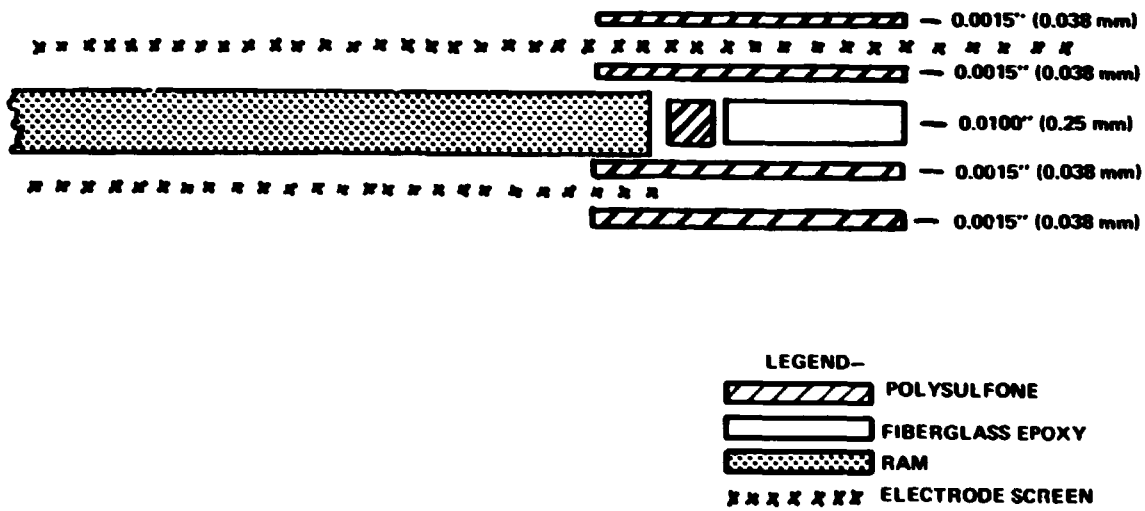

Figure 15 – Hybrid - Polysulfone Glass/Epoxy Frame Design

The main thrust of the fabrication and unitization effort in Phase III was evaluation of this type of cell frame. All cells beginning with Cell No. 31, except for Cell Nos. 33 and 34 which were delivered to NASA, were constructed using this design. Measurements of carbonate levels in the electrolyte after operating periods of various lengths indicate this frame is substantially more resistant to the cell environment than the previous standard epoxy-glass fiber frame. The new hybrid frame is almost as good as pure polysulfone and is considerably easier to fabricate. These results are discussed further in Section IV F and are summarized in Figure 30.

E. Non-Operating Cells

The carbonation results from early strip cells tested in Phase I indicated a need to develop more sensitive compatibility testing techniques to allow rapid screening of candidate materials and cell unitization designs. As a result, during Phase II, oxidation tests using gas chromotograph techniques and another method, the non-operating cell test especially developed for this program, were used to evaluate the relative carbonation characteristics of promising unitization designs. The non-operating cell provided an accelerated measurement of carbonation rates of realistic cell configurations. A cell frame represents a combination of materials not possible to simulate in simple, single fluid compatibility test.

A non-operating cell consists of a strip cell, 1.375 x 12 inches (3.5 x 30.5 cm), without an electrolyte reservoir plate, mounted between single cell end plates. A schematic drawing of this test fixture is shown in Figure 16. The cell is tested with oxygen in both reactant compartments to expose a maximum area to the oxidizing atmosphere. The cell is mounted in a 212°F (100°C) oven and the reactant passages pressurized with 16 psia (11 n/cm^2) oxygen. During Phases II and III, a test temperature of 212°F (100°C) was used as opposed to the 180°F (82.2°C) temperature used during Phase I. This increase in temperature reduced required exposure time for the same degree of carbonation from 200 to 100 hours. After the conclusion of the exposure period, the electrolyte is analyzed to determine the amount of carbonation present. By minimizing the amount of electrolyte in the cell - only the matrix and electrodes are filled with electrolyte - the non-operating cell is a sensitive indicator of carbonation produced by the cell components and structural materials.

The results of non-operating cell tests conducted during both Phases II and III are presented in Figure 17. All tests except for 10 and 10A were conducted at 212°F for 100 hours in an oxygen environment.

Cell Nos. 9 and 9A were the first hybrid polysulfone - epoxy/glass fiber frame subjected to non-operating cell carbonation tests. These tests were completed at the end of Phase II and are reported for reference. As in most of the other tests, retesting of the sample resulted in considerable reduction in carbonation levels suggesting an initial level of impurities which are leached out in the first test. Results are comparable to those of carbonation Cell No. 3, a pure polysulfone frame, showing the hybrid frame possesses the corrosion resistance of the pure polysulfone frame and the dimensional uniformity of epoxy/glass fiber frames. This became the standard UEA frame for Phase III.

Early in Phase III, Cell No. 10 was constructed to verify that the epoxy/glass fiber frame was compatible with the anode hydrogen environment. If verified, this fabrication approach could be used to manufacture Passive Water Removal (PWR) assemblies and ERP frames. These tests were conducted at 212°F (100°C) and 16 psia (11.0 n/cm^2) with a pure hydrogen atmosphere. The retest (10A) gave results comparable to the "components only" test on oxygen and indicated the suitability of this material for construction of PWR and ERP frames. As a result, all PWR's beginning with Cell No. 36 utilized an epoxy/glass fiber frame construction.

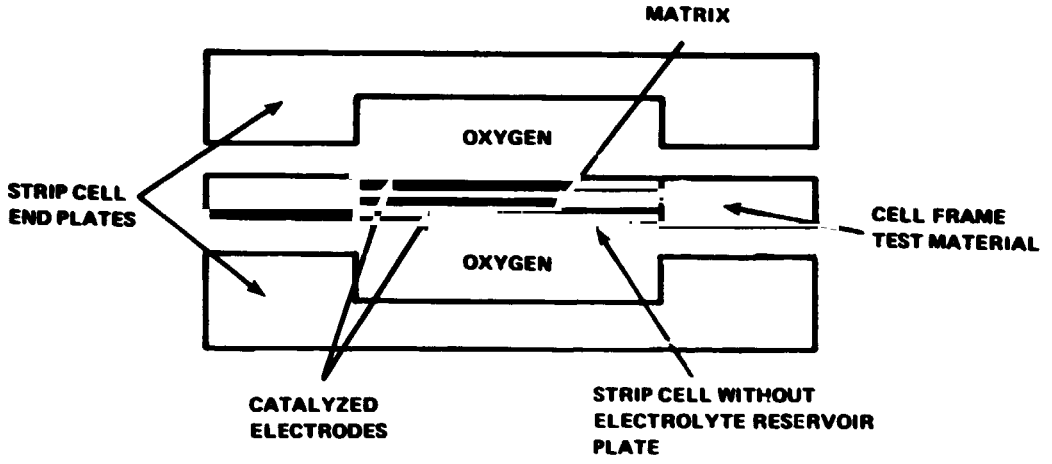

- 1.375 inches x 12.0 inches (3.5 cm x 30.5 cm) active area
- No electrolyte reservoir
- Oxygen on both electrodes - 212°F (100°C), 16 psia (11.0 n/cm^2)

Figure 16 Carbonation Test Rig

CELL	CONSTRUCTION (CURE)
1	E-755/FIBERGLASS
1A	E-755/FIBERGLASS
2	E-755/ASBESTOS (325°F)
3	POLYSULFONE
4	E-755/ASBESTOS (375°F)
4A	E-755/ASBESTOS (375°F)
5	HYPON (225°F)
5A	HYPON (225°F)
6	COMPONENTS
6A	COMPONENTS
7	E-755/ASB IMPREG
7A	E-755/ASB IMPREG
8	UARL-3 EPOXY/ASB IMPREG
9	PREPREG POLYSULFONE HYBRID
9A	PREPREG POLYSULFONE HYBRID
10	E-755/FIBERGLASS (H_2 ENVIRONMENT)
10A	E-755/FIBERGLASS (H_2 ENVIRONMENT)

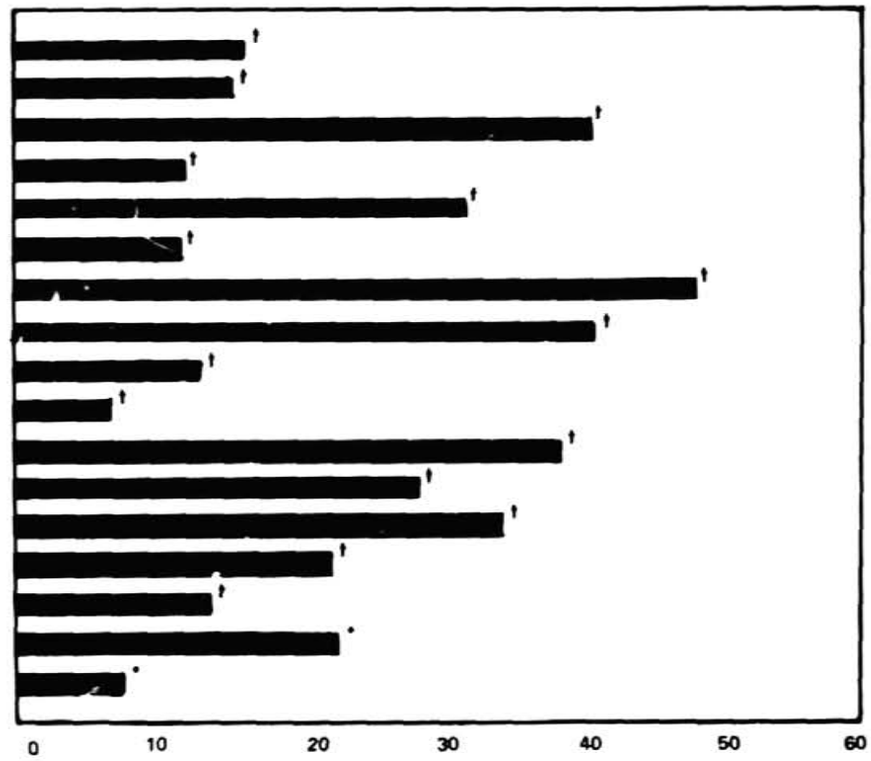

NOTES
- 0.87 GMS KOH
- 16.4 IN^2 ACTIVE AREA
- 26.7 IN PERIMETER

† TEST CONDITIONS
- 212°F (100°C)
- ~100 HOUR EXPOSURE TO OXYGEN

• TEST CONDITIONS
- 212°F (100°C)
- ~100 HOUR EXPOSURE TO HYDROGEN

Figure 17 – Non-Operating Cell Compatibility Test Results

IV. SINGLE CELL DEVELOPMENT

A. Introduction

The single cell task was a major portion of the technology advancement effort performed during Phase III of the Advanced Fuel Cell Program. This task again served as the focal point, integrating the results of system design analysis and the results of the materials development tasks. The NASA goals for operating life, weight, and system operational features call for a significant advance in fuel cell power section state-of-the-art. These goals have led to the preliminary EMS design which established the following cell requirements:

- Minimum thickness component parts and flow fields for low weight
- Plastic structural materials for low weight
- Highly compatible materials for long life
- Passive water removal
- Evaporative cooling

  } Required by the system, and their use favors long life

- Edge current collection, as a consequence of the above items.

A single cell is the smallest building block for evaluation of these cell requirements. Although a single cell does not duplicate the intercell seal geometry of a plaque, and does not require evaporative cooling for temperature control, it does provide the most cost effective approach for investigation of all the other EMS cell features.

Specifically, the single cell evaluation program had as its objectives:

(1) Test different cell component configurations and materials

(2) Define performance characteristics

(3) Evaluate methods for extending life

It has been conducted as an evolutionary program which allows results from the single cell tasks to feed back into the development process. The nature of the single cell program is depicted in Figure 18, which shows how the key development findings are fed back to improve performance and life characteristics.

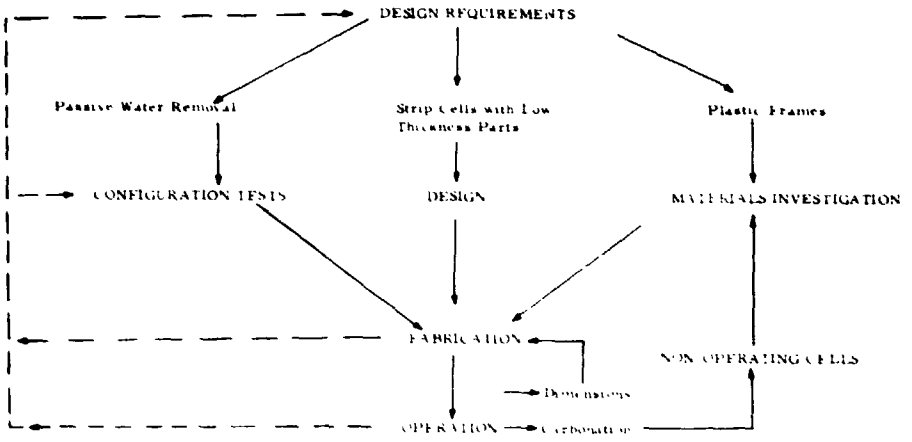

Figure 18 – Evolutionary Single Cell Development Process

B. Single Cell Design

This section describes the design of the single cell hardware and the successive single cell design configurations evaluated during the Phase III effort. The single cell test unit used to evaluate the results of unitization development for performance and endurance testing, and for the formal NASA Verification and Endurance category of testing was that developed in Phase I. It incorporates the novel features of the EMS design, namely:

- Strip cell – 12.0 x 1.375 inches (30.5 x 3.49 cm) cell area
- Edge current collection
- Improved compatibility frame unitization
- Passive water removal
- Minimum thickness flow fields and component parts.

Figure 19 shows the working elements of that cell and illustrates that the design represents a significant improvement compared to the existing state-of-the-art as represented by the cell design used in P&WA's PC17 Space Shuttle Powerplant. The direct comparison between the PC17 and the EMS cell is not completely "fair" since the EMS requirement to remove product water by the passive method requires that an additional subassembly, the water transport plate, be added to the EMS cell. Nonetheless, the passive water removal cells tested during this program were only 60 percent as thick as PC17 cells.

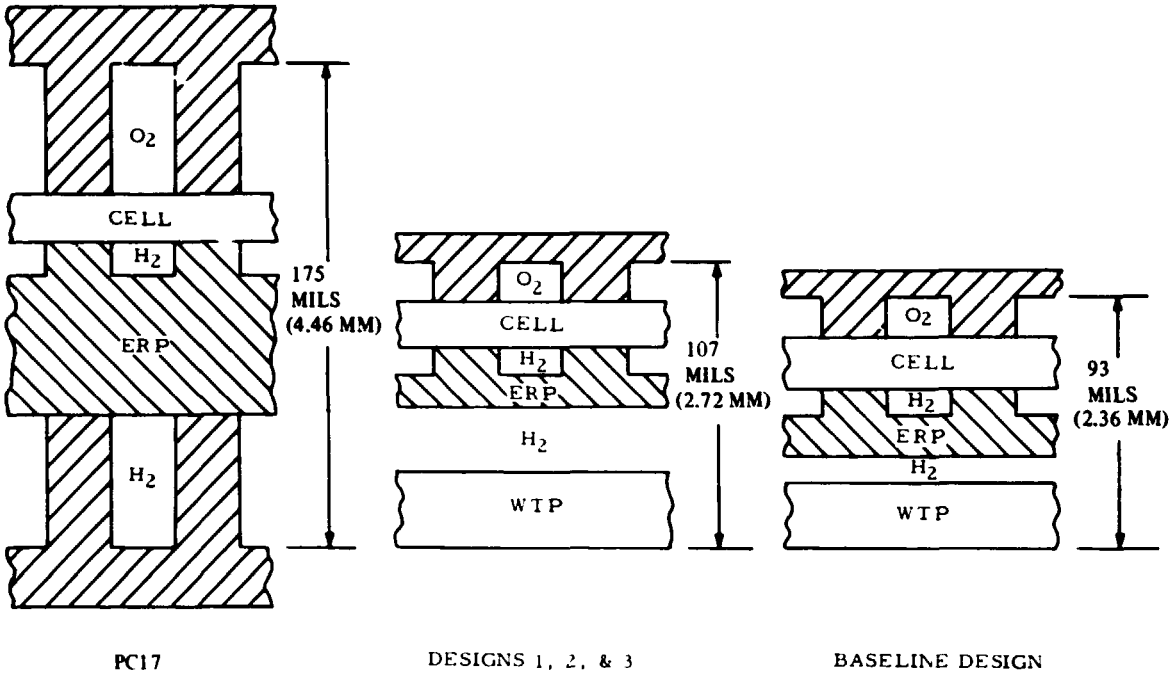

Figure 19 — Size Comparison of Cell Designs Tested

The cell is assembled of two sections: the unitized electrode assembly (UEA) and a unitized water transport plate, shown in Figure 20. These two components can be either bonded together or mated with an elastomer gasket between them to effect the required seal.

The cell test fixtures used during Phase III were the same as those used in Phases I and II. They are rigid ½ inch (1.27 cm) stainless steel plates with provision for sealing and fluid connections. Some of the features of the test fixtures, shown in Figure 21, are:

- Flow field inserts for interchange of field patterns
- O-ring sealing for easy assembly of unitized parts
- Isothermal operation to duplicate EMS Design
- Passive heat rejection for test simplicity
- Nickel plated to avoid corrosion

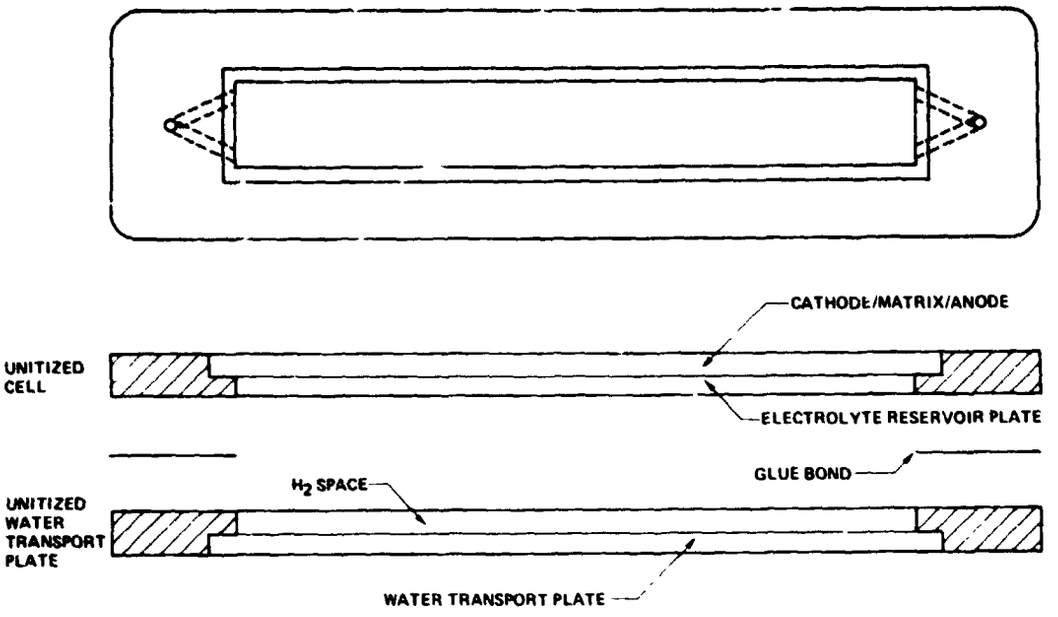

Figure 20 – Single Cell Development Plastic Frame

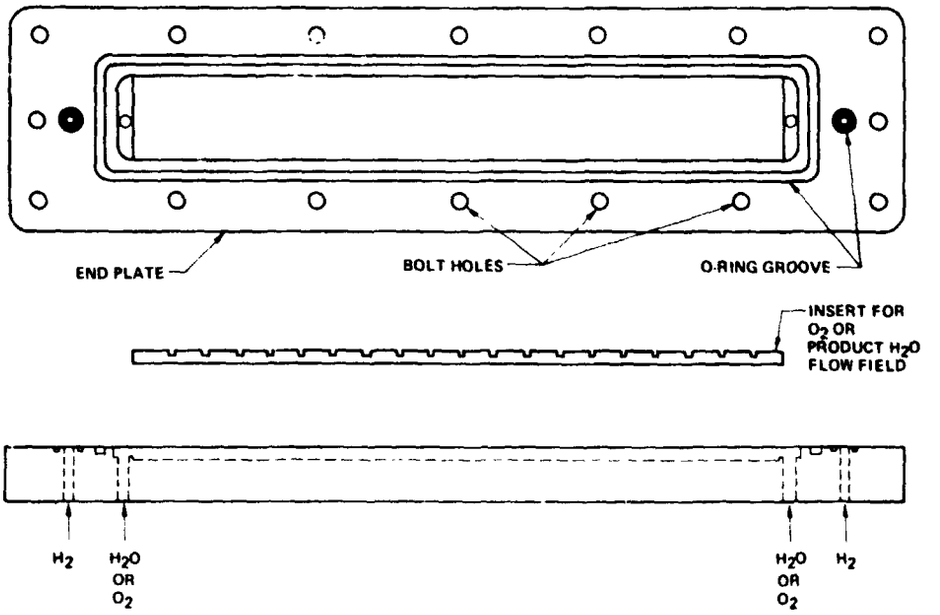

Figure 21 – Single Cell Development Test Fixture

Three thermocouples were installed in each fixture. Readings indicated uniform temperature distribution. Internal thermocouples were placed on electrodes of several cells and the temperature differed from the end plate readings by only 2 or 4°F (1.1 or 2.2°C) at the normal endurance operating conditions of 100 and 200 ASF (107.6 and 215.2 ma/cm^2).

Six different NASA-approved cell designs underwent development and testing during Phase III. The features of each of these designs are presented in Table VIII.

TABLE VIII

CELLS TESTED DURING PHASE III

Cell Number	NASA Design Number	UEA Description	PWR Description	Oxygen Field	Hydrogen Field
25	6	Epon Matrix Unit Construction PPF Electrodes Polysulfone ERP 0.031" (0.79 mm) (Bonded)	Hypon-Matrix Frame, 11-mil (0.28-mm) Sintered Ni, 10-mil (0.25-mm) RAM Goretex Membrane	Machined Insert 0.015" (0.38 mm)	Polypropylene Screen 0.023" (0.58 mm)
30	7	Polysulfone Frame PPF Anode Au-Pt Cathode Ni ERP - 22 mils (0.56 mm)	Same as 25	Same as 25	Polypropylene Screen 0.018" (0.46 mm)
31	8	Hybrid Polysulfone/ Epoxy-Glass Fiber Prepreg Frame Construction 635°F (335°C) Sintered PPF Anode Au-Pt Cathode 22 mil Ni ERP	Hybrid Polysulfone/ Epoxy-Glass Fiber Prepreg Construction, 11-mil (0.28-mm) Sintered Ni, 10-mil (0.25-mm) RAM Goretex Membrane (Hypon Frame PWR at 1504 hrs)	Same as 25	Same as 30
32	8	Same as 31	Same as 31	Same as 25	Same as 25
33	6	Hypon Matrix Unit Construction PPF Anode Au-Pt Cathode Polysulfone ERP	Hypon-Matrix Frame, 11-mil (0.28-mm) Sintered Ni, 10-mil (0.25-mm) RAM Goretex Membrane	Same as 25	Polypropylene Screen 0.029" (0.73 mm)
34	6	Same as 33	Same as 33	Same as 25	Same as 33

TABLE VIII (Cont'd)

Cell Number	NASA Design Number	UEA Description	PWR Description	Oxygen Field	Hydrogen Field
35	9	Hybrid Polysulfone/ Epoxy-Glass Fiber Prepreg Frame Construction Supported Catalyst Anode Au-Pt Cathode Ni ERP - 22 mils (0.56 mm)	Hypon-Matrix Frame, 11 mil (0.28-mm) Sintered Ni, 10-mil (0.25-mm) RAM Goretex Membrane	Same as 25	Polypropylene Screen 0.033" (0.84 mm)
36	9	Same as 35	Epoxy-Glass Fiber Frame, 11 mil (0.28-mm) Sintered Ni, 10-mil (0.25-mm) RAM Goretex Membrane	Same as 25	Same as 35
37		Hybrid Polysulfone/ Epoxy-Glass Fiber Prepreg Frame Construction PPF Anode Au-Pt Cathode Polysulfone ERP 32 mils (0.81 mm)	Epoxy-Glass Fiber Frame, 22-mil (0.56-mm) Porous Polysulfone, 10-mil (0.25-mm) RAM Goretex Membrane	Same as 25	Same as 35
38	10	Hybrid Polysulfone/ Epoxy-Glass Fiber Prepreg Frame Construction Supported Catalyst Anode 90 Au-Pt Cathode 30 mil (0.76 mm) Polysulfone ERP	Epoxy-Glass Fiber Frame, 22-mil (0.56-mm) Porous Polysulfone, 20-mil (0.51-mm) RAM Goretex Membrane	Same as 25	Same as 35
39	10	Same as 38	Same as 38	Same as 25	Same as 35
39A	10	Same as 38	Same as 38	Same as 25	Same as 35
40	11	Hybrid Polysulfone/ Epoxy-Glass Fiber Prepreg Supported Catalyst Anode 80 Au-20Pt Cathode 30 mil (0.76 mm) Polysulfone ERP	Same as 38	Same as 25	Same as 35
41	11	Same as 40	Same as 38	Same as 25	Same as 35

C Single Cell Testing

The overall goals of the single cell test program were to:

- Perform short term performance tests, with suitable diagnostics, to determine the following performance characteristics:
    - Voltage vs. current density (performance calibration)
    - Response to different operating conditions (off-design tolerance)
    - Electrolyte retention
    - Define endurance limiting phenomena and develop methods for extending cell life.

This section describes the significant test results of the single cell program during Phase III. In summary, since the program's inception, 73,424 hours of fuel cell load time were accumulated on 35 different cells. Predicted performance, off-design tolerance and electrolyte retention were demonstrated. Various cell performance deficiencies were identified by cell diagnostics and corrected. Cell endurance capability has improved markedly as a result of the research program. At the conclusion of Phase III, one single cell operated at 100 ASF had completed 10,020 hours of testing and another operated at 200 ASF had completed 6,680 hours.

The following sections discuss the performance and endurance results of Phase III. The test facilities and procedures are first described, followed by individual cell tests discussed in detail.

D. Test Facilities and Test Procedures

The test facilities used for full size, single cell testing are shown in Figures 22 and 23. These stands were originally used for work performed under contract NAS3-13229 and were adapted for passive water removal cell testing during the present contract. A schematic of the test stands is shown in Figure 24.

Reactants of fuel cell grade or better are supplied to the test stands. To eliminate test variables associated with reactant impurities, the hydrogen is further purified in a palladium-silver separator bank which reduces any contamination below detectable limits. Oxygen is purified using a Mine Safety Appliance catalytic oxidizer. Any hydrocarbons in the oxygen stream are oxidized to carbon dioxide and are removed by sodium-hydroxide scrubber columns. This system is shown in Figure 25. The carbon dioxide level downstream of the scrubber is continuously monitored by a LIRA gas analyzer. These readings indicate that the oxidizer is removing 8 to 12 ppm (equivalent) methane from the oxygen stream and that the carbon dioxide level entering the fuel cells is less than 0.5 ppm.

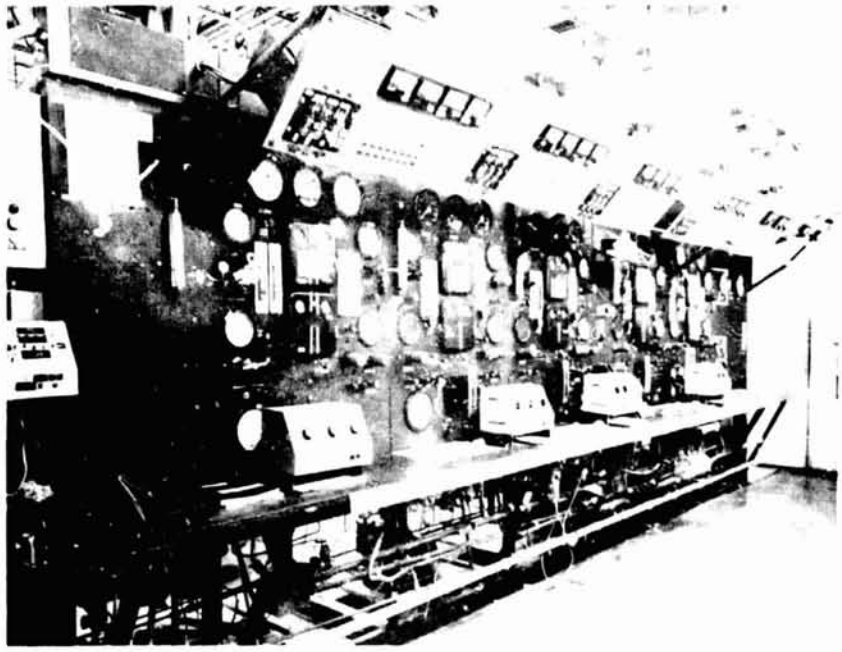

Figure 22 – Single Cell Test Facility (Front)

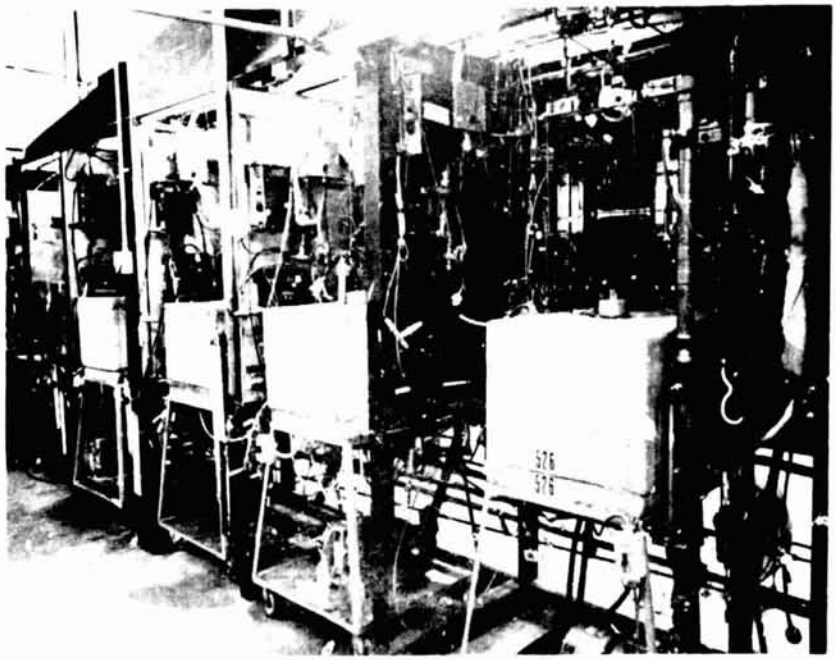

Figure 23 – Single Cell Test Facility (Rear)

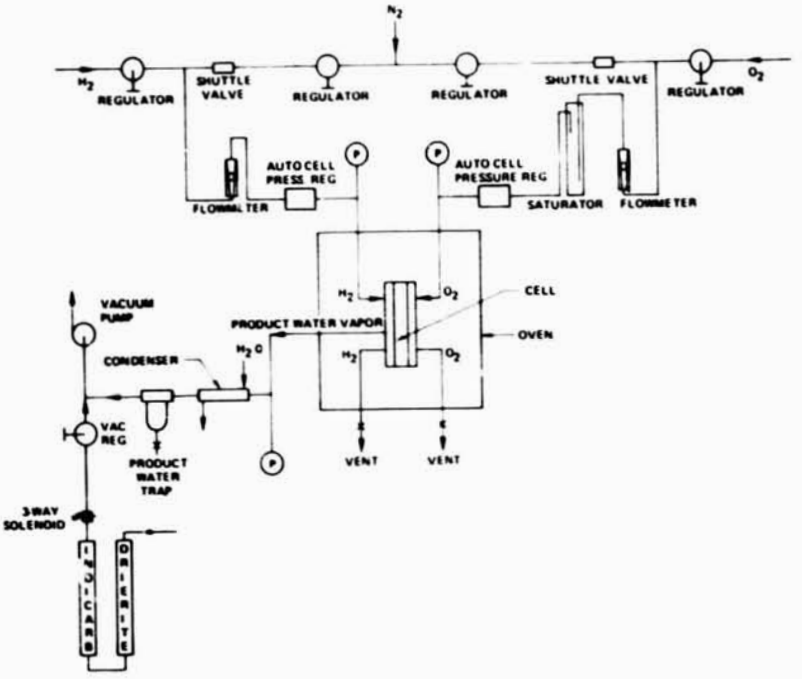

Figure 24 — Single Cell Test Stand Schematic

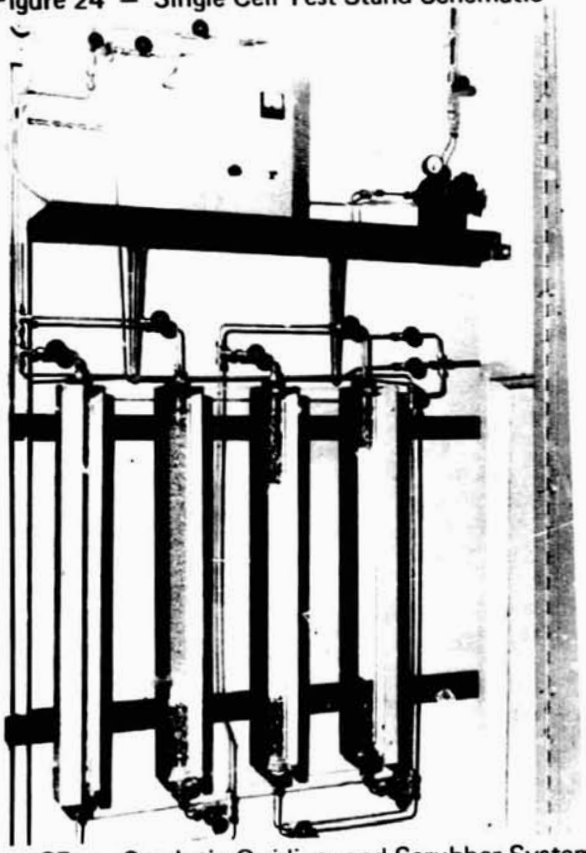

Figure 25 — Catalytic Oxidizer and Scrubber System

ORIGINAL PAGE IS
OF POOR QUALITY

Temperature control of the cells is provided by an insulated oven which is maintained within ±2°F (1.1°C) by a thermoelectric solid-state temperature controller. The relatively massive single cell end plates, in combination with the isothermal oven, maintain a uniform cell temperature. Since metallic inserts are used to form the cell's oxygen flow field, and plastic inserts for the product water field, cell waste heat is rejected primarily on the cathode side. Thus, the test rig approach realistically simulates system conditions. Cell temperature instrumentation showed that the simple oven temperature control method is effective in maintaining cell temperatures uniform within ±1.5°F (0.83°C) over a range of current densities to 300 ASF (322.8 ma/cm^2).

The product water removal system also duplicates the system design. A conventional Duo-Seal® vacuum pump is used to provide sub-atmospheric pressure sink for product water vapor. The pH of the product water is regularly monitored: Trap water samples are checked 3 times a day, using a Beckman Zeromatic® pH meter.

Single cell performance data is measured and recorded by P&WA's Automatic Data Acquisition and Recording (ADAR) System. The following parameters are recorded once every hour:

Parameter	Accuracy
Cell Voltage, volts	± 0.002 v
Cell current, amps	± 0.02 a
Oven Temperature	± 3°F (1.7°C)
Oxygen End Plate Temperature	± 3°F (1.7°C)
Water End Plate Temperature	± 3°F (1.7°C)

The ADAR system was designed to minimize experimental error and to reduce the amount of manual data handling. In addition to providing periodic scanning of the above parameters and transcribing them to engineering units, the ADAR system keeps an accurate log of total load hours. A typical ADAR printout for the NASA-LeRC Advanced Development Fuel Cells is shown in Figure 26.

```
STAND: X-528        LERC CELL-30

RIG: 37970-30   DATE:  6/21/73   TIME:  1 2   LHRS:     16

 LOAD      TOTAL
11.201      .933

TEMPERATURES
  02 SAT EXIT **  124.

  PLUS END PLATE: 1=  174.  2=  175.  3=  175.
  NEG. END PLATE: 1=  176.  2=  176.  3=  176.  4=  174.
  OVEN WALL:      1=  174.
```

Figure 26 — Typical ADAR Printout

The heart of the ADAR system is a Hewlett-Packard Model 2114A digital computer. Other major components in the system are also from Hewlett-Packard; a Model 2911 Guarded Cross-bar Scanner and Model 2402 Digital Voltmeter to scan and measure the test signals and a Model 2752 Teleprinter to print out the data.

All of the above data can also be read out directly at each station on conventional stand instrumentation. Pressure and flows are controlled and monitored by appropriate regulator, gages, flowmeters, and valves, as shown in Figure 22.

The ADAR system has been used only for automatic data acquisition. Automatic control is provided by appropriate test stand instrumentation, with provisions for automatic shutdown of any cell when certain pre-established conditions are encountered. For the NASA-LeRC single cells, these protective controls are:

Parameter	Limit
Voltage	Low (adjustable)
Current	High or Low (adjustable)
Temperature	High or Low (adjustable)
Vacuum Pressure	High or Low

These automated control and protective features have resulted in very reliable single cell operation. Over 73,400 hours of fuel cell load were attained on 35 different fuel cells with only one stand-related failure. This occurred during a Phase I test of Cell No. 10, which was flooded because of an oxygen saturator overtemperature. Some automatic shutdowns occurred because cell conditions exceeded the protective limits described above. In all of these cases, the cells were not damaged and normal testing could continue.

Single cell testing was primarily devoted to endurance testing. However, various diagnostic procedures were performed on all of the cells to document any decay mechanisms and to determine design and off-design performance characteristics of the various cell configurations.

Typical test conditions for the programs were:

Cell Current Density	100 or 200 ASF (107.6 or 215.2 ma/cm^2)
Cell Temperature	180°F (82.2°C)
Product Water Vacuum	22 inch Hg (7.4 n/cm^2)
Hydrogen Pressure	16 psia (11 n/cm^2)
Hydrogen Flow	Consumption, plus 2 minute purge every 8 hours
Hydrogen Inlet Dewpoint	Dry
Oxygen Pressure	16 psia (11 n/cm^2)
Oxygen Flow	2 x consumption
Oxygen Inlet Dewpoint	130°F (54.4°C)
Average Electrolyte Concentration	34 percent KOH

Diagnostic techniques which were regularly employed included the following:

Performance Calibrations: Voltage-current characteristics were generated to 500 ASF (538 ma/cm^2), which is somewhat above the EMS peak power operating conditions. Taken periodically, the performance calibration changes with time are valuable tools in determining the type and extent of any decay mechanisms. This is especially true of the semi-log representation of the performance data on an IR free basis which are commonly described as Tafel plots.

Tafel Plots: The Tafel region refers to the low current density portion of a performance calibration. In this region, anode and ohmic polarizations are minimal or correctable so the cell voltage is essentially cathode activation limited performance. The Tafel region extends from approximately 1 ASF (1.076 ma/cm^2) to a level where diffusion losses become significant, 10 to 100 ASF (10.8 to 107.6 ma/cm^2), which is a function of operating temperature and pressure. In the Tafel region, the semi-log voltage-current curve should be a straight line, with a slope characteristic of the catalyst/reactant combination and a level proportional to the cathode activation.

Departures from this slope are an indication of parasitic loads, either internal cell shorting or gas crossover. Thus, the Tafel slope is a useful diagnostic tool in assessing the life expectancy of an operating cell. Changes in the levels of Tafel data are also a useful tool, since they indicate changes in the activity of the catalyst, either through changes in the number of active catalytic sites or structural modifications (e.g., recrystallization), changing the effect catalyst active area.

The so-called Tafel plot is also a useful diagnostic tool at current densities above the Tafel region. At these current densities, typical of operating cells, internal resistance (IR) corrections are required. When the cell performance is thus corrected, changes in the shape of the curves can be interpreted as changes in the diffusion characteristics of the electrodes. In this region, transport limitations are encountered if the electrode structure is not adequate for delivery of reactants or removal of product water. For example, diffusion problems can be related to microscopic flooding of the Teflon pores in a wet proofed electrode, or to increased concentration gradients in a heavily carbonated cell. While the semi-log performance plots alone do not distinguish such possible causes or even anode from cathode losses, they are valuable tools, in conjunction with previous experience and post-test analysis, in evaluating any performance decay trends.

Internal Resistance (IR): Internal resistance or ohmic polarization losses are unavoidable in any cell. However, they can be minimized by matrices with high porosity and correct assembly to insure proper cell compression. In the strip cell with edge current collection, there are also resistance losses in the electrode substrates and edge frames which are measured together with the conventional ohmic loss. IR measurements are taken periodically to insure that the initial assembly is correct and that the correct cell compression is being maintained.

IR measurements are taken by the current interruption technique. Typically, a 100 ASF (107.6 ma/cm^2) load is interrupted and the resulting step change in voltage is measured on a Tektronic Type 545 oscilloscope. Since other polarizations have a long response time, the step change is a direct measure of internal cell resistance.

Dilute Oxygen Diagnostic Test: Although the Tafel and IR tests give good indication of relative cathode-matrix-anode losses at low current densities, they cannot be used to distinguish cathode and anode losses in the diffusion regime, the area of operational interest. This technique permits identification of anode and cathode losses in the diffusion regime by running performance sweeps on 20% oxygen/80% nitrogen and pure oxygen. It is based on the fact that cathode performance is proportional to the partial pressure of oxygen. A graphical procedure based on this relationship, illustrated in Figure 27, allows determination of individual electrode performance.

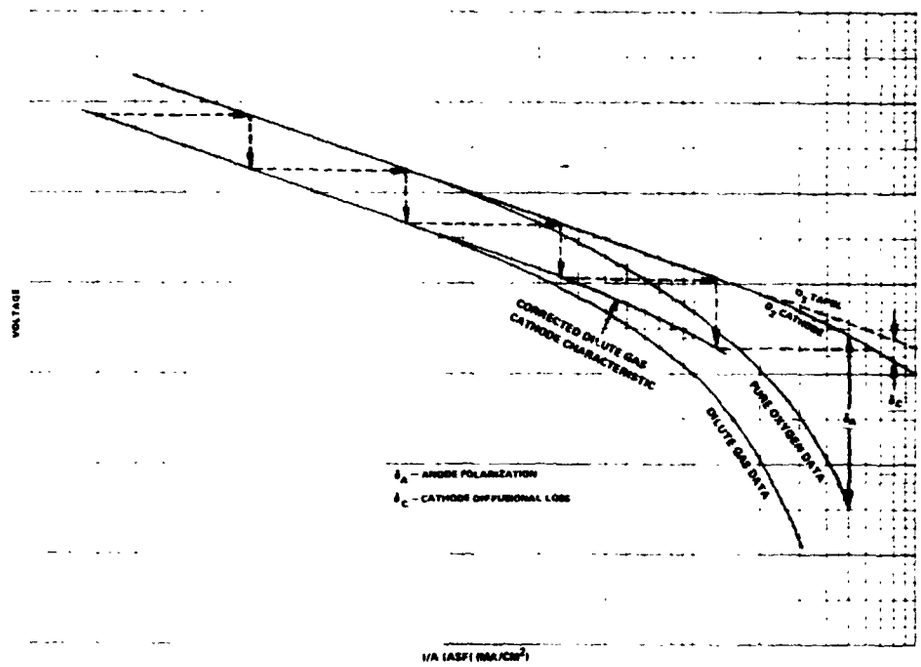

Figure 27 – Dilute Gas Diagnostic Method

A point in the activation region is selected on the dilute gas (20% O_2) data curve and the current is multiplied by 5, the ratio of oxygen partial pressures. The corrected point is plotted and compared to the O_2 data curve; if the point falls on the O_2 curve, no anode polarization has occurred. When a deviation occurs between the corrected point and the actual O_2 curve, the deviation is attributed to anode polarization. A correction is then made up to the 20 percent O_2 curve corresponding to this amount of anode polarization and the procedure is repeated.

When the true O_2 polarization curve is obtained, the difference between this curve and the generated O_2 data is anode loss. The deviation of the corrected cathode performance curve from the O_2 Tafel line is normally attributed to diffusional loss.

This approach does not separate anode losses into such categories as poisoning, flooding, concentration polarization and undescribed resistance but it does clearly show which electrode has the major effect on cell performance.

Off-Design Tolerance: If a cell is improperly filled, or if the contact between the ERP and cell is inadequate, the off-design tolerance characteristics of the cell will depart from the theoretical value. Off-design tolerance data can be generated in various ways. In the passive water removal cells, the most convenient and most severe method is to vary product water vacuum. Since the vacuum is changed almost instantaneously, the cell is subjected to a very rapid transient, taxing the transport properties of the ERP much more severely than off-design tolerance conditions imposed by slowly changing dewpoints on saturated gases.

Post-Test Analysis: All cells are subjected to post-test analysis. This includes visual (and microscopic) examination of components for observable changes in physical properties, structural defects or peculiar deposits. Because of the importance of low corrosion rates, all of the single cells in this program were carefully analyzed for carbonate conversion. Selected cells were also sectioned for laboratory tests, including floating half-cell tests of individual electrodes and measurement of catalyst activity and platinum migration.

E. Summary of Single Cells Tested

Two types of testing can be performed in the Single Cell Program. Research and Technology (R&T) tests are one type, comprising the first level of testing. These tests are performed on any items which are beyond the present state-of-the-art. This is a relatively informal level of testing in order to maximize the flow of technical information. Reviews of the progress of this testing are held regularly with the NASA Project Manager. When any item, in his judgment, is sufficiently demonstrated, the next level of testing is begun.

Verification and Endurance (V&E) tests are the second type, comprising the second and third levels of testing. All but one of the cell tests in Phase III were of this type. The Verification test is a short duration test, consisting of two weekly test cycles, interrupted by a shutdown. The objective of a Verification test is to demonstrate the ability of the article under test to perform at the conditions in question. The Endurance test is of longer duration; the weekly duty cycle is used for some tests, continuous operation for others. Both Verification and Endurance tests are of more formal nature. They require written notification to the NASA Project Manager with pertinent description of the test article. Three designs were submitted for NASA approval and were tested in Phase I of the program. In carrying out this type of test, the NASA Project manager reviews the results of the Verification test and decides which items shall undergo Endurance testing.

A statistical summary of the single cell testing during Phases I, II, and III of the program is presented in Table IX.

TABLE IX

FULL SIZE SINGLE CELL OPERATION

Number of cells tested	36
Number of configurations tested	11
Total cell test time	73,424 hours
Longest cell run (100 ASF) (107.6 ma/cm^2)	10,020 hours
Longest cell run (200 ASF) (215.2 ma/cm^2)	6,680 hours
Reasons for Shutdown:	
Stand Failure	1*
Cell Failure	3
Investigation of Decay	28
Continuing on Test	4

*During Phase I

A summary breakdown of the cells tested in Phase II into design configuration and types of tests is presented in Table X.

F. Single Cell Test Results

This section reviews the results of the cell tested during Phase III. Results of each cell test are summarized in Table XI.

Cell No. 25

Cell No. 25 was constructed using an Epon 828 impregnated UEA frame and included a PPF anode and cathode. It also featured in the UEA the first nickel-plated, porous polysulfone ERP. The configuration was approved by NASA to be Verification Design No. 6. The primary objective was to evaluate the new lightweight ERP.

Cell No. 25 accumulated 7563 hours at 100 ASF (107.6 ma/cm^2). Endurance characteristics of the cell are presented in Figure 28. After initial refurbishment at 426 hours, the cell showed a loss in wet side tolerance; see Figure 29. With continued operation, cell tolerance stabilized

and returned to normal. The poor wet side tolerance was probably because of incomplete draining of the cell electrolyte after refurbishment. Periodic tolerarce excursions performed on the cell indicated normal operation of the polysulfone ERP.

TABLE X

FULL SIZE SINGLE CELL TEST CATEGORIES

NASA Design No.	Description of Unitization	Research and Technology Test Cell Nos.	Verification and Endurance Test, Cell Nos.
6	Hypon Impreg. Matrix		25, 27, 33*, 34*
7	Laminated Polysulfone		28, 30
8	Hybrid Polysulfone/ Epoxy-Glass Fiber		31, 32
9	Hybrid Polysulfone/ Epoxy-Glass Fiber		35, 36
—	Hybrid Polysulfone/ Epoxy-Glass Fiber	37	—
10	Hybrid Polysulfone/ Epoxy-Glass Fiber		38, 39, 39A
11	Hybrid Polysulfone/ Epoxy-Glass Fiber		40, 41

*Cell Nos. 33 and 34 delivered to NASA.

TABLE XI

FULL SIZE SINGLE CELL TEST SUMMARY

Cell No.	Load Time – (Hrs.)	Performance – Volts			Initial IR (mv) @ 100 ASF (107.6 ma/cm^2)	Percent Conversion to K_2CO_3	Comments
		Initial	Peak	Final			
25	7,560	0.913	0.913	<0.700	9		Refurbished @ 5400 Hrs. and 7411 Hrs.
30	10,020	0.932	0.938	0.743	8	4.1 at 311 hrs. 42.5 at 10,020 hrs.	Refurbished at 311 Hrs.
31	3,000	0.936	0.936	0.865	10	5.6 at 320 hrs. 12.0 at 1,520 hrs. 13.3 at 3,000 hrs.	Short Removed at 1520 Hrs. Cell Refurbished
32	395	0.928	0.928	0.837	14	3.8 at 262 hrs.	Cathode Reversed
33	—	—	—	—	–	— —	Delivered to NASA
34	—	—	—	—	–	— —	Delivered to NASA
35	6,405	0.912	0.916	—	8	3.9 at 320 hrs. 42 at 6,500 hrs.	Test Continuing
36	2,290	0.918	0.918	0.847	6	5.0 at 295 hrs. 12.7 at 1,132 hrs. 9.1 at 1,843 hrs. 6.1 at 2,296 hrs.	200 ASF (215.2 ma/cm^2), 212°F (100°C), 28 PSIA (19.3 n/cm^2)
37	1,205	0.940	0.940	0.915	6	4.7 at 320 hrs. 4.4 at 1,205 hrs.	

TABLE XI (Cont'd)

FULL SIZE SINGLE CELL TEST SUMMARY

Cell No.	Load Time – (Hrs.)	Performance – Volts Initial	Peak	Final	Initial IR (mv) @ 100 ASF (107.6 ma/cm^2)	Percent Conversion to K_2CO_3	Comments
38	2,544	0.915	0.915	0.858	9	2.8 at 336 hrs. 7.3 at 2,543 hrs.	
39	345	0.912	0.912	0.905	9		200 ASF (215.2 ma/cm^2) set at 374 Hours Load Time. Performance quoted at 200 ASF (215.2 ma/cm^2)
39A	1,557	0.846	0.846		10	3.6 at 304 hrs.	Quoted at 200 ASF (215.2 ma/cm^2) Test Continuing
40	1,412	0.869	0.880		8	2.1 at 345 hrs.	Test Continuing
41	1,251	0.876	0.880		13	2.5 at 325 hrs.	Test Continuing

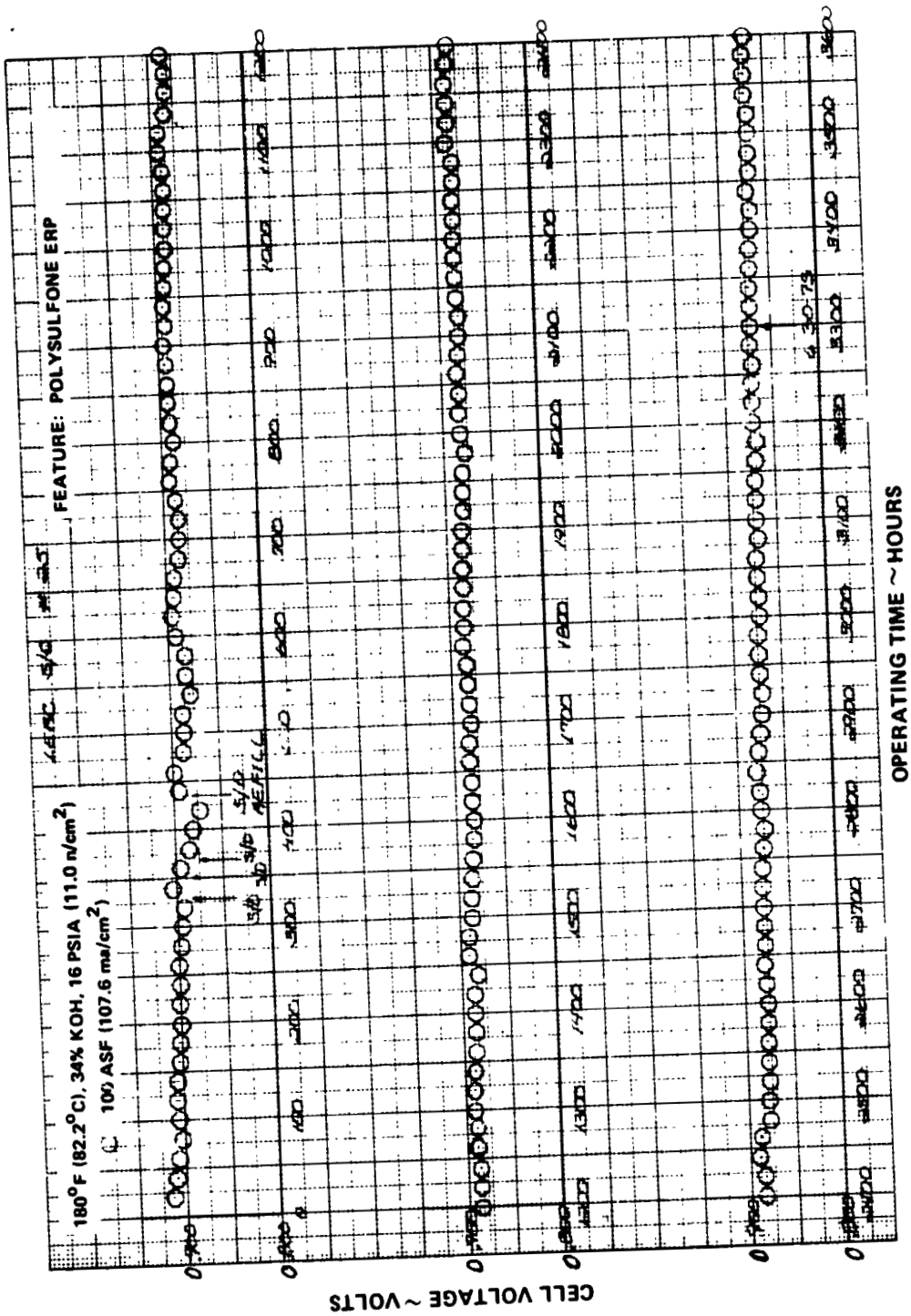

Figure 28 – Performance History of Cell No. 25

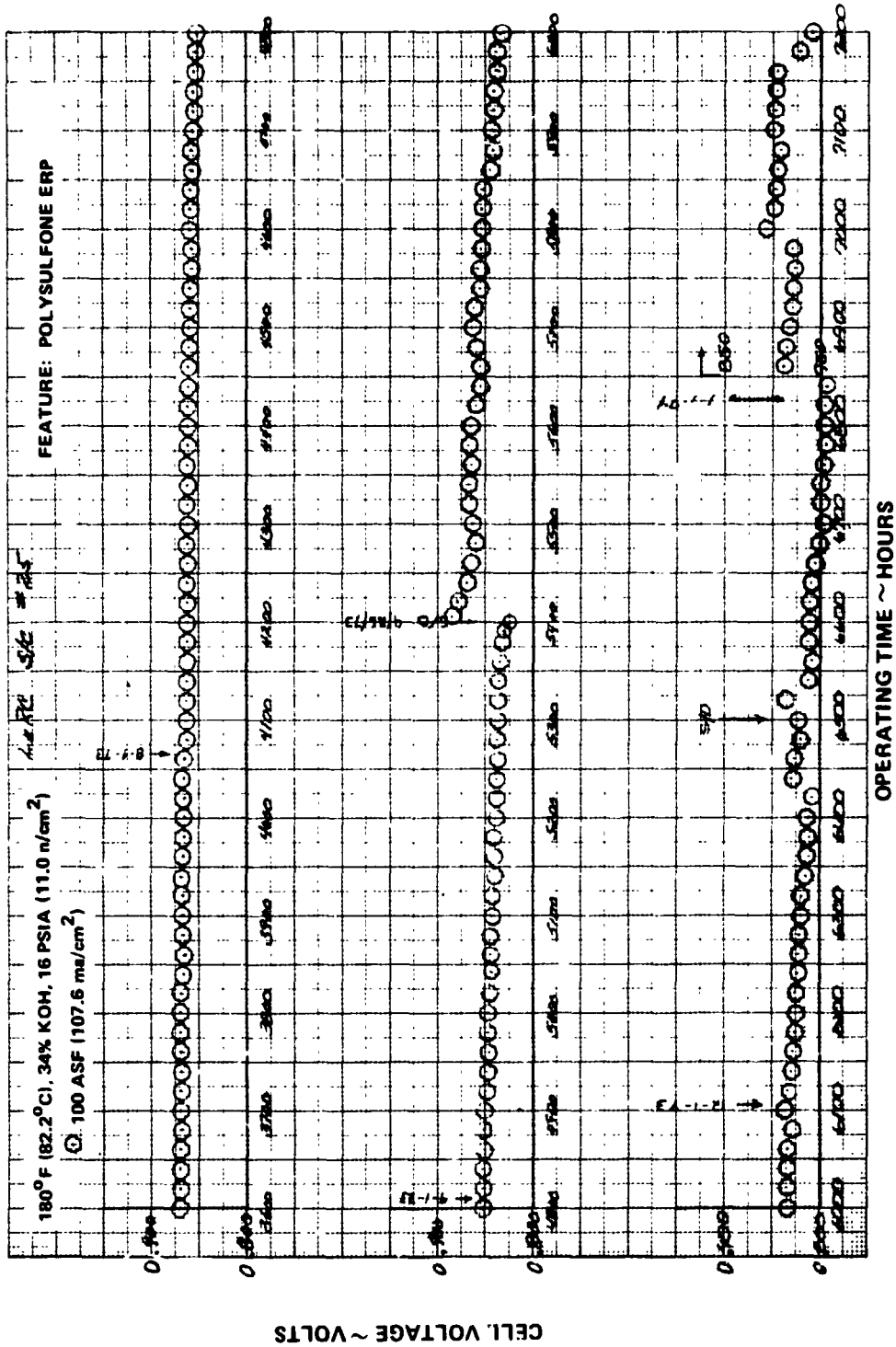

Figure 28 (Cont'd) — Performance History of Cell No. 25

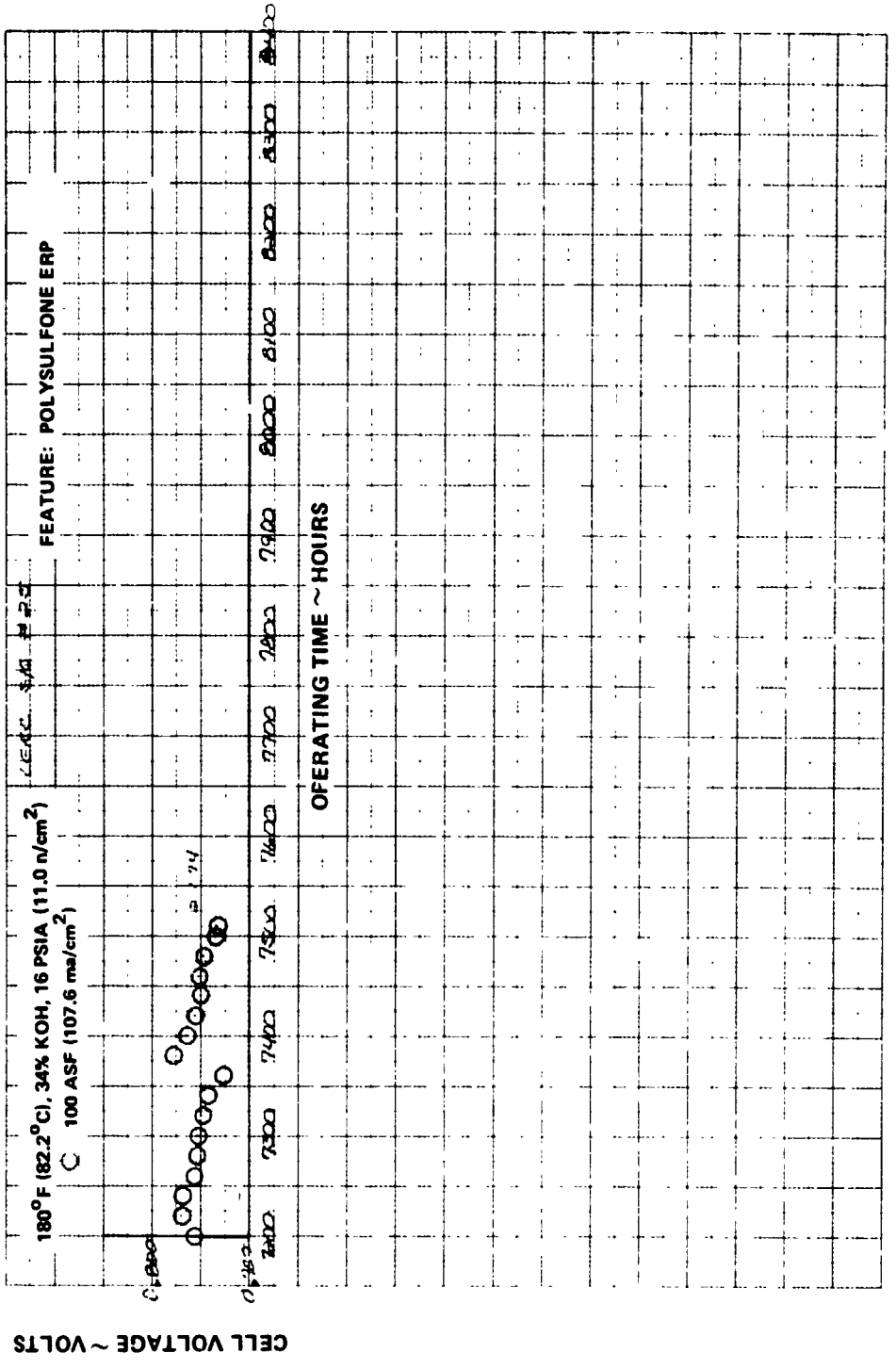

Figure 28 (Cont'd) — Performance History of Cell No. 25

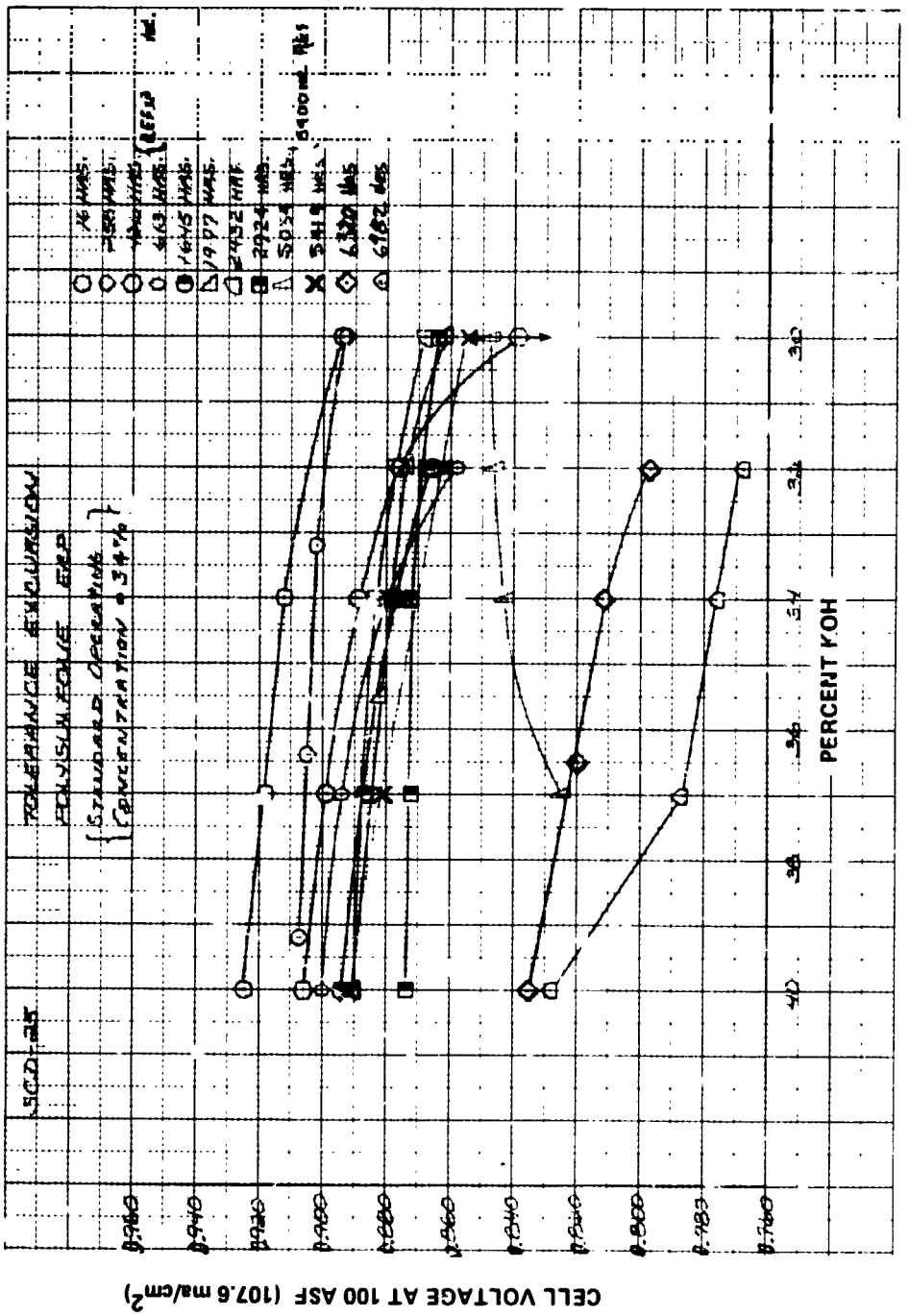

Figure 23 — Tolerance Excursion Data From Cell No. 25

A tolerance excursion performed at 5034 hours showed lack of dry side stability, an apparent indication of high K_2CO_3 levels in the electrolyte. The cell was therefore shut down for electrolyte refurbishment at 5400 hours load time and a KOH conversion level of 56 percent was determined. This carbonate level was consistent with the results of previous Hypon frame cells; see Figure 30. It was concluded that the elimination of the Hycar elasticizer from the frame material of Cell No. 25 had little effect on the electrolyte carbonation rate of single cells at these operating conditions.

Refurbishment of the cell at 5400 hours resulted in recovery of a substantial amount of lost cell performance (see Figure 28). The recovered performance, from 0.829 volts to 0.878 volts at 100 ASF (107.6 ma/cm^2), was essentially equal to the pre-refurbishment loss due to carbonate formation (48 mv). In addition, the dewpoint tolerance response was improved after refurbishment, also attributable to the removal of carbonates. The slope of the tolerance curve, Figure 29, indicates that the physical characteristics of the polysulfone ERP were not changed substantially from the start of testing. Although the cell tolerances were improved after refurbishment, the cell demonstrated a sensitivity to changes in electrolyte concentration. At 5514 hours, the cell electrolyte concentration was raised from 34 to 36.5 percent to avoid operation in the poor wet side portion of the tolerance curve. The rate of decay after refurbishment was considerably increased when compared to the overall decay rate before refurbishment. Diagnostics performed at intervals indicated that cell decay was almost solely because of increasing anode diffusion losses. The increase in anode diffusion is shown in Table XII.

Cell pressure was raised to 19.5 psia (13.5 n/cm^2) at 6430 hours, in an effort to reduce cell diffusion losses, and continued at this level for the remainder of the test. The increase in performance because of cell pressure increase is shown in Figure 31. The increase was considerably more than that expected due to activation level change only, the remaining increase being attributed to decreased cell diffusion losses. Dilute oxygen diagnostics indicated a steadily increasing level of anode diffusion after the refurbishment. Cell dewpoint tolerance excursion performed at 6982 hours showed an abnormally high performance gain on the high KOH concentration side. As shown in Figure 29, the tolerance curve slope was normal up to the 37 percent KOH level, but was abnormally high between 37 and 40 percent KOH. It was believed that this phenomenon was the result of serious anode flooding. The dewpoint excursion was normal to the point where electrolyte from the ERP was virtually depleted and further movement toward the dry side resulted in movement of the interface within the electrode. The net effect of this interface movement was a dramatic increase in performance. The return to the endurance test concentration of 36.5 percent KOH resulted in a slow deterioration in performance to the original pre-dryout performance level.

After cell refurbishment at 7411 load hours, no net improvement in performance resulted. Anode diffusion levels were not improved; K_2CO_2 analysis indicated 34 percent KOH conversion between 5400 hours and 7411 hours; see Figure 30.

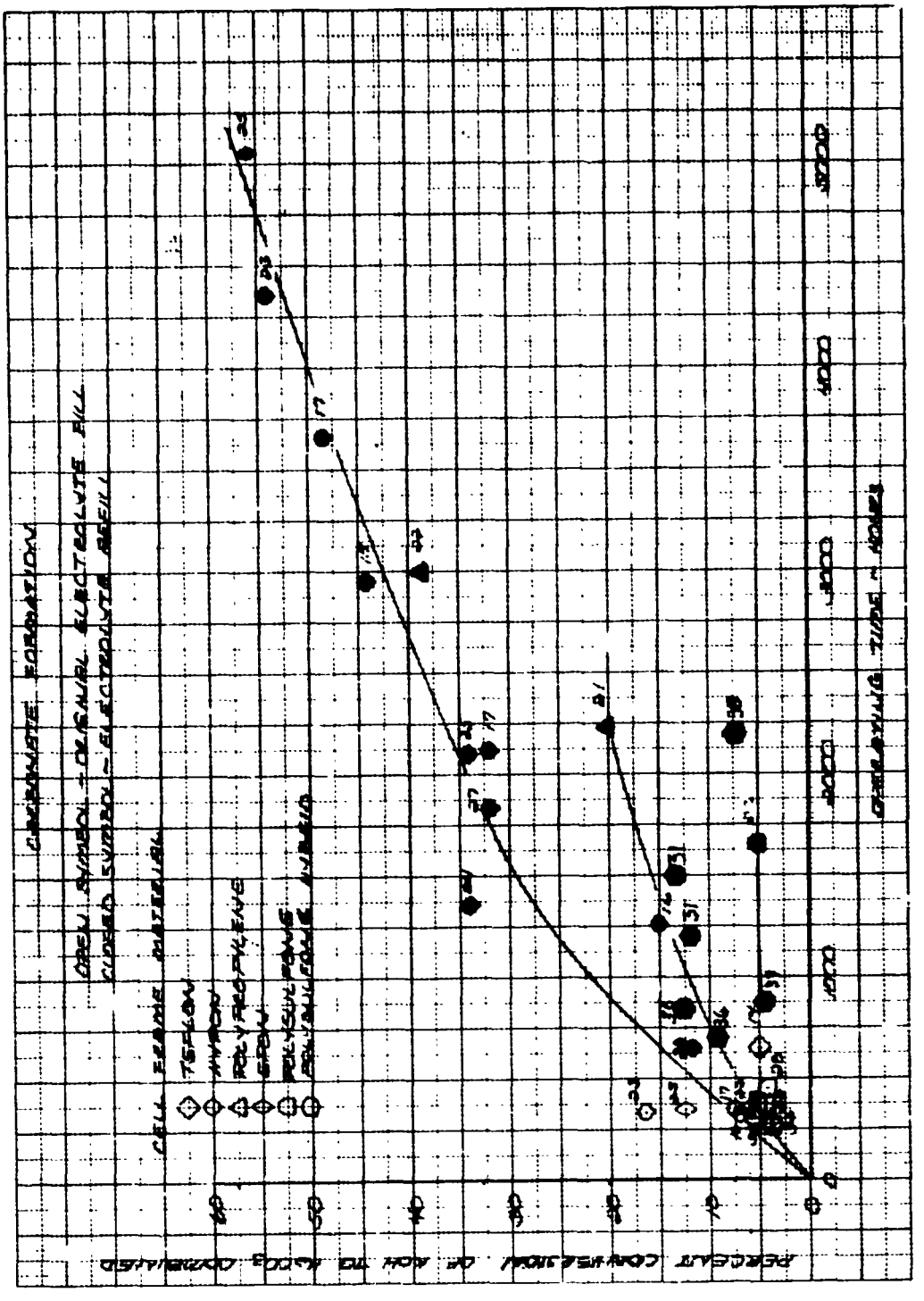

Figure 30 – Electrolyte Carbonation Data

TABLE XII

CELL No. 25 ACCOUNTABLE LOSSES

Epon Matrix – Unit Construction
PPF Electrodes – Polysulfone ERP

Rig 38498-25 0.1146 ft^2 (106.4 cm^2)
180°F (82.2°C) 34% KOH/16 PSI (11.0 n/cm^2)/PWR

	Performance					100 ASF (107.6 ma/cm^2) Diffusion Loss			
Load Time Hrs.	1.0 ASF (1.076 ma/cm^2) (Volts)	2.0 ASF (2.152 ma/cm^2) (Volts)	100 ASF (107.6 ma/cm^2) (IR Corr.)	100 ASF (107.6 ma/cm^2) (mv)	Activation Loss (mv)	Total (mv)	Anode (mv)	Cathode (mv)	(Press.) psia (n/cm^2)
23	1.038	1.022	0.925	9.0	—	12	—	—	—
328	1.024	1.008	0.902	11.0	14	12	—	—	—
523	1.014	0.997	0.892	7.0	24	11	—	—	—
1361	1.016	1.000	0.894	7.0	22	11	—	—	—
1835	1.016	1.001	0.894	7.0	22	13	—	—	—
2457	1.019	1.004	0.890	8.0	19	17	—	—	—
3281	1.010	0.992	0.882	11.5	28	24	—	—	—
5034	1.001	0.985	0.858	16.0	37	42	—	—	—
5375	0.980	0.967	0.842	15.0	57	35	23	7	—
5491	1.020	1.006	0.884	10.0	17	27	27	—	After Refurb.
6092	1.016	1.000	0.855	10.0	22	60	60	—	16 (11.0)
6527	1.016	0.993	0.813	10.0	22	94	94	—	19 (13.1)

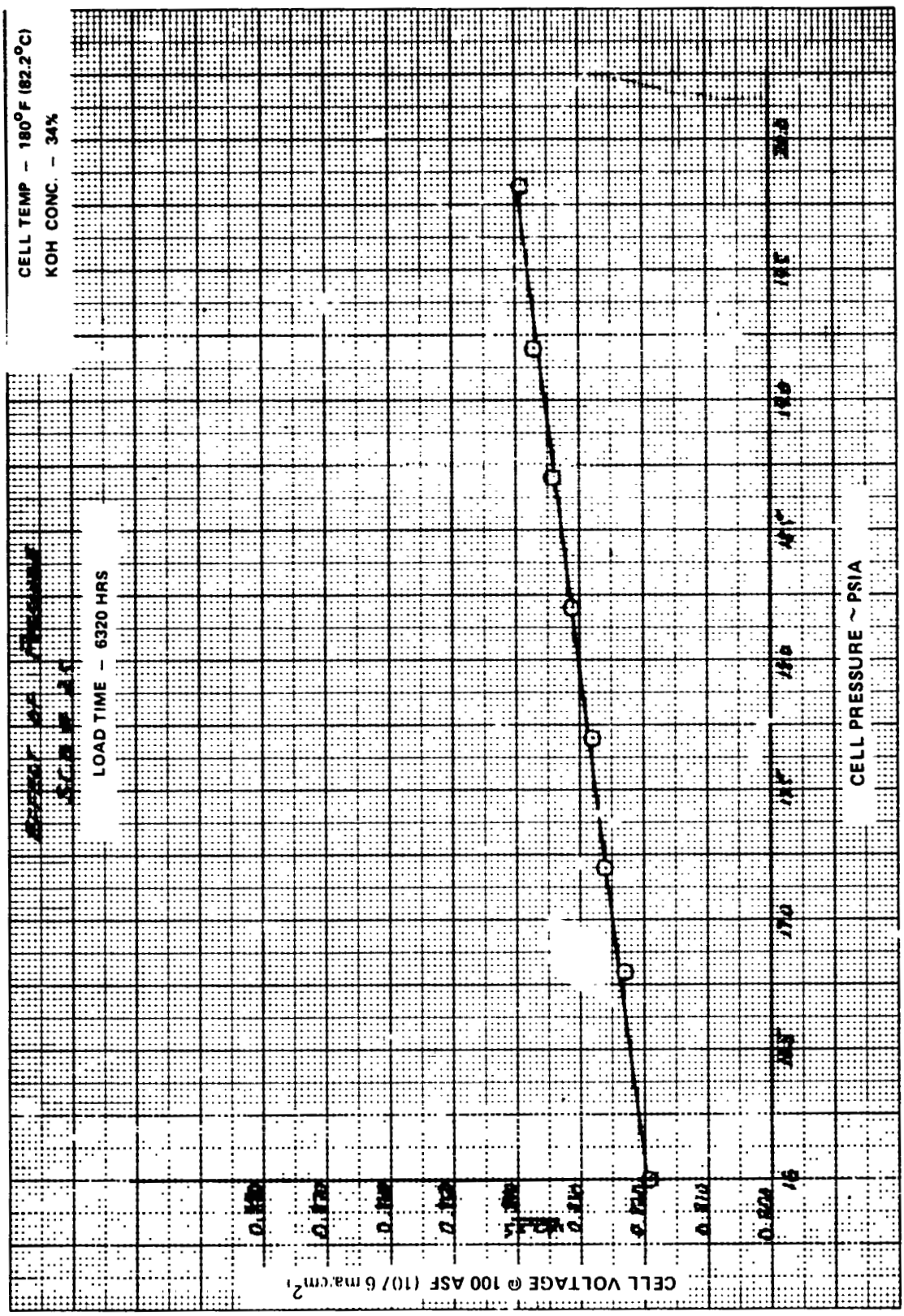

Figure 31 – Cell No. 25 Performance Improvement with Increased Pressure

The cell was shut down after 7563 hours because of performance instability. Visual observation revealed no serious deterioration of either the cell or the polysulfone ERP. Tests on the ERP indicated practically no change in effective porosity. Laboratory testing, confirmed by half-cell tests that the anode was almost completely flooded. The cathode activity was also reduced by about a factor of two. Post-test analyses of this cell are discussed in Section IIIA3.

Cell No. 30

This cell configuration was approved by the NASA Program Manager as Verification Design No. 7. Its principal feature was a laminated polysulfone frame. Attempts to fabricate a passive water removal (PWR) assembly using polysulfone film were unsuccessful. Sufficient bubble pressure could not be obtained to satisfy the 12 psi (8.27 n/cm^2) minimum differential pressure requirement. For this reason, Cell No. 30 was assembled with a Hypon PWR. The electrodes in Cell No. 30 were a PPF anode and a 90Au-10Pt cathode. The objectives of the test program were to obtain:

- Endurance experience with 90Au-10Pt cathodes
- Carbonate data for polysulfone frames.

Cell No. 30 completed 10,020 hours of endurance testing at 100 ASF (107.6 ma/cm^2), 180°F (82.2°C) and 16 psia (11.0 n/cm^2) with no refurbishment after the initial verification test period of 310 hours. The unrefurbished endurance time of the cell exceeded that of any strip cell tested to date. Figure 32 shows the performance history of this cell.

Table XIII shows voltage decay rates experienced by the cell during the testing period. After a relatively high decay rate during the initial 1000 hours, the rate stabilized at about 10 μv/hr to 4000 hours. During the next 4500 hours of testing, the average decay rate was 17 μv/hr. For the last 1500 hours, the rate increased to about 40 μv/hr. The major cause of these increasing decay rates was anode diffusion losses. Anode diffusion losses appear to be related to the rate of silicon buildup on the anode from the RAM matrix. There is evidence that buildup of this silicon layer makes the anode act as though it were flooded. Anode diffusion losses, as determined by dilute oxygen diagnostic testing at periodic intervals during the endurance testing, are shown in Table XIV. A breakdown of voltage losses, including that due to carbonates, appears in Table XV.

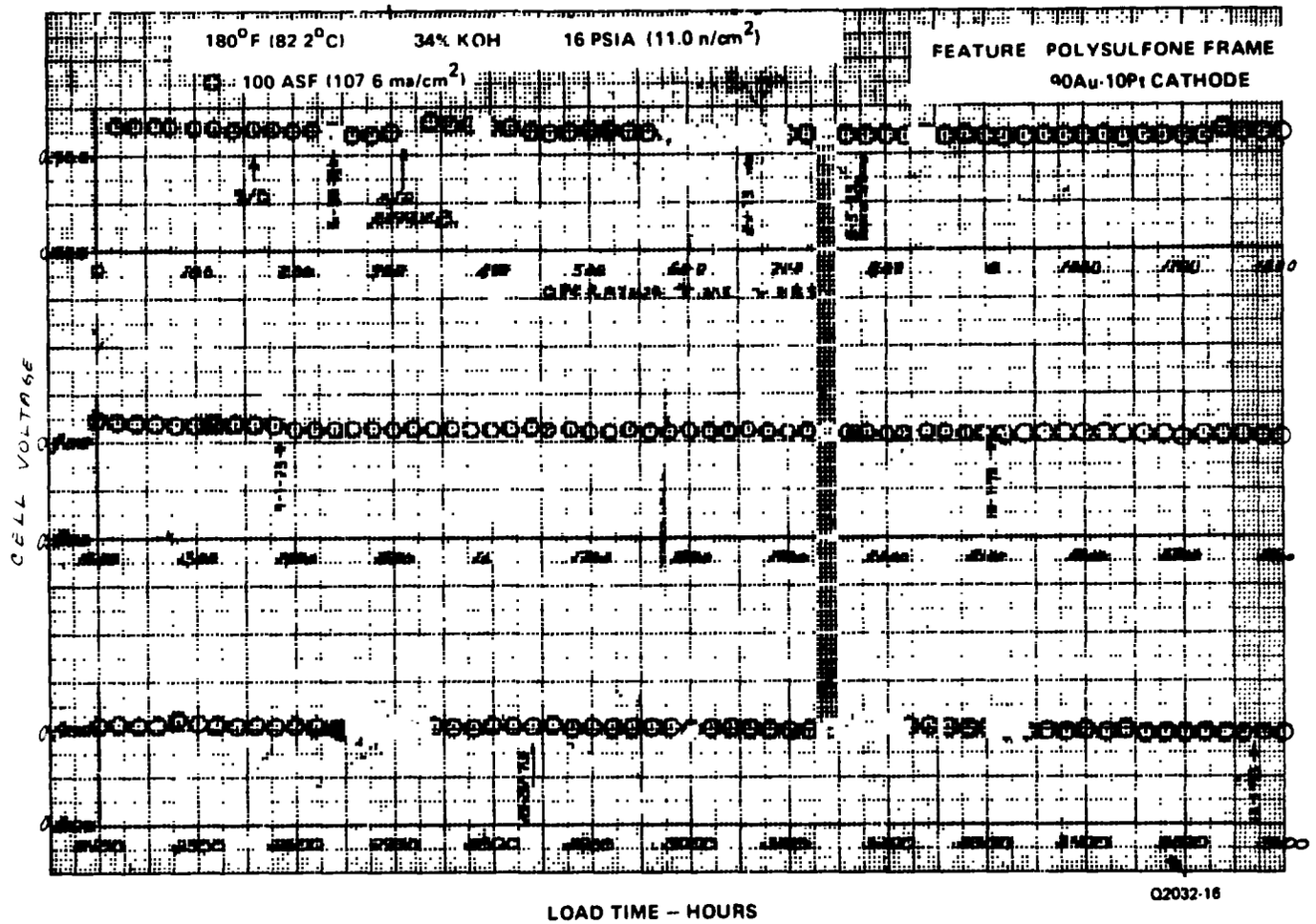

Figure 32 – Performance History of Cell No. 30

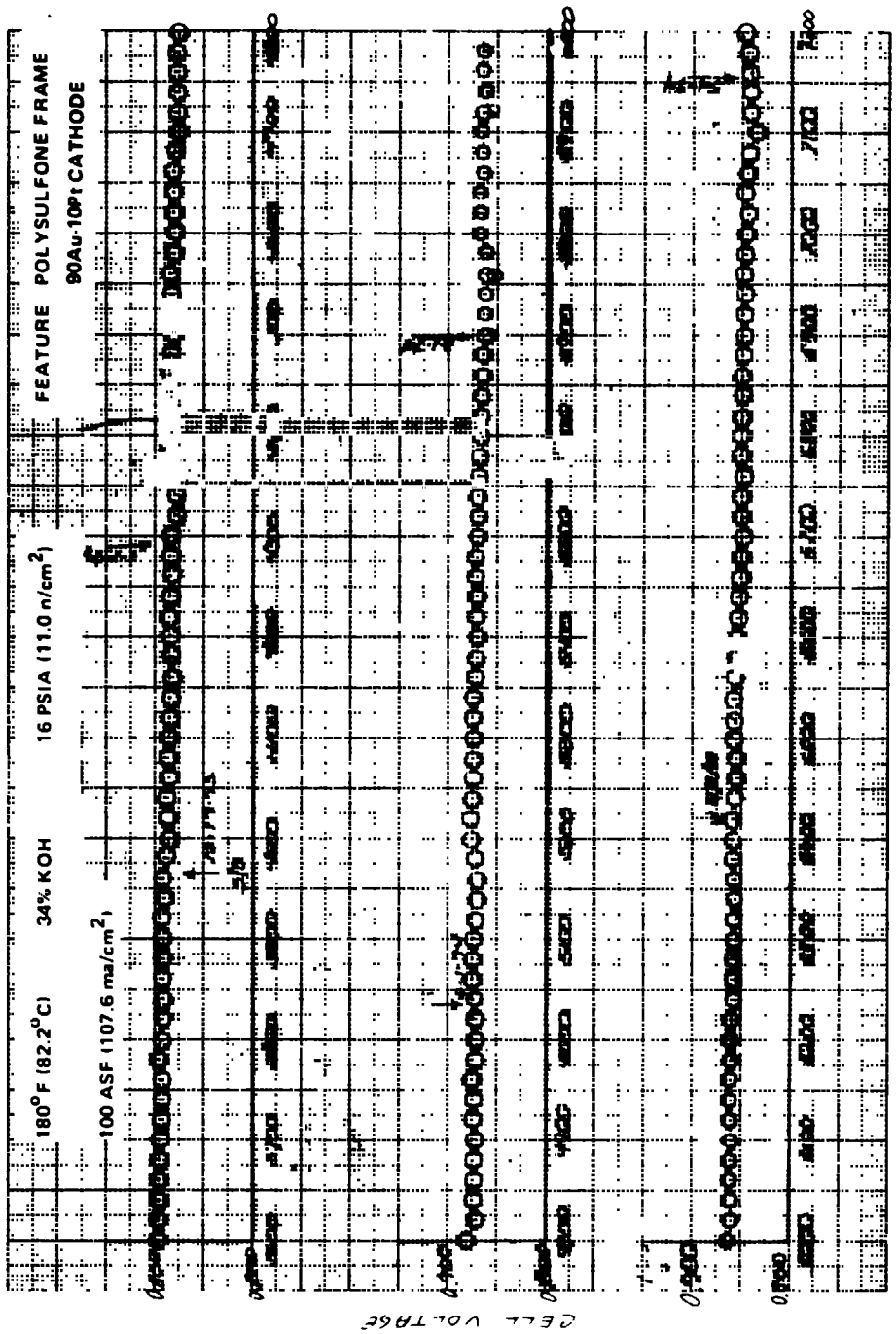

Figure 32 (Cont'd) – Performance History of Cell No. 30

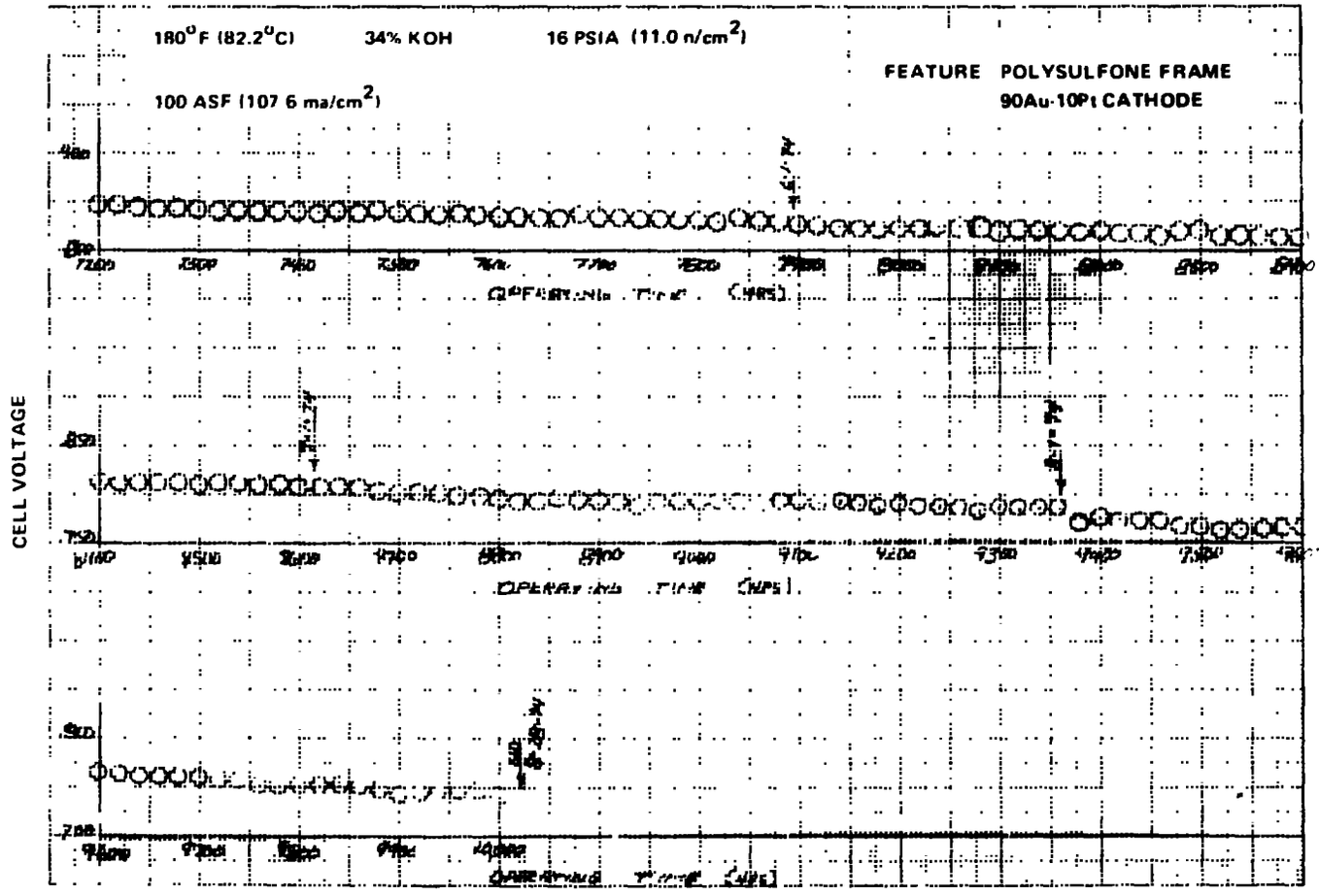

Figure 32 (Cont'd) – Performance History of Cell No. 30

TABLE XIII

CELL NO. 30 DECAY SUMMARY

Elapsed Time - Hrs	Overall Decay Rate (μv/hr)	Decay Rate for Preceding 1000-hr (μv/hr)
500	16.0	—
1000	15.0	15.0
2000	12.0	9.0
3000	11.0	9.0
4000	10.5	9.0
5000	11.8	17.0
6000	11.8	12.0
7000	12.6	17.0
8000	13.7	22.0
9000	15.4	29.0
10000	18.8	49.0

TABLE XIV

CELL NO. 30 ACCOUNTABLE LOSSES

Polysulfone Frame
90Au-10Pt Cathode
PPF Anode

Rig 37970-30 **0.1146 Ft^2 (106.4 cm^2)**
180°F (82.2°C)/34% KOH/16 psia (11.0 n/cm^2)/PWR

	Load Time, (Hrs)	Performance 1.0 ASF (1.076 ma/cm^2) (Volts)	Performance 2.0 ASF (2.152 ma/cm^2) (Volts)	Performance 100 ASF (mv' (107.6 ma/cm^2) (IR Corr.)	IR Loss 100ASF (107.6 ma/cm^2) (mv)	Activation Loss From 4 Hrs (mv)	100 ASF (107.6 ma/cm^2) Diffusion Losses Total (mv)	Anode (mv)	Cathode (mv)
	4	(1.031)*	(1.019)*	941	8.0	0	8	(8)*	(0)*
	155	(1.031)*	(1.019)*	937	8.0	0	12	--	--
Refurbished	307	(1.031)*	(1.019)*	932	8.0	0	16	--	--
	527	1.033	1.022	934	10.0	-2	15	10	5
	1138	1.028	1.016	927	11.0	3	21	14	7
	2450	1.023	1.011	917	10.0	8	26	19	7
	3026	1.021	1.009	911	11.0	10	29	--	-
	3560	1.018	1.006	907	12.0	13	31	24	7
	4346	1.012	1.000	892	13.0	19	37	27	10
	5185	1.012	1.000	886	17.0	19	44	31	13
	5784	1.012	0.999	878	14.0	19	49	36	13
	6353	1.011	0.997	868	13.0	20	57	43	14
	7211	1.008	0.994	857	14.0	23	68	52	16
	7836	1.007	0.992	845	14.0	24	80	59	21
* Estimate	8500	1.000	0.987	829	16.0	31	88	72	16
	9295	1.000	0.986	793	16.0	31	122	100	22
	10015	0.994	0.979	767	16.0	37	142	120	22

TABLE XV

CELL NO. 30 VOLTAGE LOSS BREAKDOWN
10,013 hours

	Voltage Loss - mv	
Total	182	
Activation	37	
Attributable to Carbonates	26	
IR Change	8	
Total Cell Diffusion Losses	116	22 - cathode 94 - anode

A discussion of losses as determined in post-test analysis of the individual electrodes in this cell is presented in Section IIA3.

Post-test analysis of the KOH in the cell showed that 42.5 percent of the original fill KOH had been converted to carbonates. The results appear in Figure 30. The conversion value for this polysulfone frame is considerably lower than that for previously tested Hypon frame cells and indicates that polysulfone frame materials can effectively be used for extended time periods at these conditions. The results of the carbonate analysis are presented as a combined result; i.e., an average carbonate percentage of the Passive Water Removal (PWR) assembly and Unitized Electrode Assembly UEA. It is consistent with the results presented from other tests.

The cell tolerance response was normal to about 6640 hours where a flattening out or "drooping" occurred at the higher electrolyte concentrations. This phenomenon is normally associated with carbonate buildup to the point where dry side tolerance is affected. Tolerance excursions at load times of 7880 hours and 10,015 hours, Figure 33, showed continued deterioration on the high concentration side of the tolerance curve. To minimize the risk of running on the dry side, the cell electrolyte concentration was lowered to 33 and 32 percent at about 8400 and 8800 hours respectively. The remaining endurance testing was conducted at 32 percent KOH concentration.

Teardown inspection showed the cell to be in excellent condition. Throughout the test, no signs of crossover or shorting were evident.

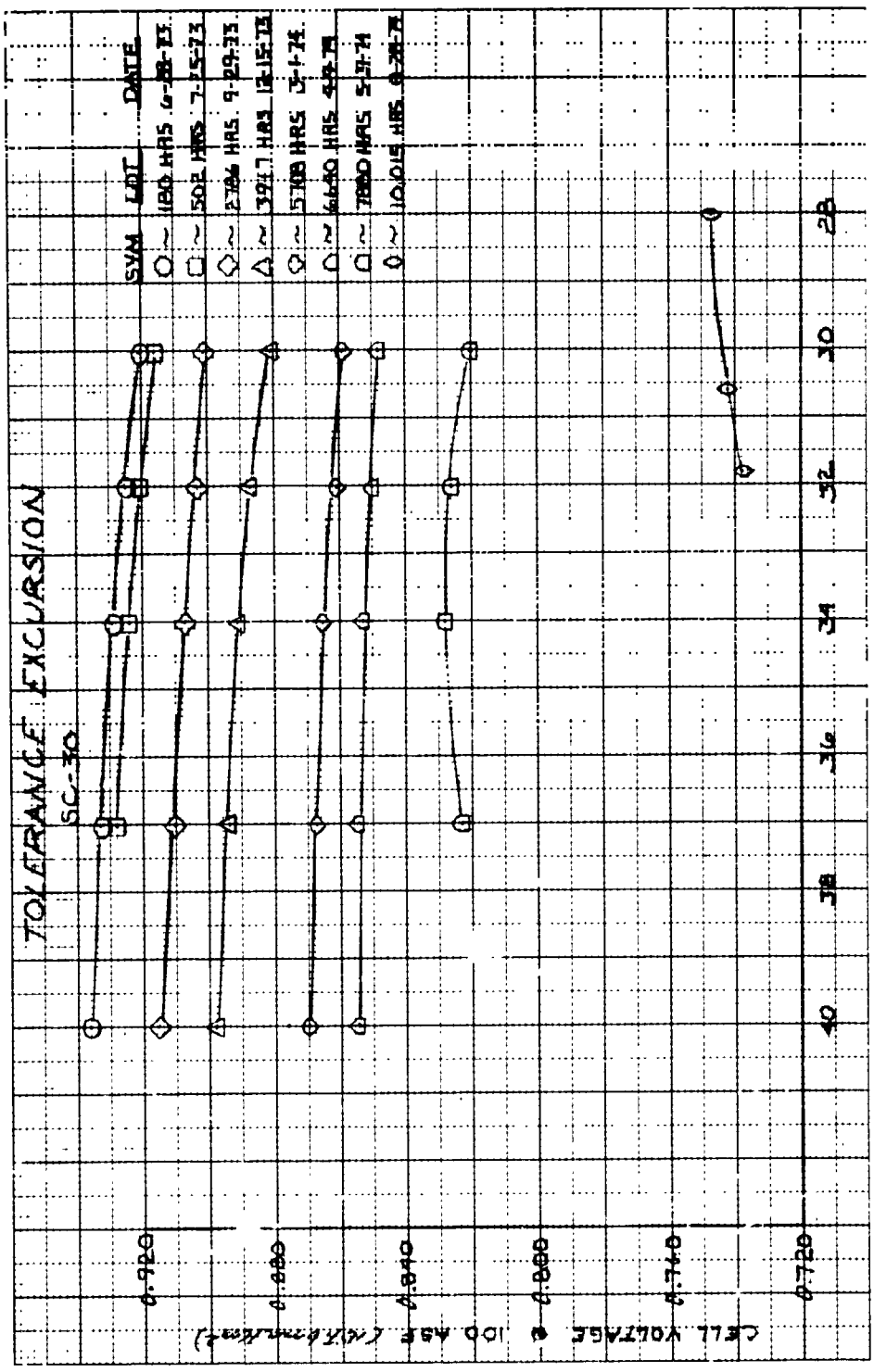

Figure 33 — Cell No. 30 Tolerance Exursion Data

Cell Nos. 31 and 32

These cells were of the configuration approved by the NASA Program Manager as Verification Design No. 8. These were the first of the hybrid polysulfone/epoxy-glass fiber frame cells described in Section IIID. Both cells were fabricated with PPF anodes, 90Au-10Pt cathodes, and sintered at a higher temperature of 635°F (335°C) to make them more hydrophobic and to retard flooding. The objectives of the test were to evaluate the corrosion resistance of the hybrid polysulfone-epoxy-glass fiber frames and the performance and endurance characteristics of the high sinter temperature anodes.

Both cells were fabricated with nickel ERP's and initial testing was performed with hybrid polysulfone-epoxy glass fiber Passive Water Removal (PWR) assemblies. The PWR in Cell No. 31 was replaced with a Hypon frame PWR after 1504 hours because of damage incurred on the hybrid PWR during teardown. Cell No. 31 accumulated 3000 hours load time. Its operating history is presented in Figure 34. Carbonate conversion determinations were made after the verification test of each cell. Additional carbonate conversion values were obtained for Cell No. 31 after 1504 hours, after 3000 hours, and at the end of testing. Carbonate values are shown in Figure 30. The values obtained are considerably lower than those for Hypon frame cells.

The initial performance level of Cell No. 31 was excellent. However, cell tolerance excursion at the start of testing indicates an abnormal performance loss at higher electrolyte concentrations. This phenomenon was apparently because of the higher anode sintering temperature. Subsequent refills of the cell resulted in an improvement in the cell dry side tolerance, though the refills at 312 and 1504 hours did not result in fully normal tolerance response. Tolerance results as obtained are presented in Figure 35. In addition to the poor tolerance behavior, the cell decay rate was quite high. It was postulated that the decay was magnified by the fact that only a portion of the catalyst was wetted and that this portion was more sensitive to poisoning. Because of the extreme hydrophobicity of the anode, the movement of electrolyte was not reversible within the electrode resulting in poor tolerance response. The tolerance response of Cell No. 32 also showed poor dry side response, see Figure 36, but was not as abnormal as that of Cell No. 31. Dilute oxygen testing test on both cells showed relatively high anode diffusion levels.

Cell No. 32 accumulated 395 hours of testing. Teardown of this cell revealed that the cathode was installed with catalyst layer away from the matrix. Cell performance was reasonable until the cell was refurbished. After refurbishment, cell performance was poor, forcing shut down of the rig. The operating history of the cell is presented in Figure 37.

The test results of these cells indicated that the higher sintering temperature of the anodes, while offering promise of longer life, render the anodes overly hydrophobic at these test conditions.

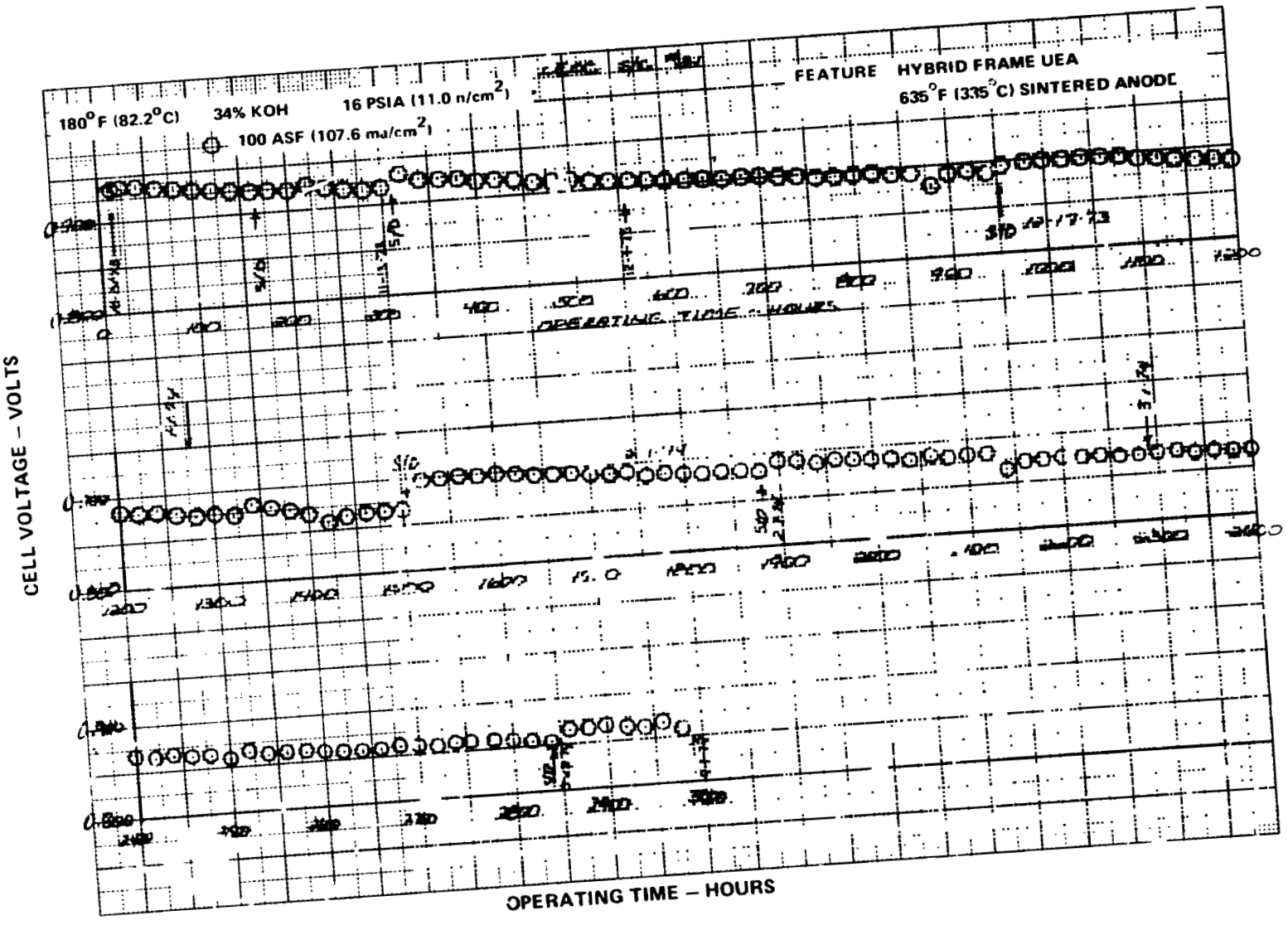

Figure 34 – Performance History of Cell No. 31

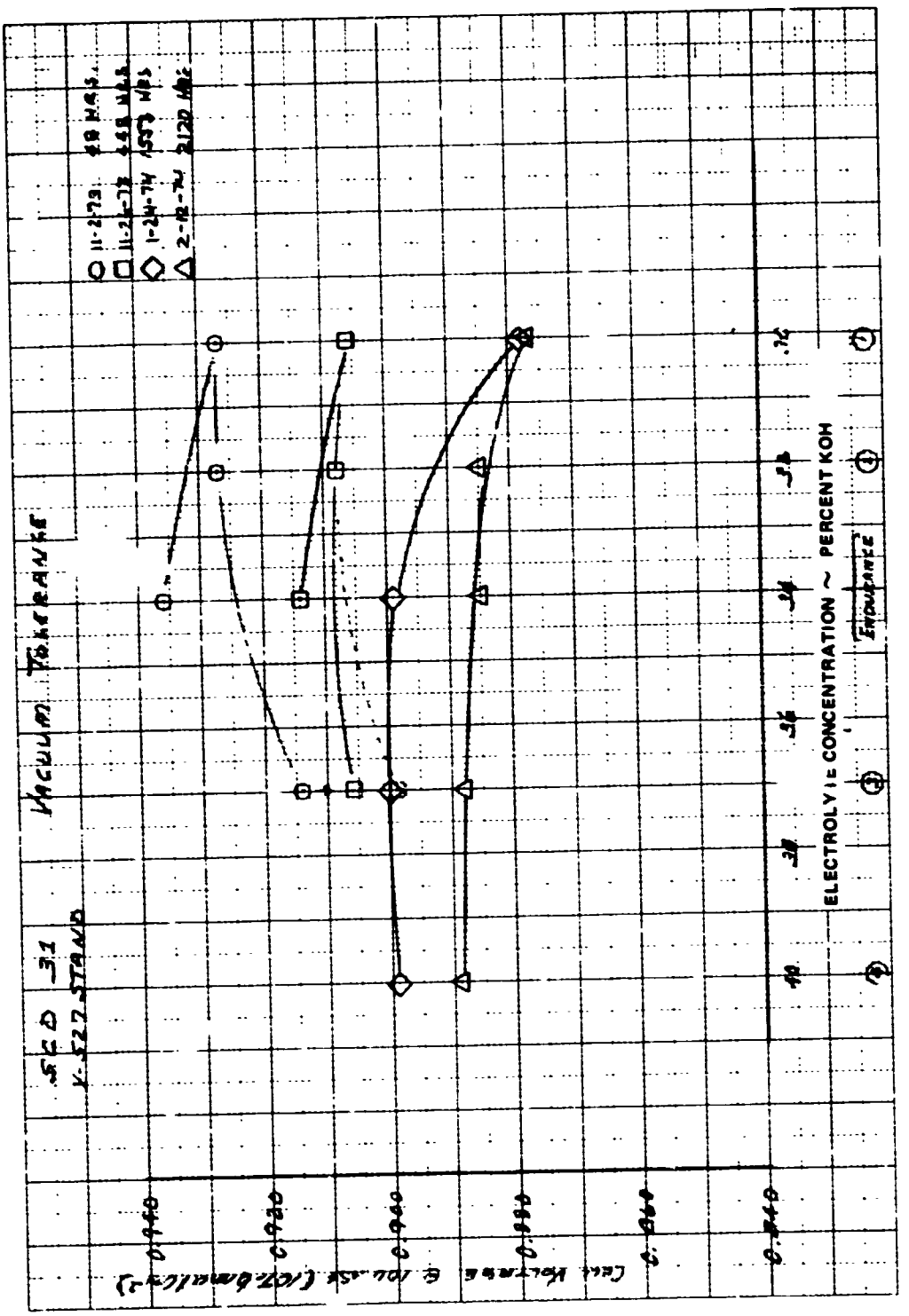

Figure 35 – Cell Nr. 31 Tolerance Excursion Data

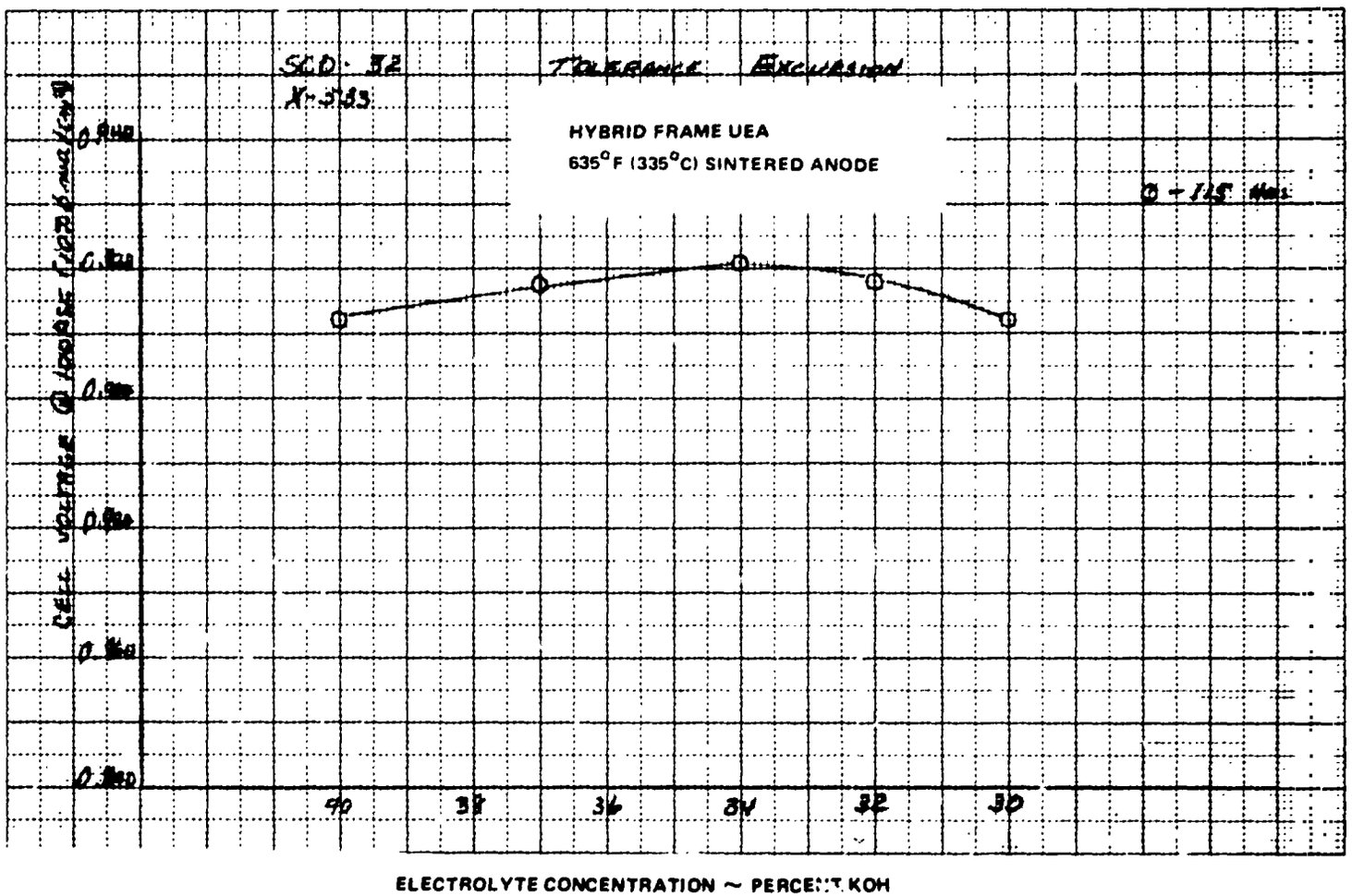

Figure 36 — Cell No. 32 Tolerance Excursion Data

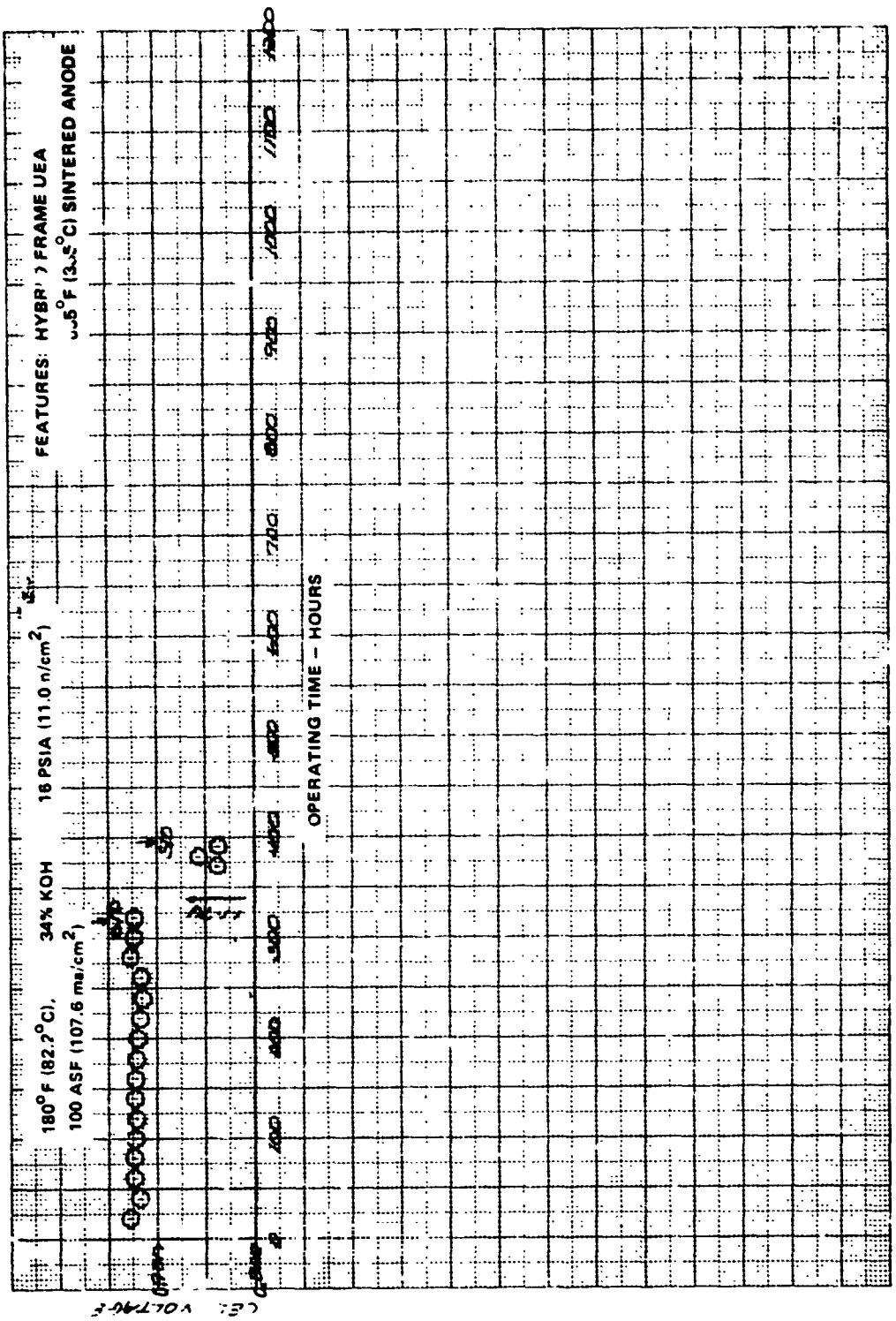

Figure 37 – Performance History of Cell No. 32

Cell Nos. 33 and 34

Cell Nos. 33 and 34 were both delivered to the NASA LeRC for evaluation. Both were of the Verification Design No. 6 and were identical to Cell No. 25.

Cell Nos. 35 and 36

Cell Nos. 35 and 36 were of the configuration approved by the NASA Program Manager on Verification Design No. 9. Frame construction was of the hybrid polysulfone/epoxy-glass fiber. Supported catalyst anodes were used in each cell as well as 90Au-10Pt cathodes. The primary test objectives were to evaluate the supported catalyst anodes and to further evaluate hybrid polysulfone frame corrosion resistance in the fuel cell environment.

Cell No. 35 has accumulated 6405 hours of operation at 100 ASF (107.6 ma/cm^2) and continues on test; see Figure 38. Cell performance was very stable during the initial 5000 hours of testing. The decay rate exhibited during this time period was about 8.5 μv per hour; lower than any cell tested to date. A summary of cell accountable losses appears in Table XVI. The low initial performance was because of somewhat higher than normal anode diffusion levels. The bulk of the cell performance decay was due to anode diffusion and cathode activation. A small but noticeable electrical short appeared at about 4000 hours load time.

An unexplained step drop in cell performance level occurred at about 5200 hours accompanied by an increase in decay rate. Although the reason for this drop is not clear, diagnostics performed at 5697 hours indicate a significant increase in the value of the cell electrical short and a large increase in anode diffusion. Typical diagnostic data appears in Figures 39 and 40.

The tolerance excursion data for Cell No. 35 showed a sharp drop off in cell voltage at concentration values below 34 percent KOH, probably due to an overfill condition. Tolerance response after refill was normal, see Figure 41. A tolerance excursion performed at 6008 hours showed a loss in dry side tolerance. This is normally an indicator of carbonate level increase.

The primary conclusion of this test is that the supported catalyst anode exhibits stable performance under these operating conditions. This cell remains on test.

Cell No. 36 accumulated a total of 2296 hours of operation. Of this total, 1811 hours were at conditions of 212°F (100°C), and 28 psia (19.3 n/cm^2). Of the 1811 hours, 1325 hours of testing were conducted at 200 ASF (215.2 ma/cm^2). KOH concentration was a nominal 34 percent throughout the test. The operating test history of this cell is shown in Figure 42.

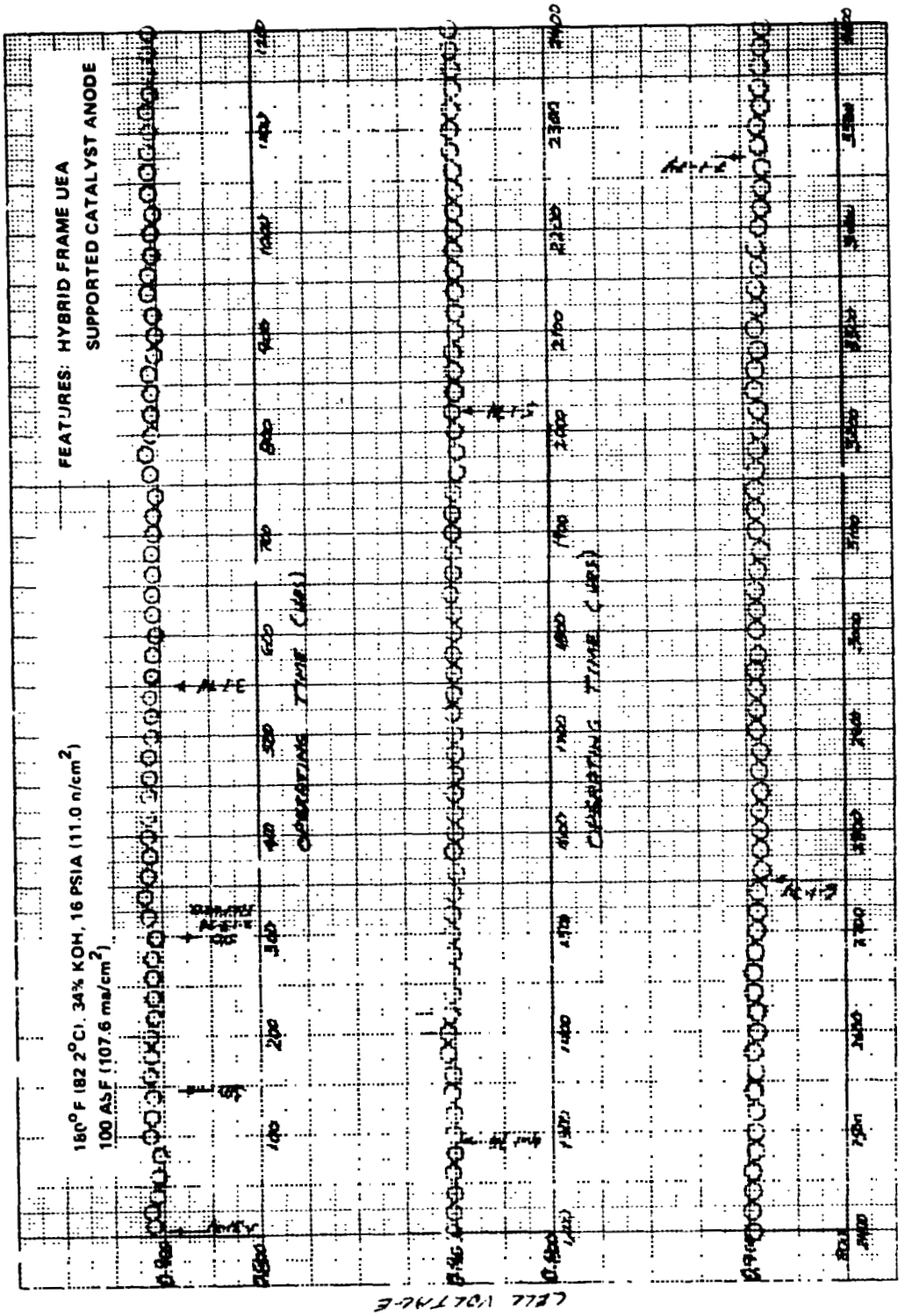

Figure 38 — Performance History of Cell No. 35

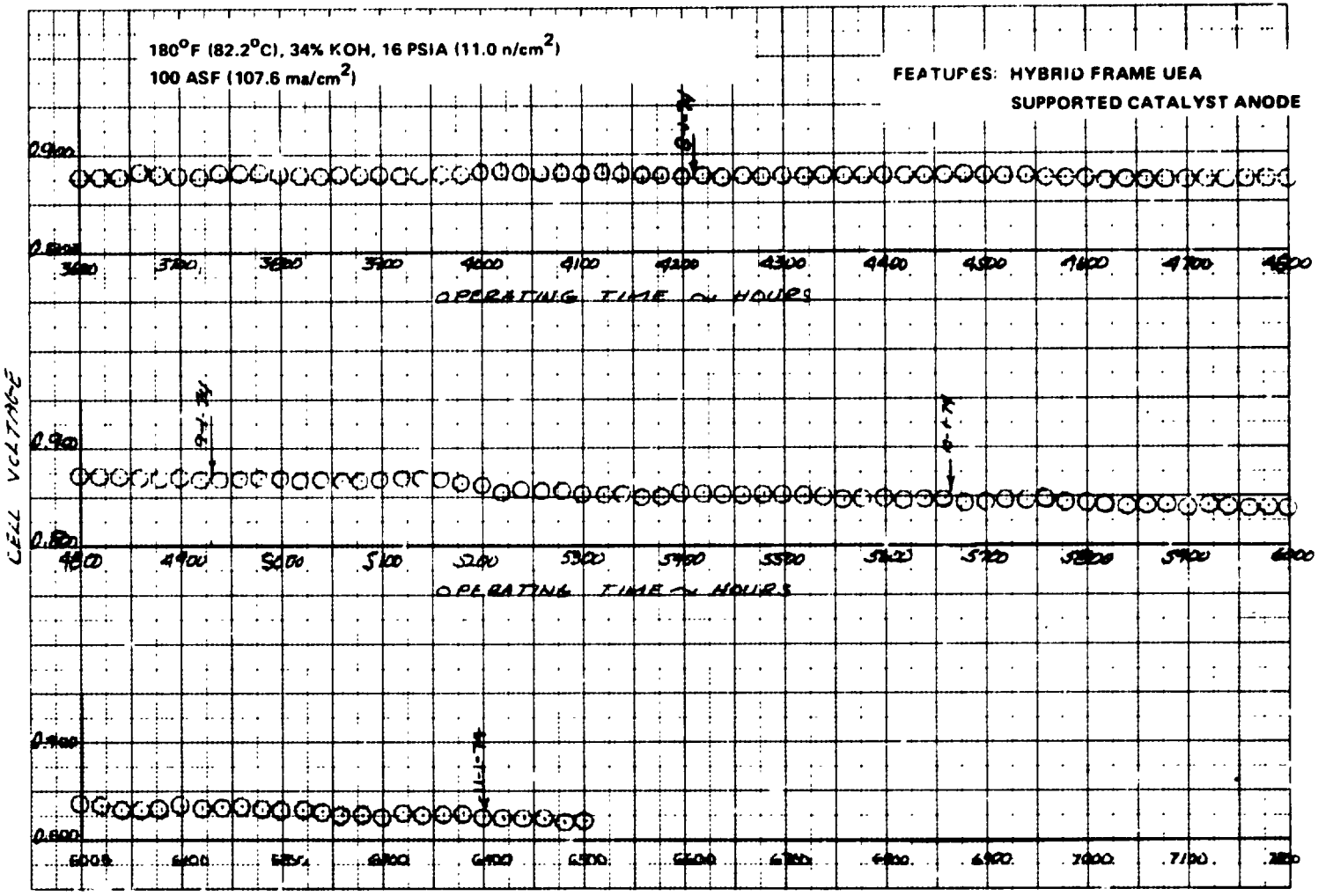

Figure 38 (Cont'd) — Performance History of Cell No. 35

TABLE XVI

CELL NO. 35 ACCOUNTABLE LOSSES

Hybrid Frame-Polysulfone-
Fiberglass Epoxy 90Au-10Pt Cathode
Supported Catalyst Anode

Rig 38503-35 0.1146 Ft^2 (106.4 cm^2)
180°F (82.2°C)/34% KOH/16 psia (11.0 n/cm^2)/PWR

Load Time (Hrs)	Performance 1.0 ASF (1.076 ma/cm^2) (Volts)	Performance 2.0 ASF (2.152 ma/cm^2) (Volts)	Performance 100 ASF (107.6 ma/cm^2) (IR Corr.)	IR Loss 100 ASF (107.6 ma/cm^2) (mv)	Activation Loss (mv)	100 ASF (107.6 ma/cm^2) Diffusion Losses Total (mv)	Anode (mv)	Cathode (mv)
87	1.035	1.023	0.917	8	–	34	30	4
290	1.038	1.025	0.917	10	–	37	33	4
322	1.041	1.030	0.922	7	–	38	33	5
1020	1.032	1.021	0.913	8	3	35	31	4
1713	1.029	1.017	0.904	8	6	41	37	4
2527	1.027	1.014	0.898	8	8	45	39	6
3360	1.023	1.011	0.887	8	12	48	42	6
4150	1.021	1.008	0.882	8	14	57	49	8
5060	1.013	1.000	0.873	8	22	59	52	7
5697	1.009	0.997	0.854	10	26	72	66	6
6014	1.007	0.994	0.844	8	28	83	77	6

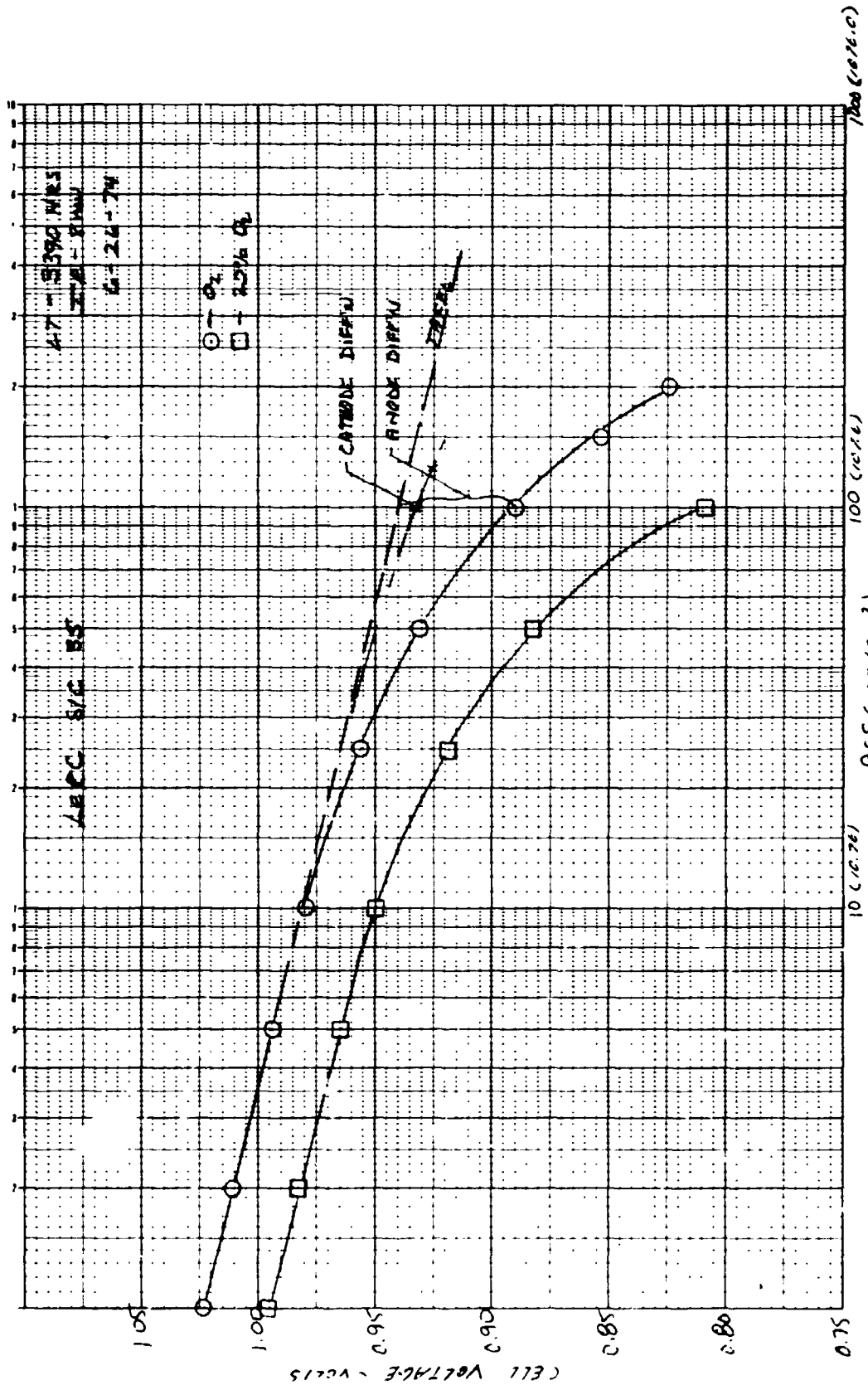

Figure 39 – Cell No. 35 Dilute Oxygen Diagnostic Data (3390 Hours)

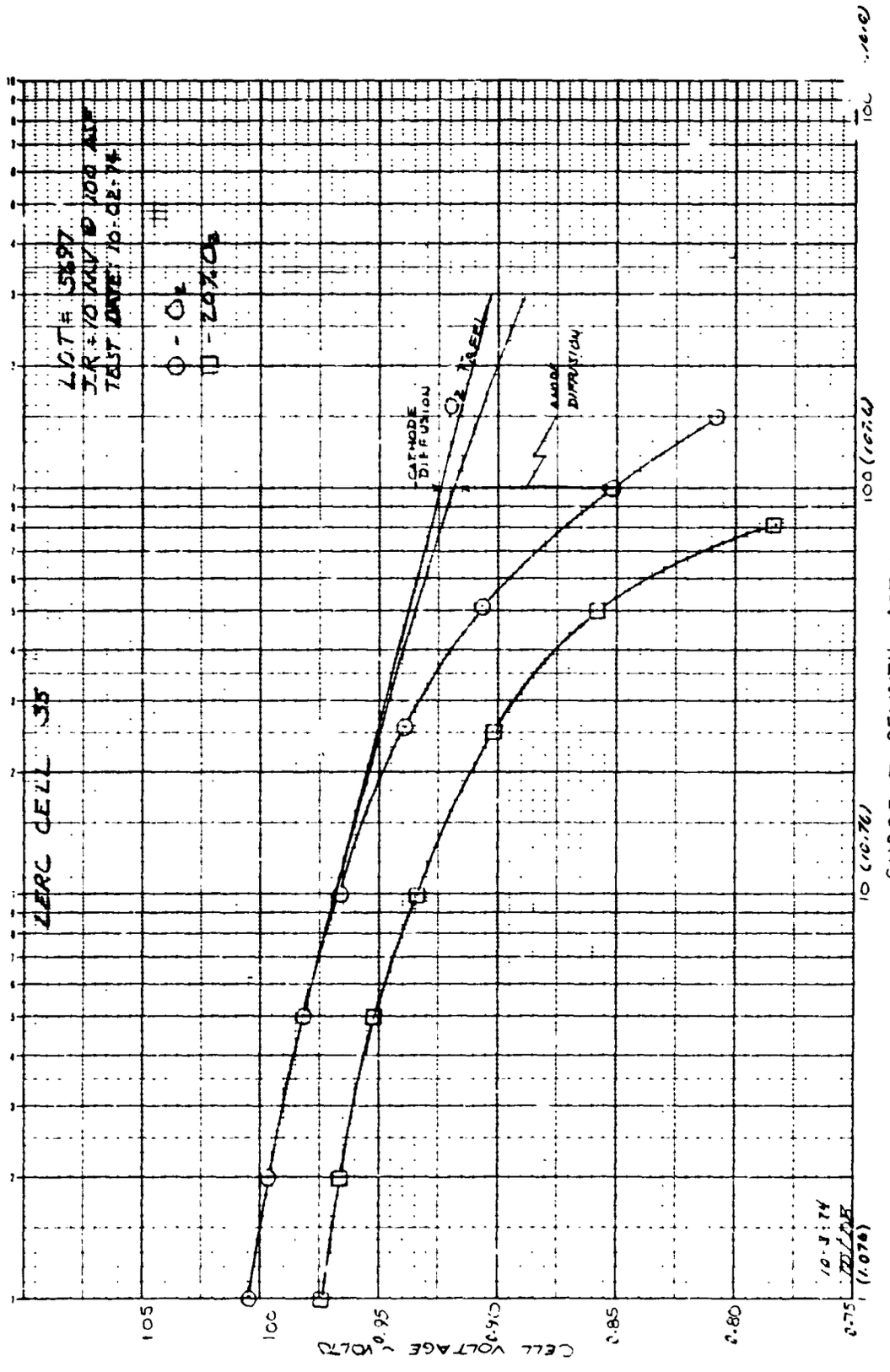

Figure 40 — Cell No. 35 Dilute Oxygen Diagnostic Data (5697 Hours)

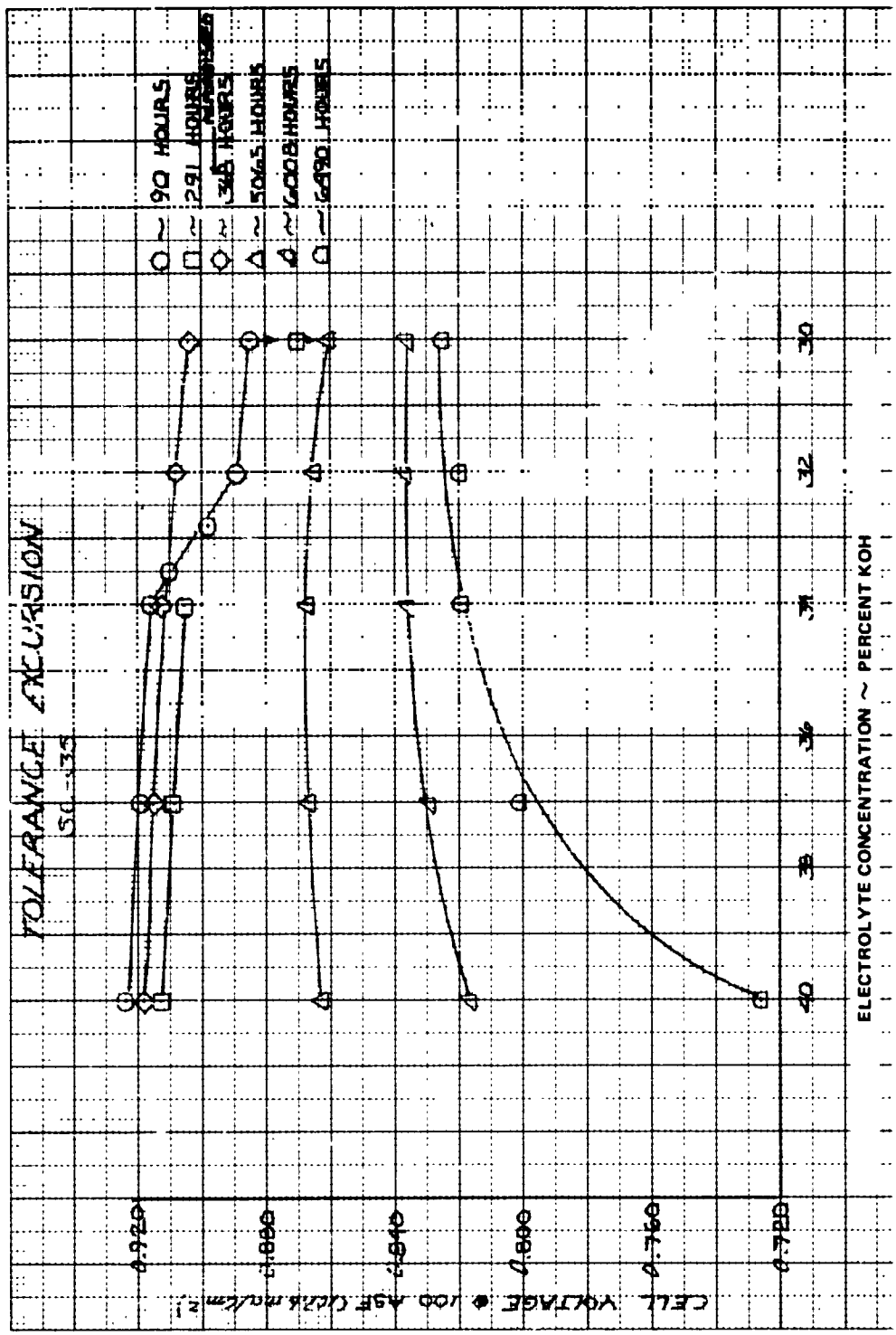

Figure 41 – Cell No. 35 Tolerance Excursion Data

ORIGINAL PAGE IS
OF POOR QUALITY

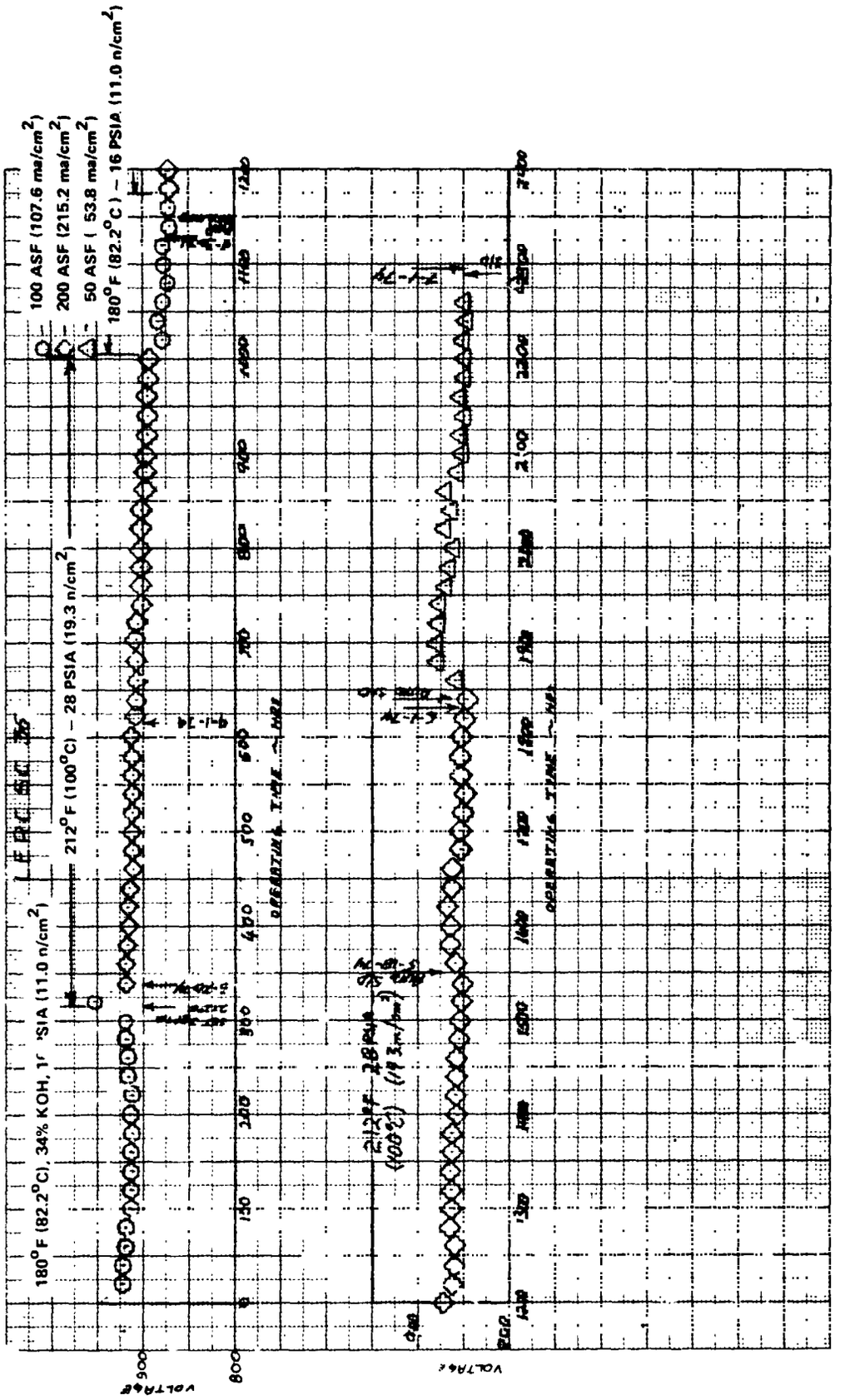

Figure 42 — Performance History of Cell No. 36

Initial cell performance at 180°F (82.2°C) and 16 psia (11.0 n/cm^2) was comparable to that of Cell No. 35. After the verification test period and refurbishment, cell endurance conditions of 212°F (100°C), 28 psia (19.3 n/cm^2) and 200 ASF (215.2 ma/cm^2) were set. These conditions were maintained for the bulk of the remaining test time. The objective of this test was to evaluate frame corrosion characteristics and electrode endurance qualities at elevated temperature, pressure, and current density.

Electrolyte conversion test results are shown in Figure 30. It is apparent from the results that operating temperature of 212°F (100°C) did not result in an appreciable increase in electrolyte conversion level, verifying the suitability of polysulfone for operation at elevated temperature.

However, at the conditions of this test, problems with the passive water removal assembly were encountered. Pressure differential across the PWR at these conditions is 20 psid (13.8 n/cm^2) as opposed to the 12 psid (8.3 n/cm^2) nominal pressure differential at 180°F (82.2°C) operating temperature. Partial leakage occurred across the PWR at about 1000 hours operating time forcing shutdown and replacement of the PWR assembly. Replacement was made with a PWR incorporating a 0.020 in. (0.51 mm) asbestos matrix in place of the original 0.010 in. (0.25 mm) asbestos matrix. Operation of the PWR was normal for 743 hours when leakage again developed. However, refill of the cell was sufficient to eliminate the problem. Teardown showed that the PWR gas crossover was apparently a result of local dryout of the matrix and not mechanical failure.

Cell No. 36 was refilled twice after the initial verification period. With each refill, cell performance was lost. After the 1100-hour refill, 20 percent oxygen diagnostics showed that cell voltage loss due primarily to increased anode diffusion. Other cells have shown anode diffusion loss increase after refill and the problem has been attributed to anode flooding or over-wetting. Since this occurred after a relatively short time in this cell, it is assumed that the 212°F (100°C) operating temperature accelerates this process. A refill after 1843 hours resulted in poor cell performance.

A summary of the cell accountable losses up to 1173 hours appears in Table XVII. A breakdown of cell losses was not obtainable after cell shorting began at about 1500 hours load time. The cell was shut down at 2293 hours because of UEA crossover. It is believed that crossover was the result of cell shorting.

Cell No. 37

Cell No. 37 was fabricated with a hybrid polysulfone/epoxy-glass fiber frame, PPF anode, 90Au-10Pt cathode, and polysulfone ERP's in both the UEA and PWR. The PWR frame was made with epoxy-glass fiber. This cell was not constructed to an official NASA Verification Design and was tested primarily to obtain additional hybrid frame configuration corrosion data.

The cell accumulated 1207 hours load time at 100 ASF (107.6 ma/cm^2). The operating test history is shown in Figure 43. The KOH conversion level (4.4 percent) exhibited by this cell

TABLE XVII

CELL NO. 36 ACCOUNTABLE LOSSES

Hybrid Frame-Polysulfone-
Glass Fiber/Epoxy, 90Au-10Pt Cathode
Supported Catalyst Anode

Rig 38505-38 0.1146 ft^2 (106.4 cm^2)
34% KOH/PWR

Load Time (Hrs)	Performance 1.0 ASF (1.076 ma/cm^2) (Volts)	2.0 ASF (2.152 ma/cm^2) (Volts)	100 ASF (107.6 ma/cm^2) (IR Corr.)	IR Loss (mv) 100 ASF (107.6 ma/cm^2)	Activation Loss (mv)	100 ASF (107.6 ma/cm^2) Diffusion Losses Total (mv)	Anode (mv)	Cathode (mv)	(Temp) °F (°C)	(Press) psia (n/cm^2)
36	1.037	1.024	0.925	8.0	–	27	25	2	180 (82.2)	16 (11.0)
282	1.039	1.027	0.928	8.0	–	27	24	3	180 (82.2)	16 (11.0)
316	1.052	1.039	0.961	6.0	0	10	3	7	212 (100)	28 (19.3)
845	1.042	1.030	0.944	6.0	10	17	7	10	212 (100)	28 (19.3)
1173	1.047	1.035	0.935	6.0	5	31	21	10	212 (100)	28 (19.3)

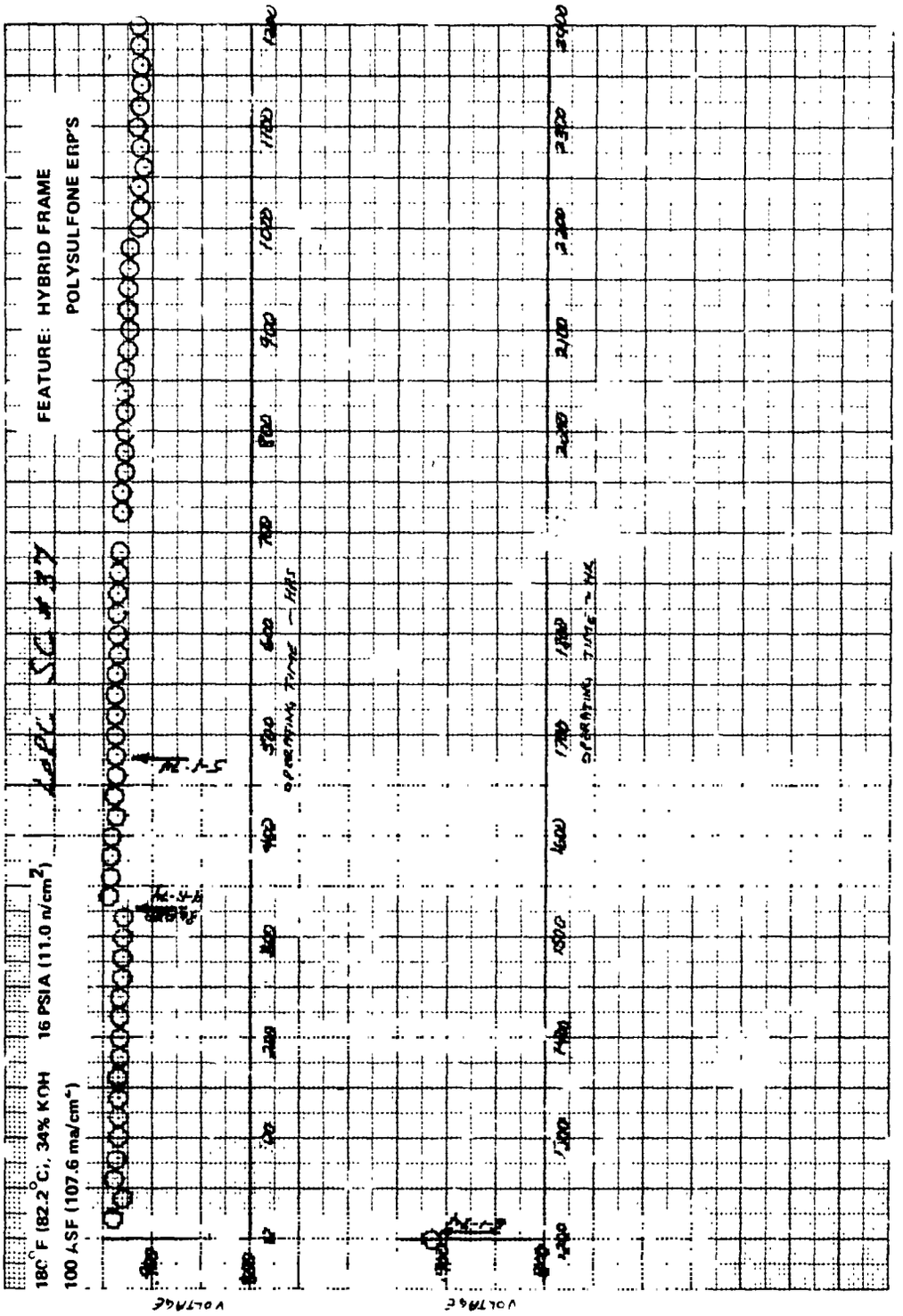

Figure 43 — Performance History of Cell No. 37

was considerably lower than the values obtained from previous hybrid polysulfone/epoxy-glass fiber frame cells; see Figure 30.

Performance degradation was considerably higher than normal. This was believed to be due to the continuous loss of electrolyte from the cell via the PWR during the entire test period. Daily monitoring of the cell product water revealed high pH, indicative of the loss of electrolyte. Post-test inspection of the PWR hydrophobic membrane revealed several small pinholes through which electrolyte could have been lost. An additional indicator that electrolyte loss did occur during the course of testing was the favorable performance response to wet side operation near the end of testing. As seen in Figure 44, tolerance response was normal after refill but showed poor dry side response near the end of testing. Initial tolerance response indicated an apparent poor fill which was corrected by refilling.

Cell Nos. 38, 39 and 39A

Cell Nos. 38, 39, and 39A were constructed with hybrid polysulfone/epoxy-glass fiber frames, supported catalyst anodes, 90Au-10Pt cathodes and polysulfone ERP's in both the UEA and PWR assembly. They were Verification and Endurance tested as NASA approved Design No. 10.

Cell No. 38 accumulated 2543 hours at the 100 ASF (107.6 ma/cm^2) endurance condition. The performance history of the cell is presented in Figure 45. The post-test carbonate analysis of the cell indicated a low KOH conversion value, comparable to that of Cell No. 37, as shown in Figure 30. The value is considerably lower than the carbonate values obtained in earlier hybrid polysulfone/epoxy-glass fiber framed cells.

Accountable losses, as determined by dilute oxygen diagnostics, appear on Table XVIII. Anode diffusion losses were consistent with those of other cells with supported catalyst anodes (Cell Nos. 35 and 36). However, anode diffusion losses increased quite rapidly with time. Figure 46 shows the poor wet side tolerance response of the cell, believed due to poor electrolyte transfer characteristics of the polysulfone electrolyte reservoir plate. To avoid large fluctuations, an operating electrolyte concentration of 38 percent was set at about 615 load hours and maintained throughout the remainder of the test.

The cell was automatically shut down after 2543 hours because of Passive Water Removal (PWR) assembly crossover. At this point, the cell was removed from the test stand and post-test carbonate analysis performed. A recheck indicated that the PWR assembly had resealed itself. Crossover apparently was because of a local dryout condition and not due to failure of the component. Visual examination of the ERP after test showed poor nickel plating coverage. It was concluded that the poor plating plus a somewhat higher hydrophobicity of the anode were responsible for the poor electrolyte transfer and decay characteristics.

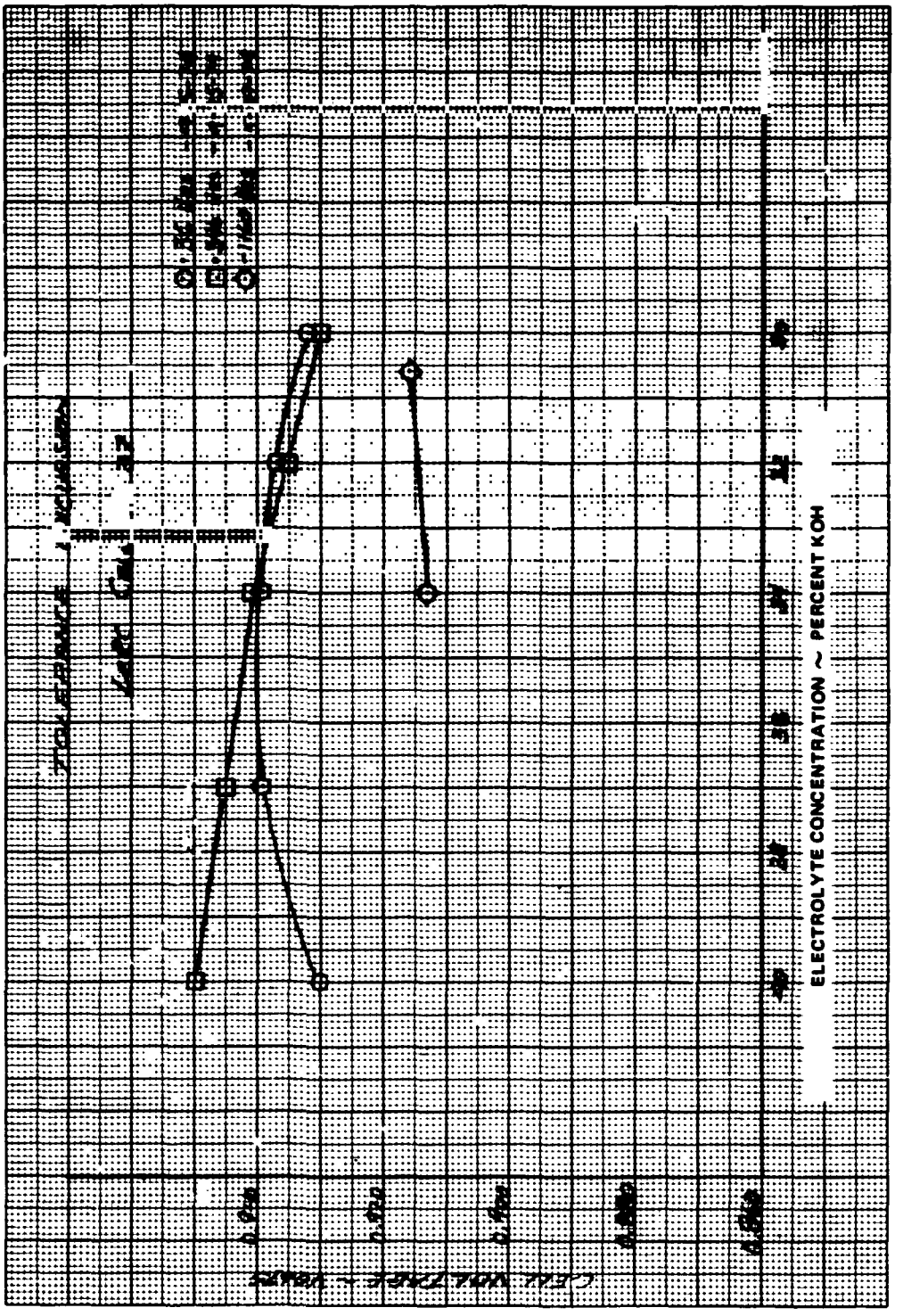

Figure 44 – Cell No. 37 Tolerance Excursion Data

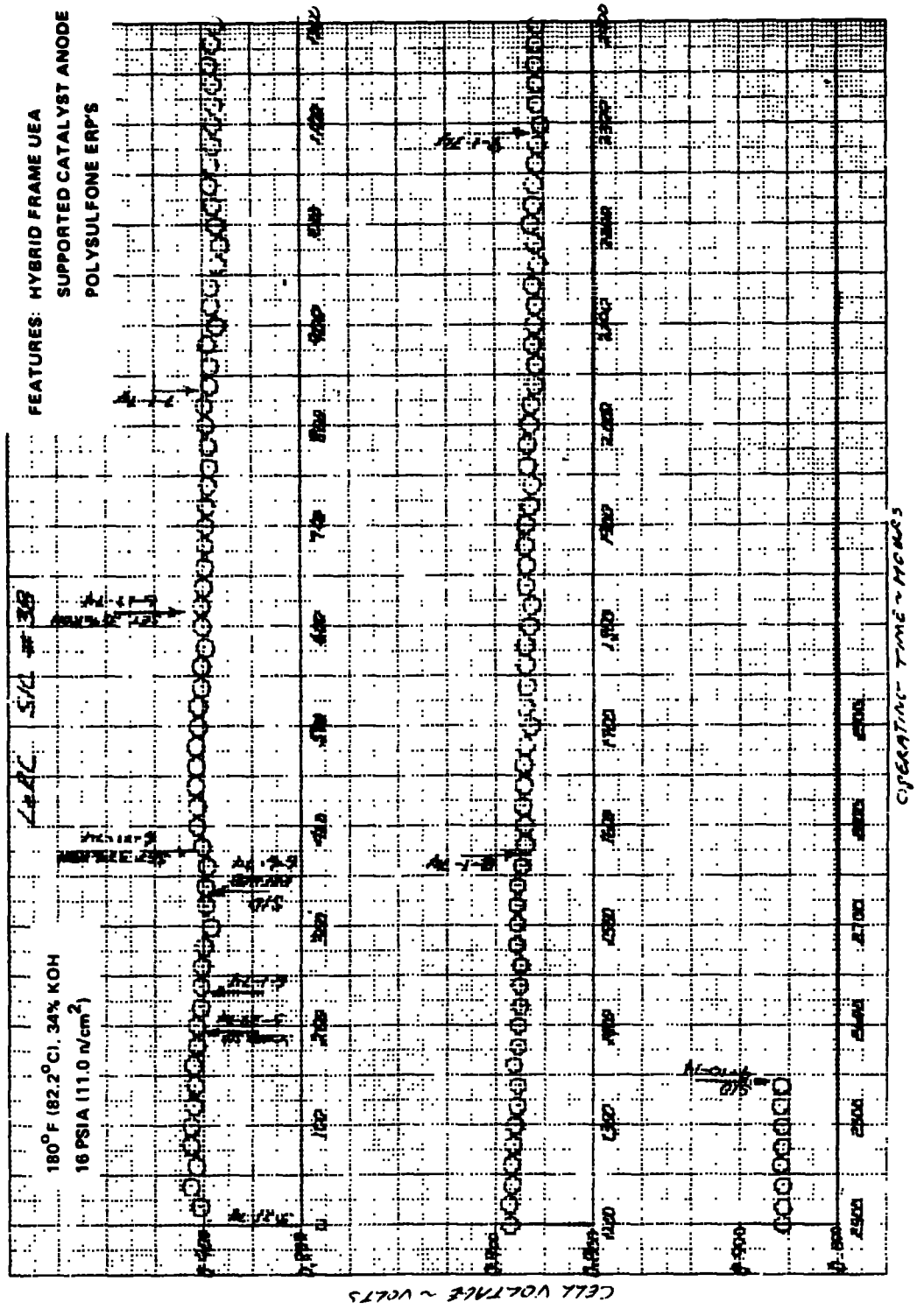

Figure 45 — Performance History of Cell No. 38

TABLE XVIII

CELL NO. 38 ACCOUNTABLE LOSSES

Hybrid Frame - Polysulfone
Fiberglass Epoxy, 90Au-10Pt Cathode,
Supported Catalyst Anode
Polysulfone ERP's

Rig 38505-38 0.114 Ft^2 (105.9 cm^2)
180°F (82.2°C)/34% KOH/16 PSIA (11.0 n/cm^2)/PWR

	Performance			IR Loss		100 ASF (107.6 ma/cm^2) Diffusion Losses		
Load Time (Hrs)	1.0 ASF (1.076 ma/cm^2) (Volts)	2.0 ASF (2.15 ma/cm^2) (Volts)	100 ASF (107.6 ma/cm^2) (IR Corr.)	100 ASF1 (107.6 ma/cm^2) (mv)	Activation Loss (mv)	Total (mv)	Anode (mv)	Cathode (mv)
68	1.028	1.017	0.906	9	–	40	34	6
189	1.031	1.020	0.913	9	–	35	26	9
385	1.034	1.024	0.908	9	–	42	35	7
1388	1.028	1.016	0.882	9.5	–	68	58	10

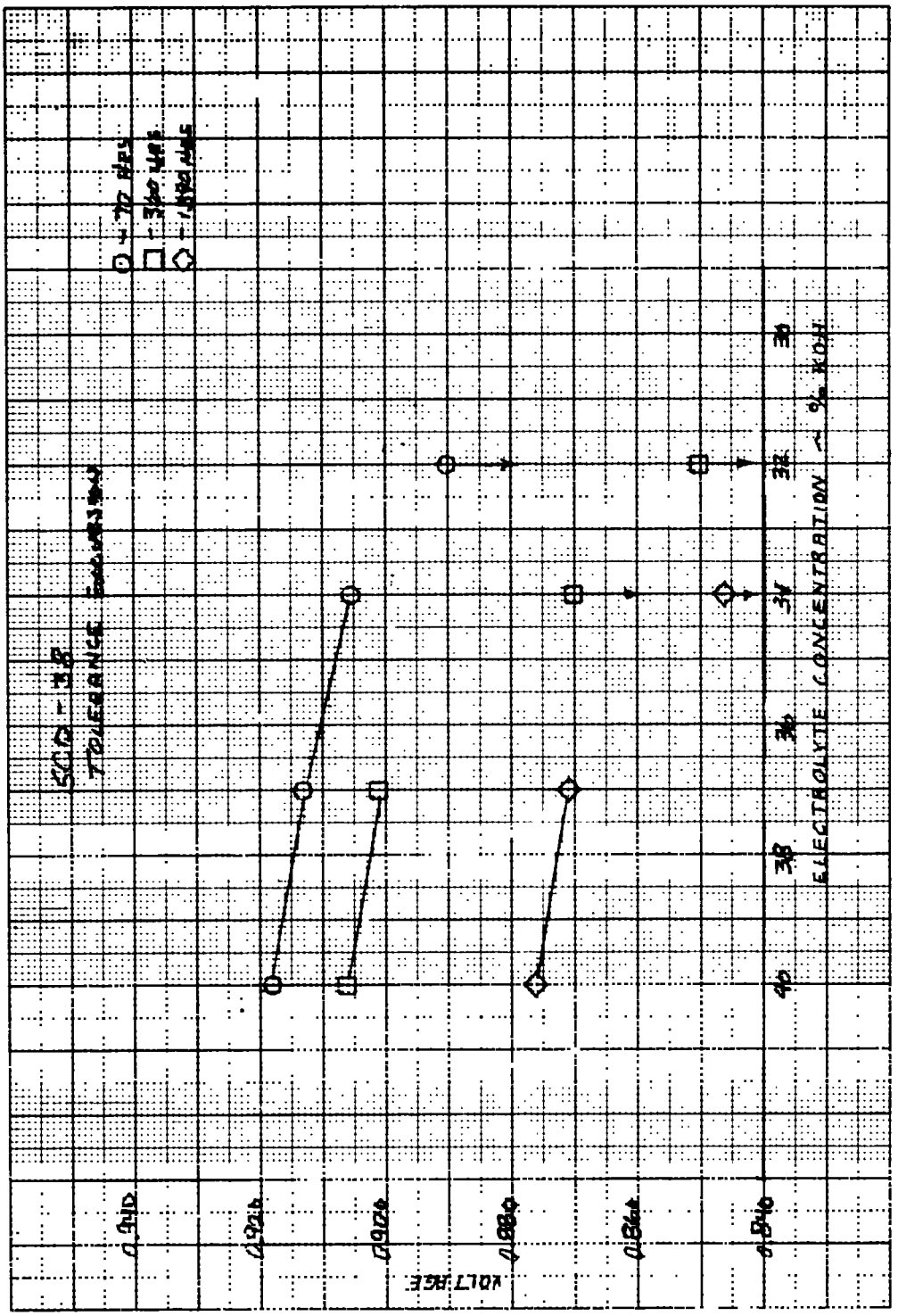

Figure 46 — Cell No. 38 Tolerance Excursion Data

Cell No. 38 showed poor initial performance and tolerance response. After several disassemblies and rebuilds, the cell UEA developed minor crossover. It was concluded that the poor initial performance was the result of poor electrolyte takeup properties of the ERP. Poor takeup was believed to result from inadequate nickel plating of the ERP. However, later testing of Cell Nos. 39A, 40 and 41 showed that the initially poor performance in all of these cells was due to incomplete filling of the anode. This was concluded from the abnormally high anode diffusion losses measured in dilute oxygen diagnostic tests. Subsequent refilling of the cell resulted in improved cell performance and reduced anode diffusion losses. Since the anodes of these cells and that of Cell No. 39 were from the same electrode batch, it can be assumed that the poor initial performance of Cell No. 39 was also because of insufficient anode fill resulting from overly hydrophobic anodes. Cell No. 39 accumulated 345 hours at 100 ASF (107.6 ma/cm^2). The operating test results are presented in Figure 47. Improved performance was obtained after rebuilding the cell with a nickel ERP and again after a second rebuild and additional testing with a polysulfone ERP. As determined from testing of later cells, the performance improvement was due to both the refill associated with the rebuild and the ERP change. Cell accountable losses appear in Table XIX. The cell was shut down when it became somewhat erratic with pressure fluctuations because of UEA crossover.

Cell No. 39A was built with a new UEA and all the other components from Cell No. 39. As discussed previously, the cell required a refill because of poor performance as the result of insufficient anode wetting. After refill, performance was consistent with other supported catalyst anode cells. The operating history of this cell is presented in Figure 48, and cell accountable losses appears in Table XX. Cell load was increased to 200 ASF (215.2 ma/cm^2) after 374 hours. The cell has accumulated 1557 hours total load time with 1183 hours accumulated at 200 ASF (215.2 ma/cm^2). Cell performance has been relatively stable at these conditions. Cell testing is continuing.

Cell Nos. 40 and 41

These cells were fabricated with hybrid polysulfone/epoxy-glass fiber frames. Both cells incorporate supported catalyst anodes, 80Au-20Pt cathodes, and polysulfone ERP's. These cathodes, because of higher alloying and surface area characteristics, are expected to give the same performance and endurance characteristics with half the catalyst loading of the 90Au-10Pt cathodes. This configuration was approved by the NASA Program Manager to be Verification Design No. 11. The objectives of the test were to evaluate the stability and performance of 80Au-20Pt cathodes.

As previously discussed, both cells required a refill before good performance was obtained because of the relative hydrophobicity of the anodes. Both cells showed lower 100 ASF (107.6 ma/cm^2) performance levels than previous cells, apparently due to the slightly lower cathode activity combined with the anode diffusion losses consistent with other supported catalyst anodes.

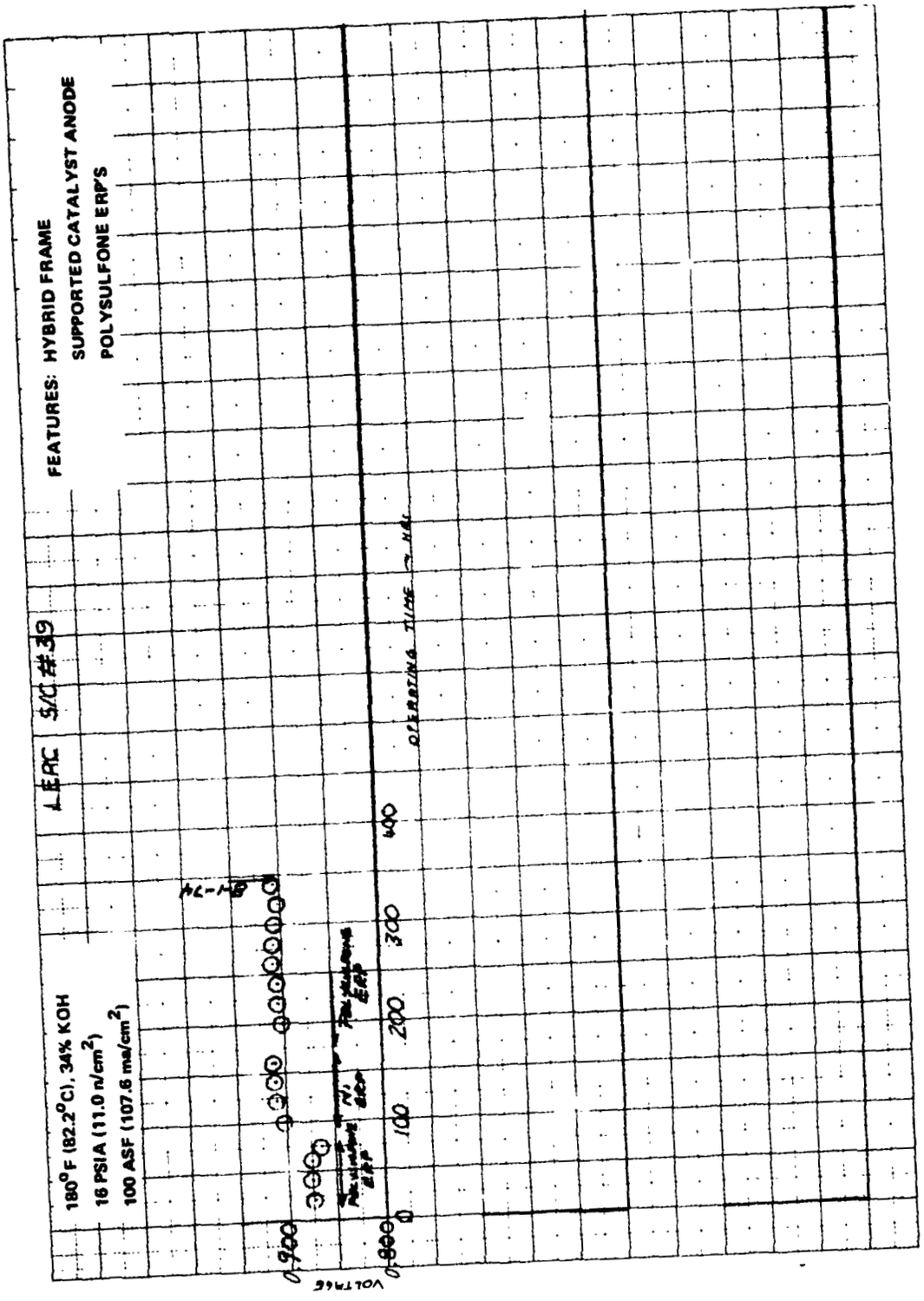

Figure 47 — Performance History of Cell No. 39

ORIGINAL PAGE IS
OF POOR QUALITY

TABLE XIX

CELL NO. 39 ACCOUNTABLE LOSSES

Hybrid Frame – Polysulfone
Glass Fiber Epoxy, 90Au-10Pt
Cathode, Supported Catalyst
Anode, Polysulfone ERP'S

Rig 38507-39 0.114 Ft^2 (105.9 cm^2)
180°F (82.2°C)/34% KOH/16 PSIA (11.0 n/cm^2)/PWR

Load Time Hrs.	Performance 1.0 ASF (1.076 ma/cm^2) (Volts)	Performance 2.0 ASF (2.152 ma/cm^2) (Volts)	Performance 100 ASF (107.6 ma/cm^2) (IR Corr.)	IR Loss (mv)	Activation Loss (mv)	Diffusion Losses Total (mv)	Diffusion Losses Anode (mv)	Diffusion Losses Cathode (mv)	
24	1.033	1.021	887	11	—	63	52	11	Polysulfone ERP
115	1.028	1.016	918	8	5	25	21	4	Ni ERP
190	1.028	1.015	914	9	5	24	20	4	Polysulfone ERP

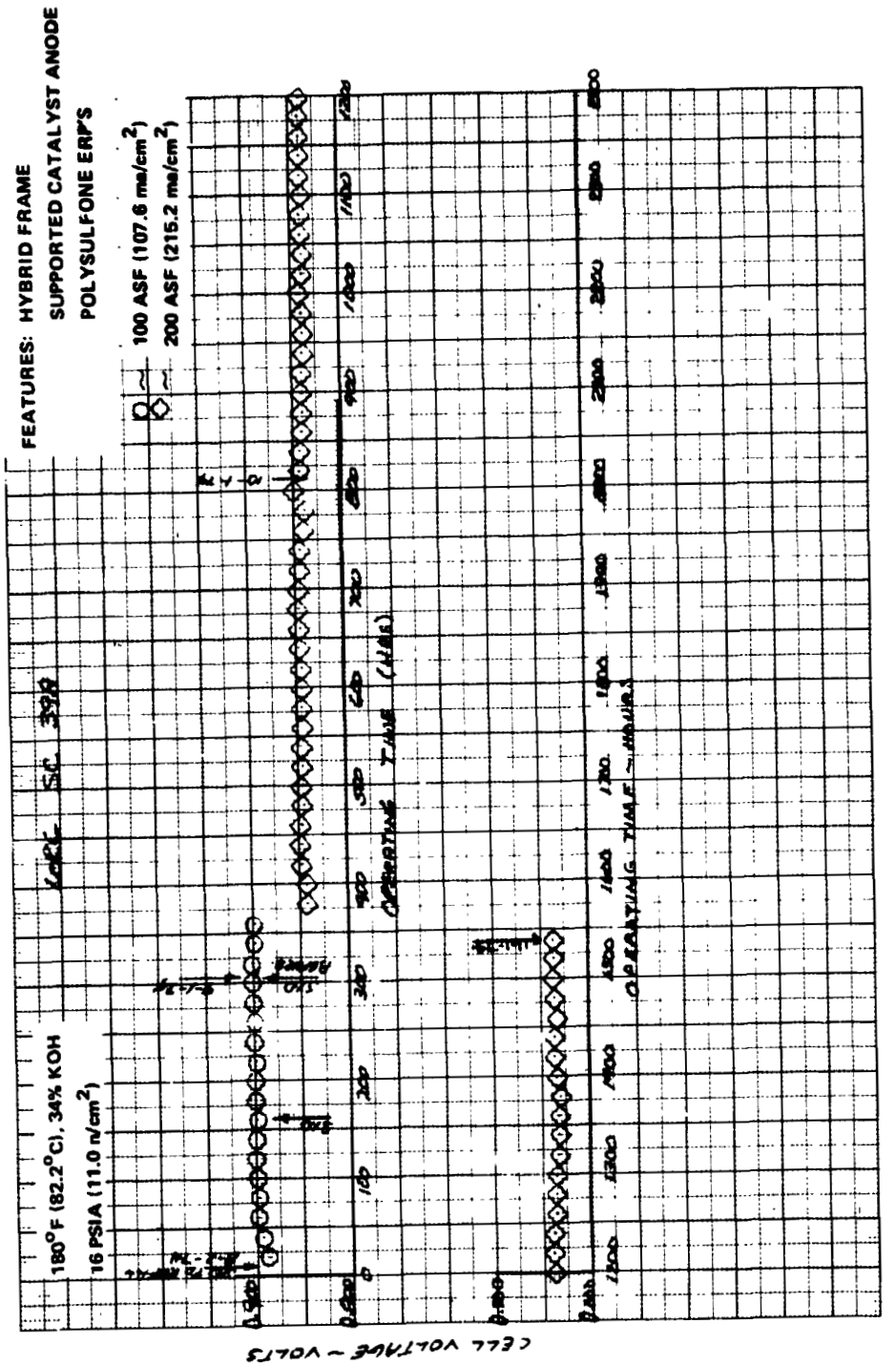

Figure 48 — Performance History of Cell No. 39A

TABLE XX

CELL NO. 39A ACCOUNTABLE LOSSES

Hybrid Frame – Polysulfone
Glass Fiber Epoxy, 90Au-10Pt
Cathode, Supported Catalyst
Anode, Polysulfone ERP'S

Rig 38507-39A 0.114 Ft^2 (105.9 cm^2)
180°F (82.2°C)/34% KOH/16 PSIA (11.0 n/cm^2)/PWR

Load Time Hrs.	Performance 1.0 ASF (1.076 ma/cm^2) (Volts)	Performance 2.0 ASF (2.152 ma/cm^2) (Volts)	Performance 100 ASF (107.6 ma/cm^2) (IR Corr.)	IR Loss (mv)	Activation Loss (mv)	Diffusion Losses Total (mv)	Diffusion Losses Anode (mv)	Diffusion Losses Cathode (mv)	
2	1.023	1.009	81[illegible]	14	--	87	82	5	
118	1.030	1.017	914	12	--	25	17	8	After Refill
303	1.031	1.018	915	10	--	30	23	7	
324	1.023	1.009	906	10	8	30	23	7	After Refurb.
1839	1.025	1.013	905	12	6	35	28	7	

Cell No. 40 has accumulated 1436 hours load time at 100 ASF (107.6 ma/cm^2). The operating test results are presented in Figure 49. The cell decay rate since initiation of testing has remained extremely low. Accountable losses of the cell are presented in Table XXI. Good tolerance response was demonstrated after refurbishment of the cell; see Figure 50. The cell is continuing on test.

Cell No. 41 has accumulated 1275 hours at 100 ASF (107.6 ma/cm^2). The operating history of this cell is presented in Figure 51. The accountable losses of the cell are shown in Table XXII. Tolerance response was normal. This cell is continuing on test. To date, Cell Nos 40 and 41 both show very stable performance characteristics.

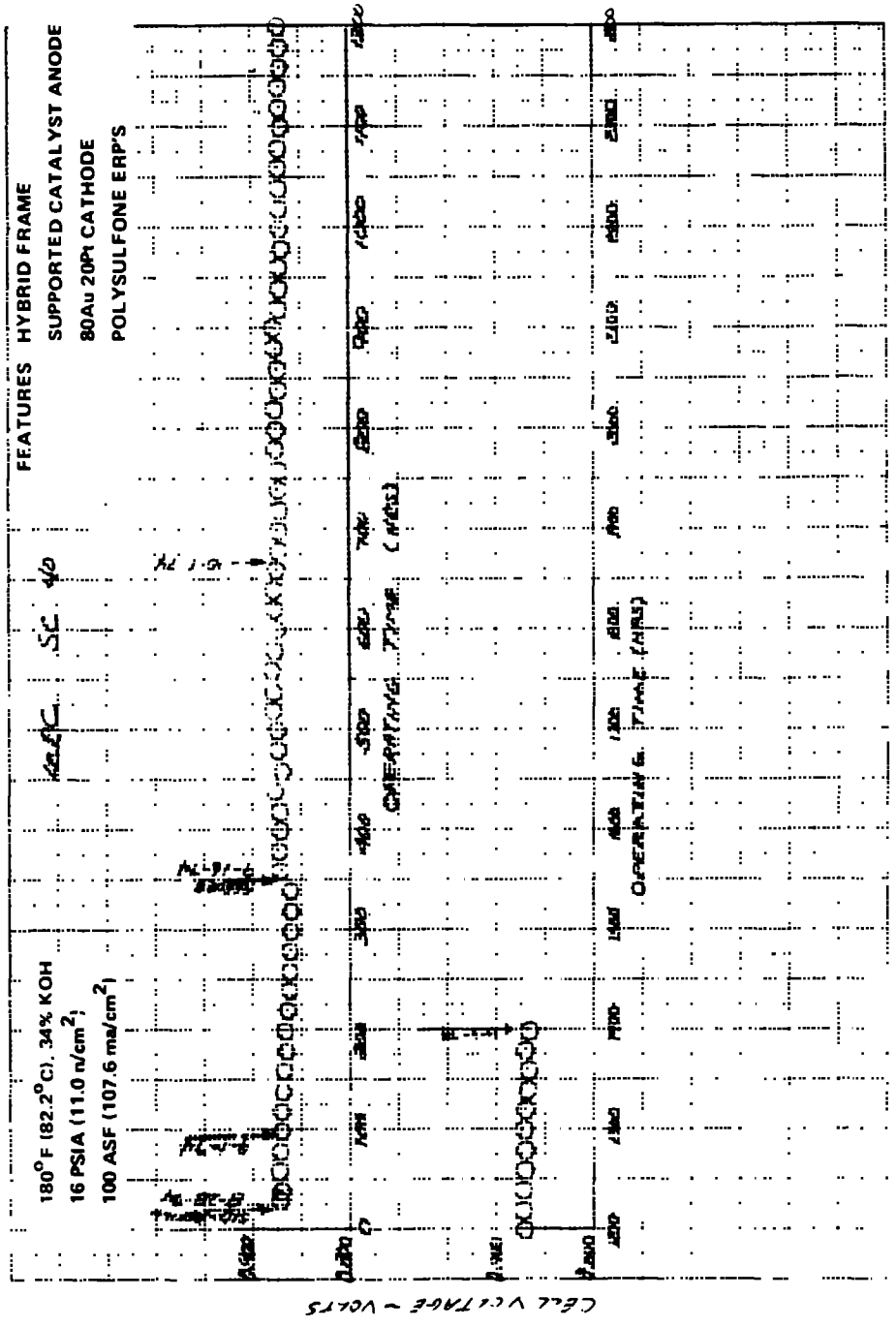

Figure 49 — Performance History of Cell No. 40

TABLE XXI

CELL NO. 40 ACCOUNTABLE LOSSES

Hybrid Frame-Polysulfone-Fiberglass Epoxy, 80Au-20Pt Cathode, Supported Catalyst Anode, Polysulfone ERP's

Rig 38740-40 0.1146 ft^2 (106.4 cm^2)
180°F (82.2°C)/16 psia (11.0 n/cm^2)/34% KOH/PWR

Load Time (Hrs.)	Performance 1.0 ASF (1.076 ma/cm^2) (Volts)	Performance 2.0 ASF (2.152 ma/cm^2) (Volts)	Performance 100 ASF (107.6 ma/cm^2) (IR Corr.)	IR Loss 100 ASF (107.6 ma/cm^2) (mv)	Activation Loss (mv)	100 ASF (107.6 ma/cm^2) Diffusion Losses Total (mv)	Anode (mv)	Cathode (mv)	
18	1.029	1.015	0.835	8	—	104	93	11	
32	1.029	1.016	0.880	8	—	67	55	12	Refilled
335	1.019	1.007	0.867	9	10	64	55	9	
367	1.018	1.005	0.882	10	11	41	36	5	After Refurb.
1018	1.016	1.004	0.881	10	13	53	45	8	

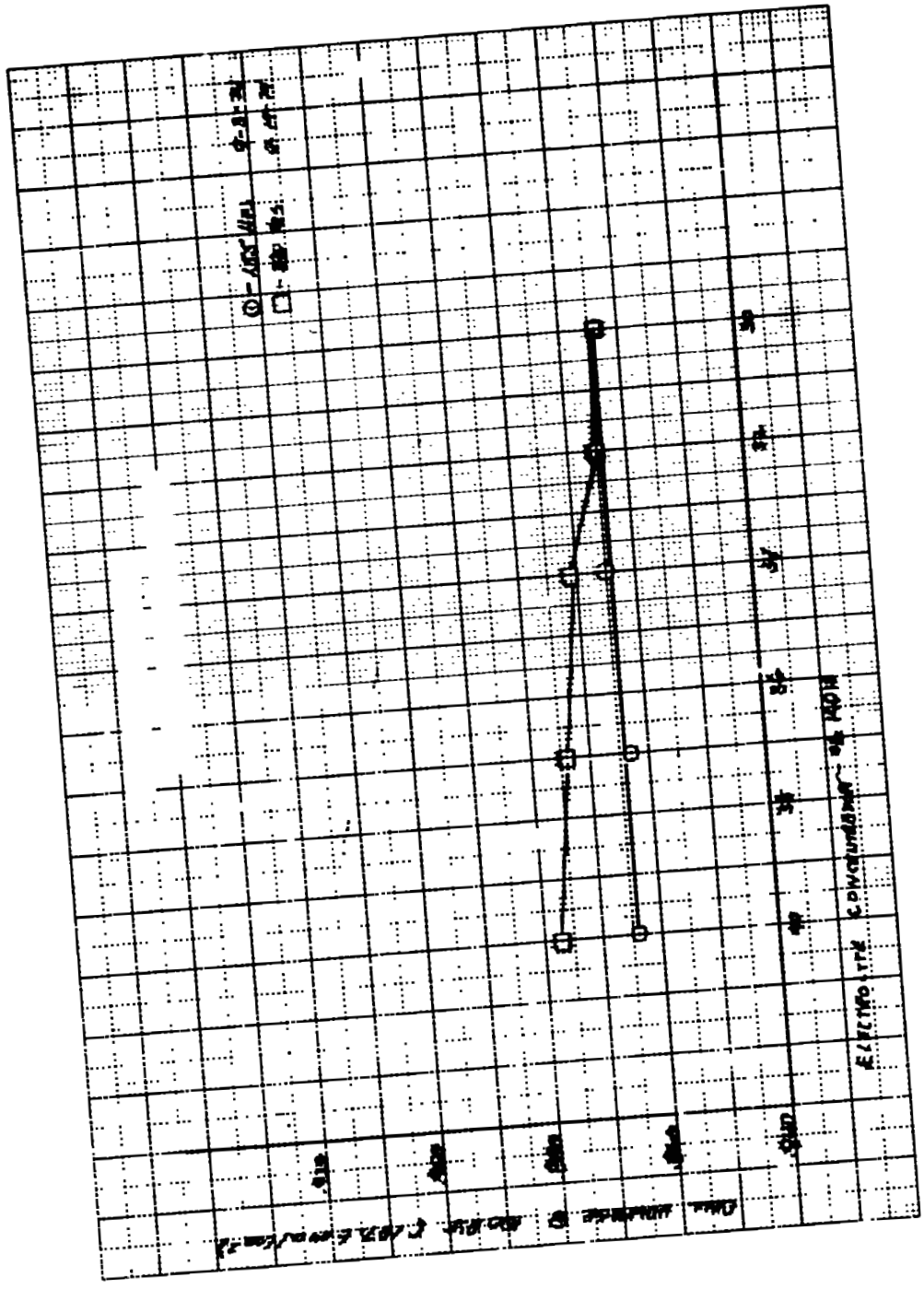

Figure 50 — Cell No. 40 Tolerance Excursion Data

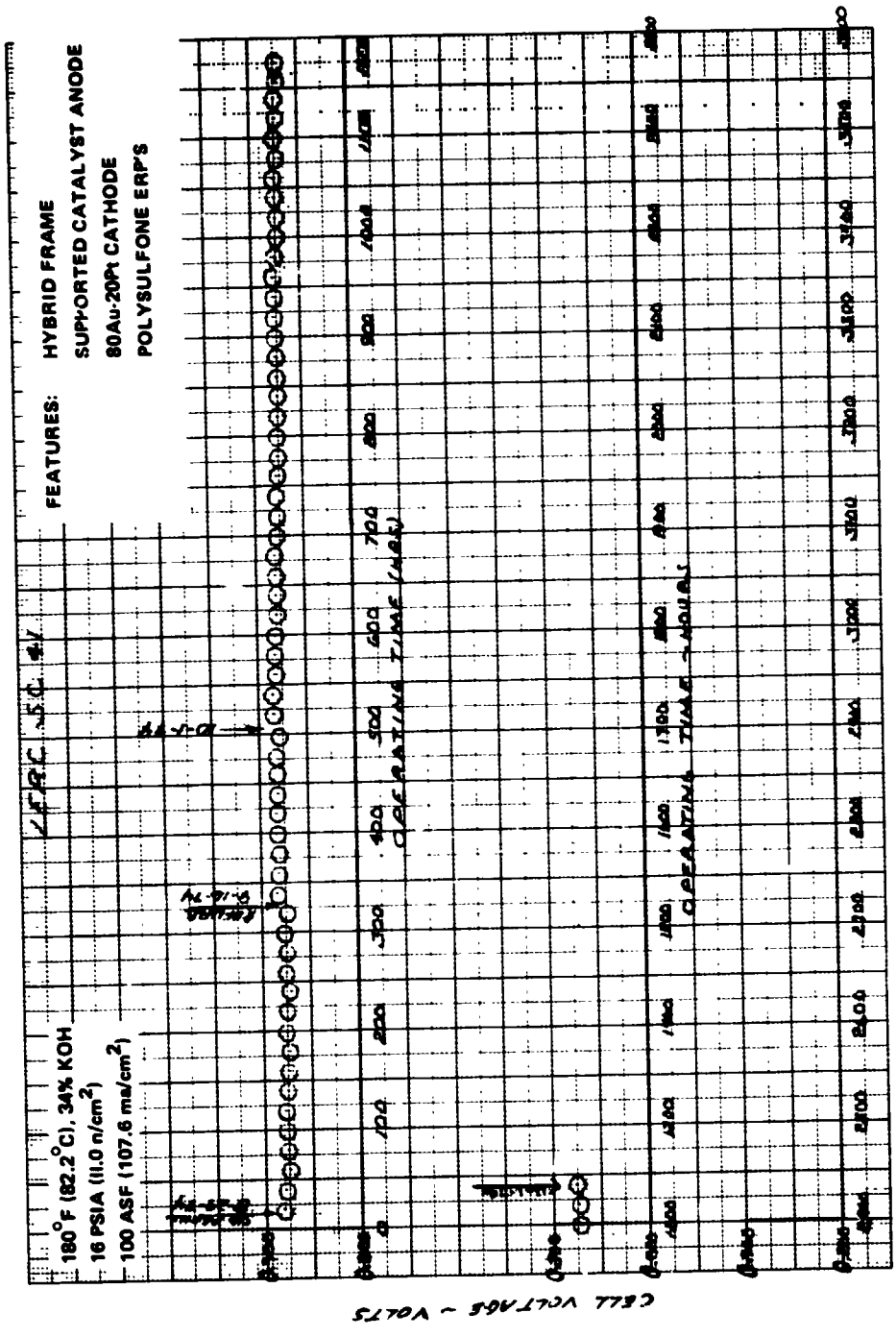

Figure 51 – Performance History of Cell No. 41

TABLE XXII

CELL NO. 41 ACCOUNTABLE LOSSES

Hybrid Frame-Polysulfone-
Fiberglass Epoxy, 80Au-20Pt
Cathode, Supported Catalyst
Anode. Polysulfone ERP's

Rig 38750-41 0.1146 Ft^2 (106.4 cm^2)
180°F (82.2°C)/16 psia (11.0 n/cm^2)/34% KOH/PWR

	Performance			IR Loss		100 ASF (107.6 ma/cm^2) Diffusion Losses			
Load Time (Hrs)	1.0 ASF (1.076 ma/cm^2) (Volts)	2.0 ASF (2.152 ma/cm^2) (Volts)	100 ASF (107.6 ma/cm^2) (IR Corr.)	100 ASF (107.6 ma/cm^2) (mv)	Activation Loss (mv)	Total (mv)	Anode (mv)	Cathode (mv)	
14	1.027	1.013	0.815*	15	—	130	120	10	
62	1.026	1.011	0.889	14	1	49	42	7	After Refill
322	1.022	1.010	0.888	14	5	42	37	5	
347	1.026	1.014	0.901	13	1	31	20	11	After Refurb.
1527	1.022	1.009	0.888	14	5	51	40	11	

V. SYSTEM DESIGN STUDIES

A study was performed to determine how the conceptual design of the Engineering Model System would be changed to accommodate the requirements of the Space Tug application, particularly the lower power and voltage. Major conclusions are:

- The EMS schematic is modified by substituting a pumped liquid cooling loop for the original evaporative cooling system and (if water recovery is needed) by incorporating a static condenser/separator to condense product water vapor and remove it for storage. Passive water removal in the stack is retained.

- The EMS stack configuration is modified by changing the number of 0.1146-ft^2 (106.4-cm^2) cells per plaque from six to two and by reducing the number of plaques from 88 to either 17 or 34 depending on the desired Tug power level. Use of the two-cell plaque keeps the multicell plaque option open for future higher power, higher voltage requirements.

- Estimated weight of a complete 3-kw cell stack (34 plaques with coolers and end-plates) is 17 pounds (8 kilograms) which is consistent with a Tug powerplant minimum weight of 33 pounds (15 kilograms), assuming water recovery is not required. Stack dimensions (including end plates) are 7.2 inches thick x 5.6 inches wide x 14.5 inches long (18.3 x 14.2 x 36.8 cm).

A. Introduction

During Phase III, a study was performed to define alternative Engineering Model System (EMS) configurations tailored to the requirements of the Space Tug Powerplant. Specifically, the study set out to resize the total cell area and number of cells in the stack to meet lower Tug power and voltage requirements and to determine if alternative heat and water removal concepts could simplify the system or stack, reduce weight, or reduce volume. This was possible because the design requirements of the Space Tug Powerplant are significantly different than those of the original Phase I EMS; see Table XXIII. The original requirements strongly influenced the choice of some of the EMS concepts and subsystems. The new Tug requirements permit a greater choice of processes for heat and water removal. For example, the EMS technical specification included a requirement to provide an open cycle heat removal capability. This constraint led to evaporative stack cooling with static separation of the water/steam mixture within the stack. Another ground rule required that motor-driven pumps and blowers could not be used. This led to passive water removal and a "static" condensation process. During Phase III, no Tug requirement for open-cycle heat removal could be foreseen by either the government or potential prime contractors. This allowed circulating liquid, either single or two-phase, to be considered. Minimizing ancillary power requirements by eliminating electrical motor-driven pumps remains a worthwhile objective but may not necessarily be optimum from the standpoints of total weight and development difficulty.

TABLE XXIII

COMPARISON OF DESIGN REQUIREMENTS

	ENGINEERING MODEL SYSTEM – PHASE I	SPACE TUG – PHASE III
Life		
Qualification Endurance (hours)	10,000 with refurbishment	2500 without refurbishment
Expected Usage (hours)	–	700
Electrical		
Voltage:		
normal range (volts)	117±5%	30±2.5
peak power (volts)	100	–
Power:		
normal range within voltage (kw)	1.4 - 7.0	0.5 -1.5
peak (kw)	21	1.5 or 3.0
average (kw)	–	0.5 - 1.0
Ancillary Component Power	Minimized	Minimized
Degradation, max. (μv/hr./cell)	5	–
Thermal		
Heat Rejection Mode:		
nominal	Spacecraft radiator	Interface exchanger(s) with Spacecraft Radiator Loop
peak power	open cycle/steam venting/etc.	
Coolant Outlet Temperature to Radiators	Maximum consistant with life and performance	–
Reactants		
Fuel and Oxidant	Propulsion grade, H_2 and O_2 –	Propulsion grade H_2 and O_2 or High purity H_2 and O_2
Specific Fuel Consumption	0.7lb/kw-hr. (0.32 kg/kw-hr)	–
Source Pressure psia (n/cm^2)		
Propulsion grade	35 - 1000 (24-690)	15 - 1000 (10-690)
High purity	–	
Structural		
Weight	20lb/kw (9 kg/kw)	–
Volume	0.5ft^3/kw (14000 cm^3/kw)	–

Seven candidate FCP configurations are described along with the Phase I system configuration. The Phase I EMS system employs evaporative cell cooling and passive water removal. Five of the potential Phase III configurations employ passive water removal as well, but differ from the Phase I system by using fluid cooling, either water or a fluorocarbon liquid. Another configuration is cooled by both liquid and recirculated hydrogen, and the hydrogen flow is also used to remove the product water. The remaining configuration uses evaporative cell cooling and passive water removal as in the EMS, but accomplishes these functions with two separate subsystems rather than the single loop in the EMS.

The liquid cooling is described as single phase in the discussion that follows. However, it could alternatively be two-phase circulation with boiling taking place within the cell stack. The vapor in the two-phase mixture could then be condensed in a condenser/interface heat exchanger. An open-cycle option could be added by provision of an external vapor separator in place of the condenser.

B. Alternative System Concepts

Phase I EMS - This system, shown in Figure 52, was discussed in detail in the Final Report for Phase I, but a brief description is included here for reference. The Phase I EMS cell stack employs evaporative cooling and passive water removal. Steam formed in the stack coolers and the product water vapor are mixed at the stack outlet and, under closed cycle operation, condensed. The condensate is then returned to the stack coolers through a reactant-driven water pump. The excess water goes to a water storage tank, i.e., the product water portion of the condensate. During open cycle operation, the combined steam flows are vented to space, and cooling water comes from the water storage tank.

Stack temperature is maintained at a constant value by a pressure regulator in the cooler stream outlet line that regulates the steam compartment pressure. Water is fed into the cooler on demand through a pressure difference regulator that seeks to maintain a constant water-steam pressure difference. The stack combined steam outlet pressure is controlled in the closed cycle mode by a regulator that controls the pump recirculation loop ejector flow. In open cycle operation, a pressure regulator performs this function by controlling the vent flow. Proper ejector flow is maintained under all conditions by regulating the flow in a bypass loop in parallel with the ejector to maintain a constant ejector outlet pressure.

Hydrogen that may carry over into the water loop in the product water vapor is removed from the loop to the overboard vent line through a small hydrogen separator.

Reactants are supplied through coupled regulator valves that control the inlet pressure to the stack. The hydrogen, before going to the stack, passes through and actuates the diaphragm water pump that feeds cooling water to the stack. The oxygen passes through an ejector that induces a recirculation of oxygen from the stack to the oxygen feed line. This serves to humidify the inlet oxygen stream and prevent electrolyte drying during extended operation (10,000 hours for Phase I). Purge valves are provided to permit control of reactant impurities.

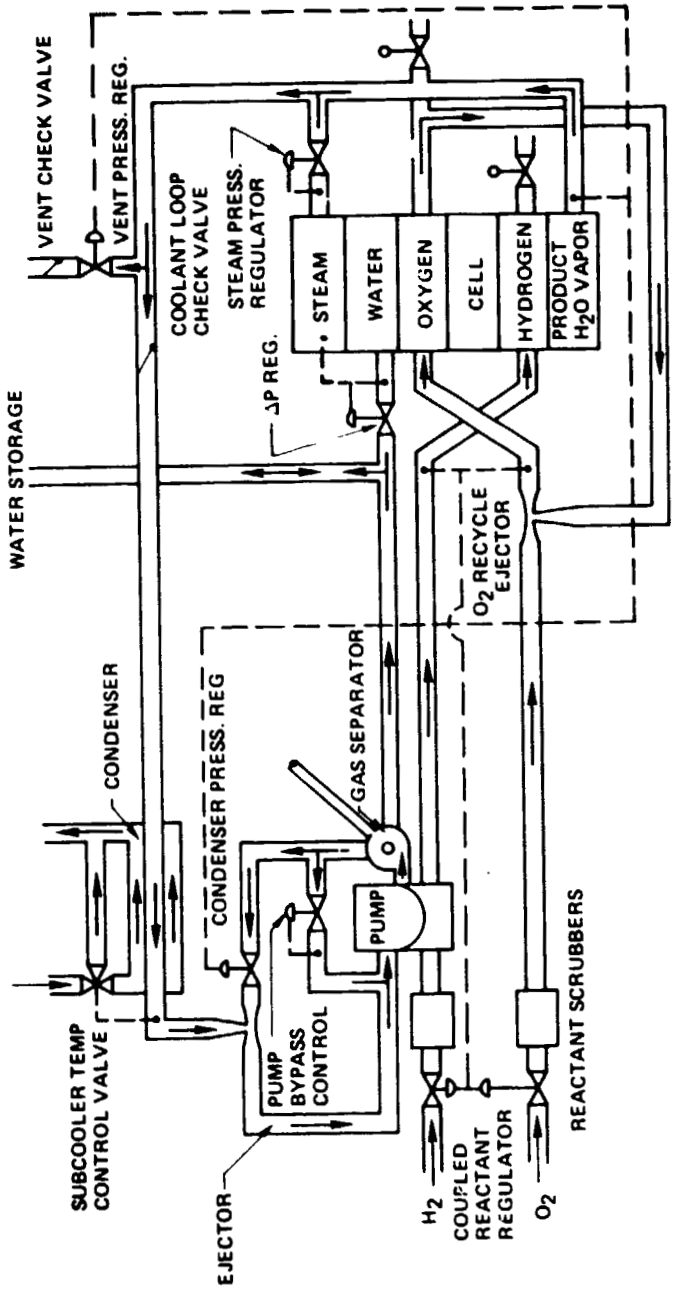

Figure 52 – Phase I Engineering Model System Schematic

Phase III Options - Seven candidate FCP configurations were considered in the Phase III system study. Five of these employ passive water removal and fluid cooling. These five all have the same basic powerplant schematic except for product water conditioning. That basic schematic is shown in Figure 53. Reactants are fed into the stack and vented from the stack via a reactant control. The stack is cooled by a single-phase or two-phase fluid cooling loop containing a pump, accumulator, startup/sustaining heater, and bypass leg with thermal control valve. This loop is cooled in turn by a vehicle cooling loop through an external heat exchanger. Product water vapor pressure in the passive water removal cavities within the stack is controlled by a vent regulator. The first five options differ only in the method of condensing and disposing of the product water. These different methods are as follows:

Option	Description
1	Static condenser/separator cooled by spacecraft coolant
2	Static condenser/separator cooled by fuel cell coolant
3	Jet condenser system cooled by spacecraft coolant
4	Jet condenser system cooled by fuel cell coolant
5	Jet condenser contained in fuel cell cooling loop

The schematics for the static condenser system and the jet condenser system are shown in Figures 54 and 55 respectively.

Option 6 uses fluid cooling, but product water is removed by evaporation into a circulating hydrogen stream rather than into a low pressure steam cavity. Some of the waste heat is also removed in the hydrogen.

Option 7 uses passive water removal and evaporative cell cooling with internal steam separation as in the EMS, but the functions are kept in two separate subsystems rather than combined.

Phase III Option I – Figure 56 shows the schematic for this configuration. It employs a cell stack that features passive water removal and heat rejection to a circulated fluorocarbon coolant. The coolant is pumped through the stack by a motor driven pump, picking up heat. It is circulated around the loop and through an interface heat exchanger where the heat is rejected to the spacecraft coolant loop. A bypass line around the heat exchanger is used for low load operation when the full cooling capacity of the heat exchanger is not required. A start/sustain heater at the stack inlet, controlled by a temperature switch at the stack outlet, serves as a means to warm the stack rapidly on startup and to maintain the stack temperature at low load. The loop is provided with an accumulator, pressurized from the reactant supply.

Product water passes from the stack through a pressure regulator that controls the vapor cavity pressure to a fixed value. It then passes through a 3-way valve that directs it to the overboard vent through which it is dumped to space, or directs it to a static condenser/separator where it is condensed before being stored on-board, avoiding venting for extended periods if necessary.

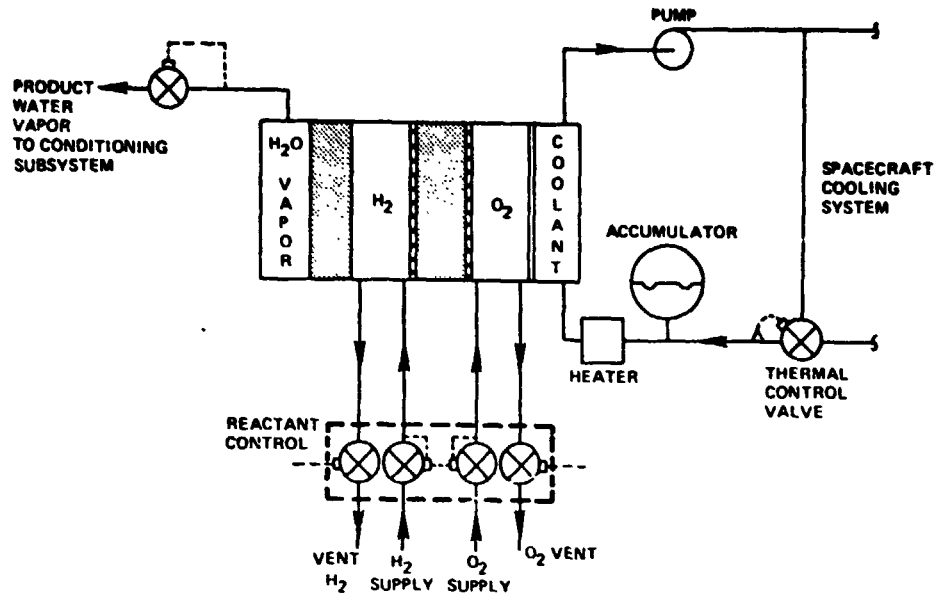

Figure 53 – Basic Powerplant Schematic for Options 1–5 with Product Water Conditioning Omitted

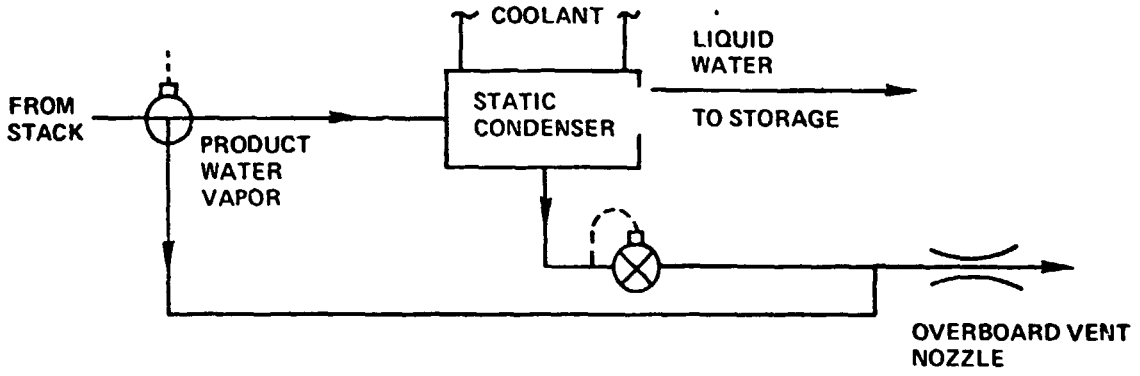

Figure 54 – Static Condenser System Schematic

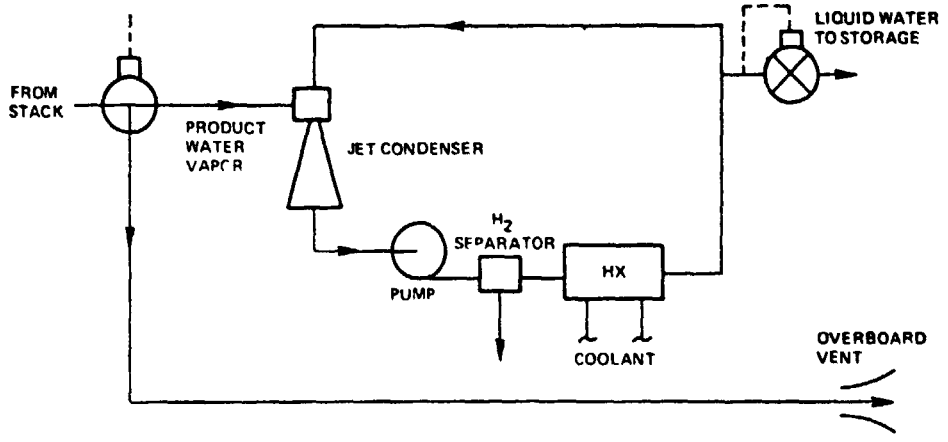

Figure 55 – Jet Condenser System Schematic

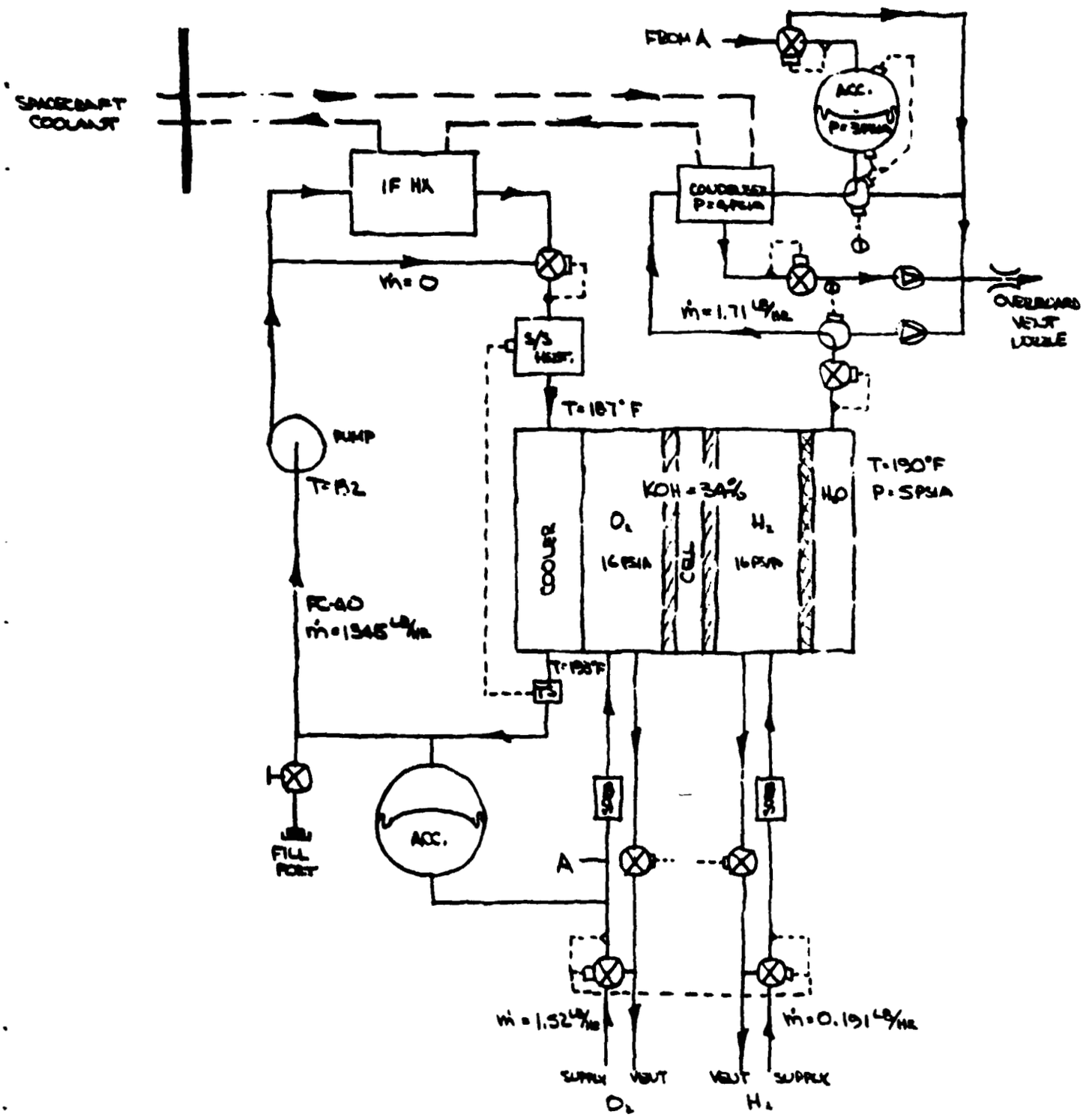

Figure 56 – Option 1 (Non-Integrated Static Condenser/Separator Schematic)
Net Power Output (dc) = 2000 Watts

The static condenser/separator is essentially a two-chamber device separated by a hydrophilic matrix. Product water vapor enters the steam cavity where it contacts cooling coils and condenses. It is immediately taken up by the matrix through which it passes by means of a pressure differential maintained across the matrix. The maximum pressure in the steam chamber is limited by a pressure regulator in a vent line to space that allows non-condensables to be dumped overboard. The pressure downstream from the matrix is maintained by the pressure regulator that controls the product water accumulator pressure. A 3-way valve at the accumulator inlet either allows the accumulator to fill from the condenser, or allows it to dump overboard.

The condenser/separator, in this option, is cooled directly by spacecraft coolant as is the interface heat exchanger. Spacecraft coolant flows first through the condenser and then through the interface heat exchanger to permit minimum weight heat exchangers.

Reactants are supplied through coupled regulator valves that control the inlet pressure to the stack. Purge valves are provided to permit removal of accumulated reactant impurities.

Phase III Option 2 – This configuration, shown in Figure 57, is the same as Option 1 except that the condenser/separator is integrated into the powerplant coolant loop. For this concept, the temperature at the outlet of the interface heat exchanger must be significantly lower than in Option 1. To accomplish this objective without rejecting more heat than necessary, a provision for reducing the flow through the heat exchanger is made by providing a line bypassing both the heat exchanger and condenser. This bypass flow is controlled to maintain a given temperature after the two loops rejoin at the inlet of the start/sustain heater. The bypass loop around the heat exchanger is still necessary during startup.

Phase III Option 3 and Option 4 – These two systems, shown in Figures 58 and 59 respectively, are the same as Options 1 and 2 respectively except that product water vapor condensation is accomplished by means of a jet condenser in a separate water circulation loop. The jet condenser takes the place of the static condenser/separator and may save system weight.

When condensation of the product water vapor is desired, the vapor is directed by a 3-way valve to the water circulation loop. Although the pressure level in the loop is generally higher than in the product water vapor cavity in the cell stack, flow from the stack to the loop is induced by means of the jet condenser which, acting as an ejector, creates a locally lower pressure as its nozzle throat. As the vapor contacts the cooler water of the loop and as the pressure recovers in the diverging section of the jet condenser, the vapor condenses, raising the temperature of the flow stream.

After passing through a motor driven pump, the water stream goes to a heat exchanger (not a condenser) where the heat picked up through the condensation of the vapor is rejected. In Option 3, the heat is rejected directly to the spacecraft coolant as in Option 1. In Option 4, the heat is rejected to the powerplant coolant loop as in Option 2.

Before returning to the jet condenser, any hydrogen carryover into the water loop is removed in a hydrogen separator. This could be a dynamic device or a Ag-Pd tube as used in the Apollo Command Module.

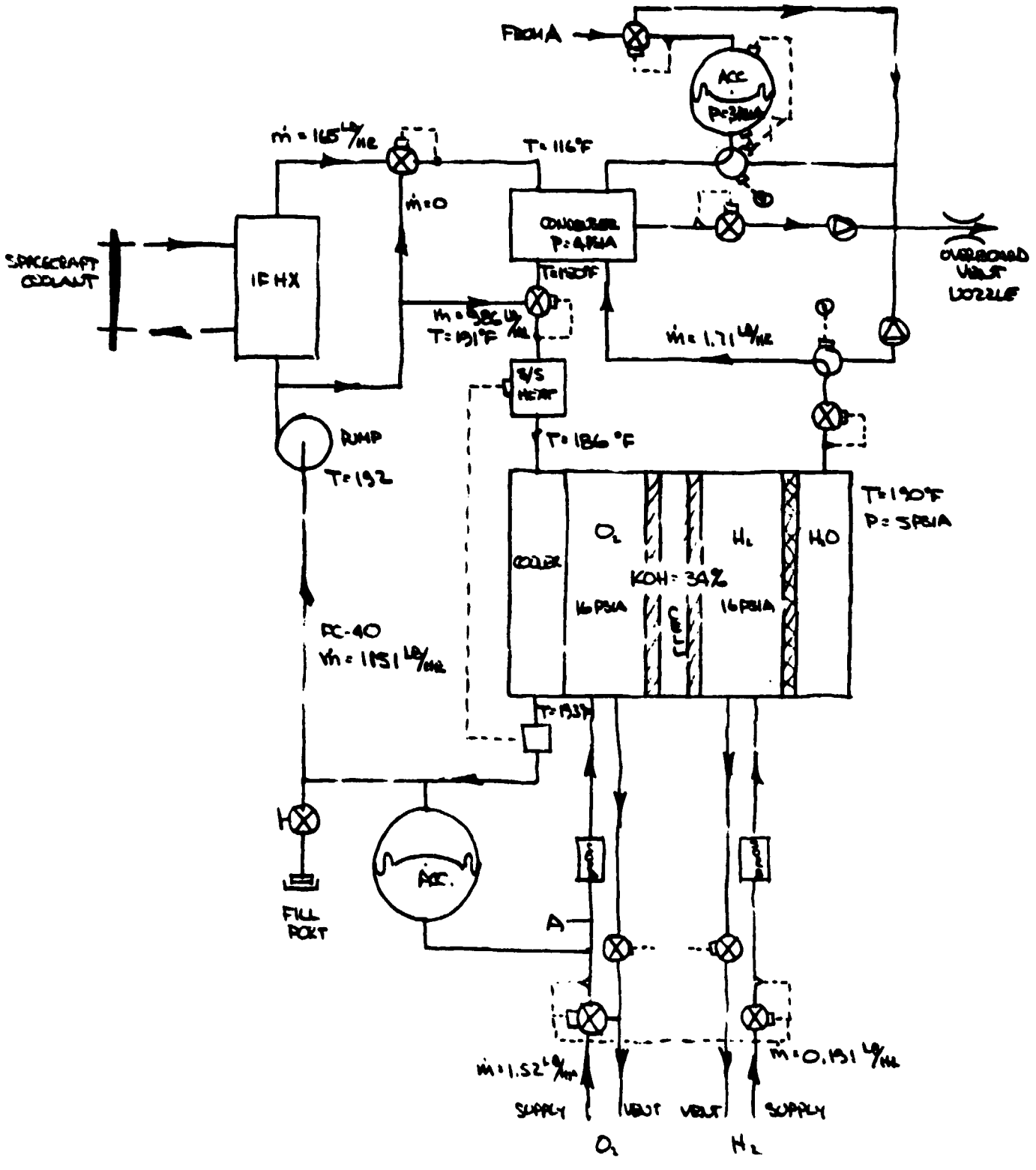

Figure 57 -- Option 2 (Integrated Static Condenser/Separator)
Net Power Output (dc) = 2000 Watts

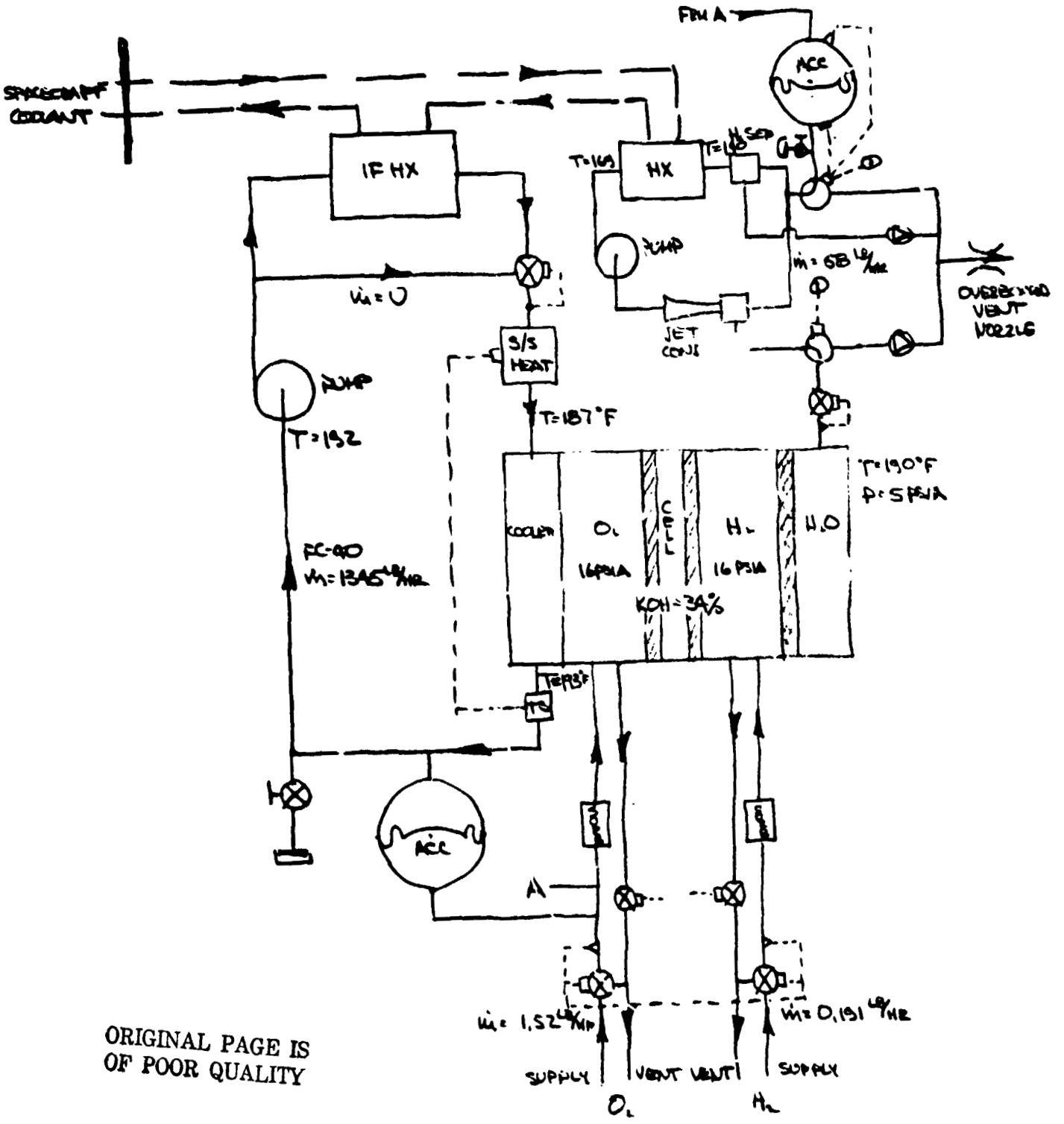

ORIGINAL PAGE IS
OF POOR QUALITY

Figure 58 – Option 3 (Non-Integrated Jet Condenser)
Net Power Output (dc) = 2000 Watts

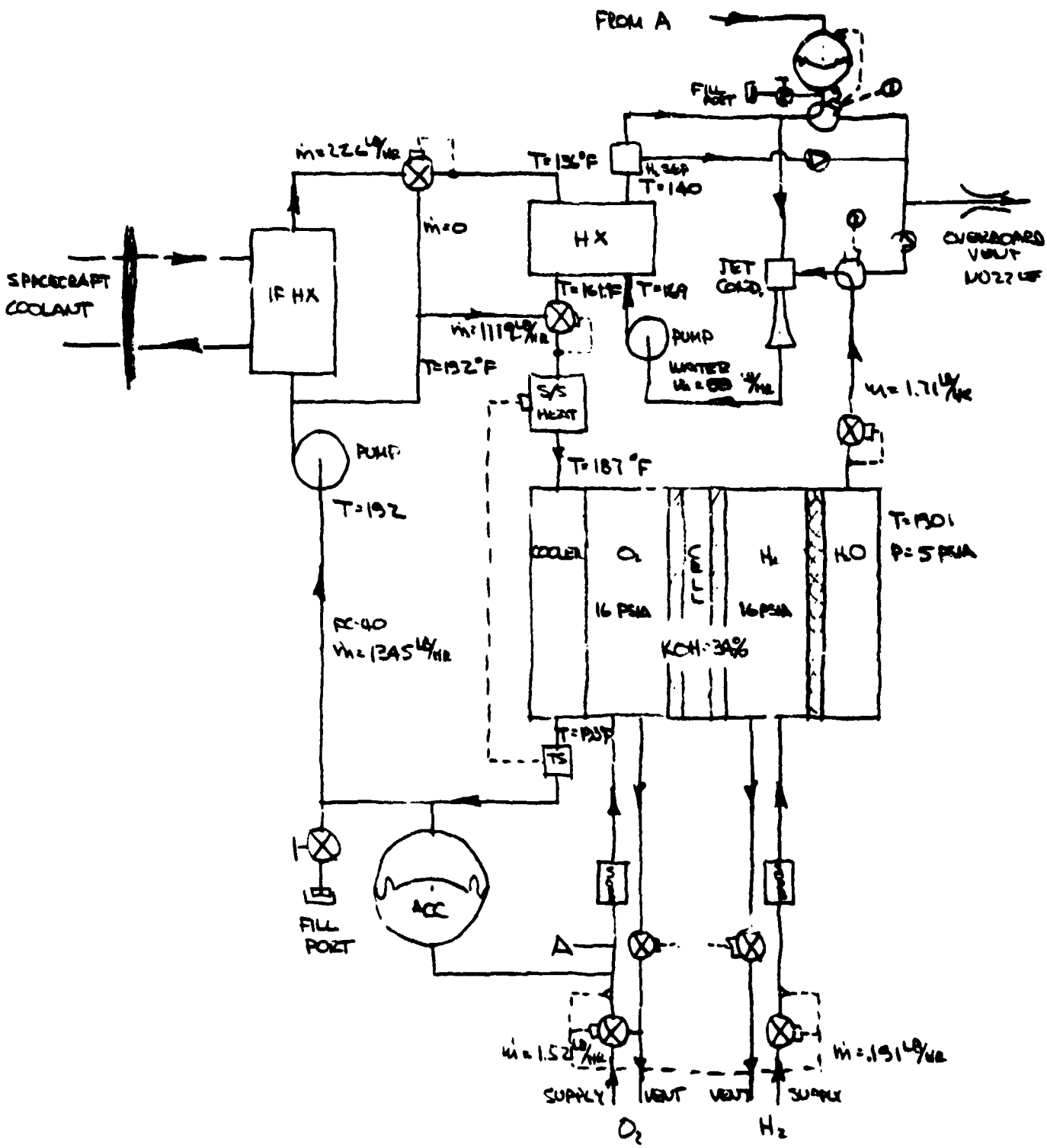

Figure 59 – Option 4 (Integrated Jet Condenser)
Net Power Output (dc) = 2000 Watts

Phase III Option 5 – A jet condenser is also employed in this configuration, but, as is shown in Figure 60, it is integrated directly into the powerplant cooling loop. For this to work, the powerplant coolant must be water as the coolant is mixed with the product water for condensation. Otherwise, the system is similar to the Phase III options previously described.

The new components in this coolant loop are a hydrogen separator, a regenerative heat exchanger, and a jet condenser. The hydrogen separator removes any hydrogen carried into the coolant loop with the product water vapor. The regenerative heat exchanger is used at low load to drop the temperature of the coolant entering the interface heat exchanger so that the coolant exiting the interface heat exchanger can be lowered to meet the inlet requirement of the jet condenser without rejecting excessive heat. Data in the literature indicates it is not desirable to achieve jet condenser inlet temperature control by reducing the flow in the interface heat exchanger/jet condenser loop because the jet condenser requires a constant flow for proper operation.

In this system, the product water, when not vented directly overboard, is collected in the coolant loop and in time causes the loop accumulator to fill up. On response from a high level switch signal, the accumulator is dumped through a 3-way valve to the overboard vent.

While this is occurring, the 3-way valve at the stack outlet directs the product water vapor to the same vent. The product water vapor may be vented at any time.

Phase III Option 6 – All of the preceding systems operate at low pressure (~15-30 psia). This option, shown in Figure 61, uses a higher pressure to reduce the effect on performance of low reactant partial pressure. This configuration is essentially the same as that being designed for the Space Shuttle Orbiter Program. The preliminary operating conditions and flow rates are based on the DM-2, a Space Shuttle demonstrator powerplant operated for 5070 hours under NASA contract.

The coolant loop is the same configuration as employed in Options 2 and 1. The product water vapor is removed from the stack by a recirculating hydrogen loop. Hydrogen enters the stack, and, as it passes through, some is consumed and replaced by water vapor while the stream receives some of the heat rejected by the stack. After leaving the stack, it passes through a condenser where the product water vapor is condensed and the stream cooled. The gas-water mixture then goes to a hydrogen pump-separator where the liquid water is removed and the gas returned to the stack inlet. Hydrogen used in the stack is replaced in the loop at the stack outlet. Purge venting is also accomplished from the loop of the stack outlet but upstream of the hydrogen inlet point.

Product water may be either vented to space or stored in a product water accumulator. The accumulator will discharge automatically at a high level signal. Both the 3-way valve and the accumulator dump valve act in concert so that both will be open to the vent nozzle at the same time.

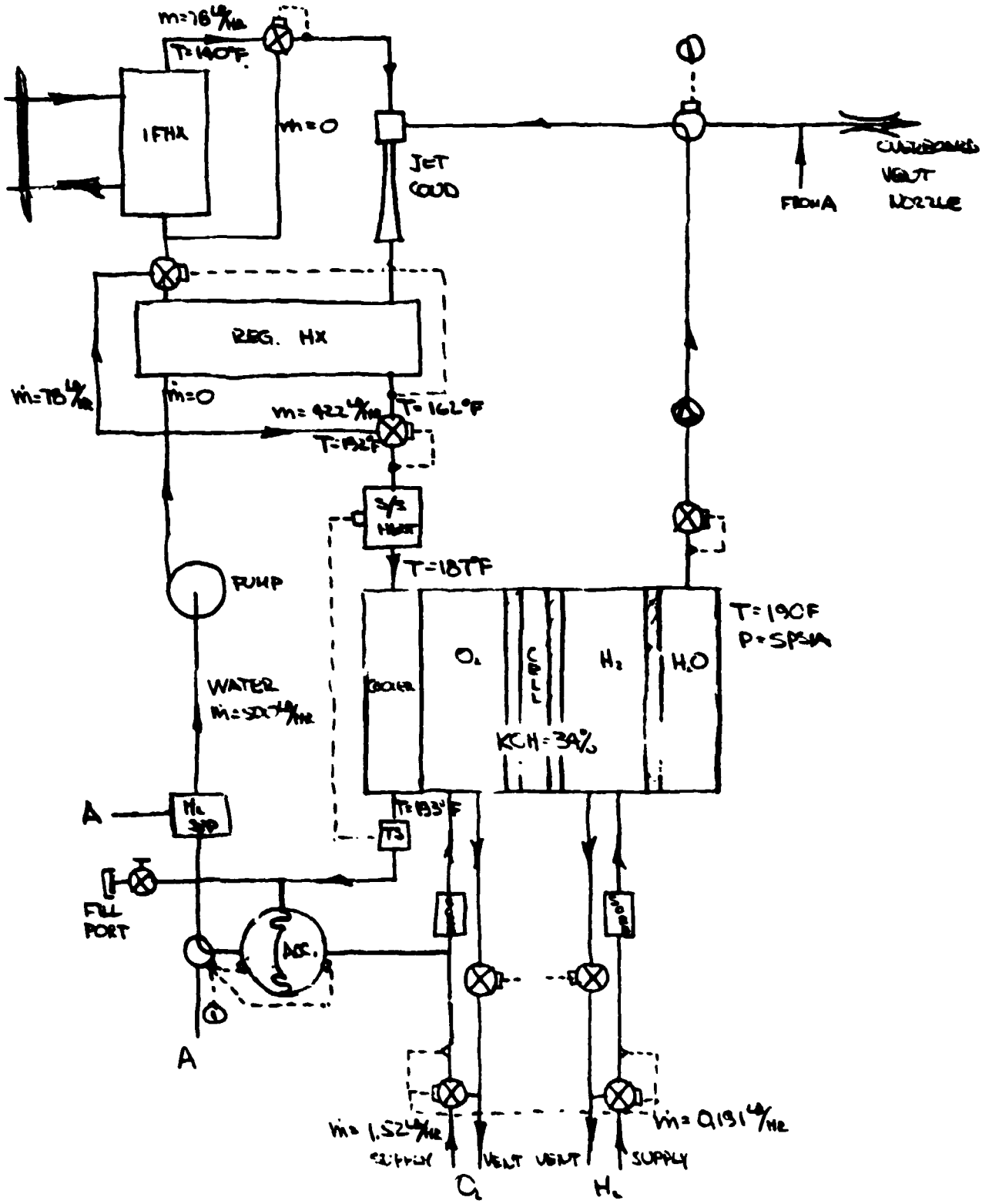

Figure 60 — Option 5 (Main Loop Jet Condenser)
Net Power Output (dc) = 2000 Watts

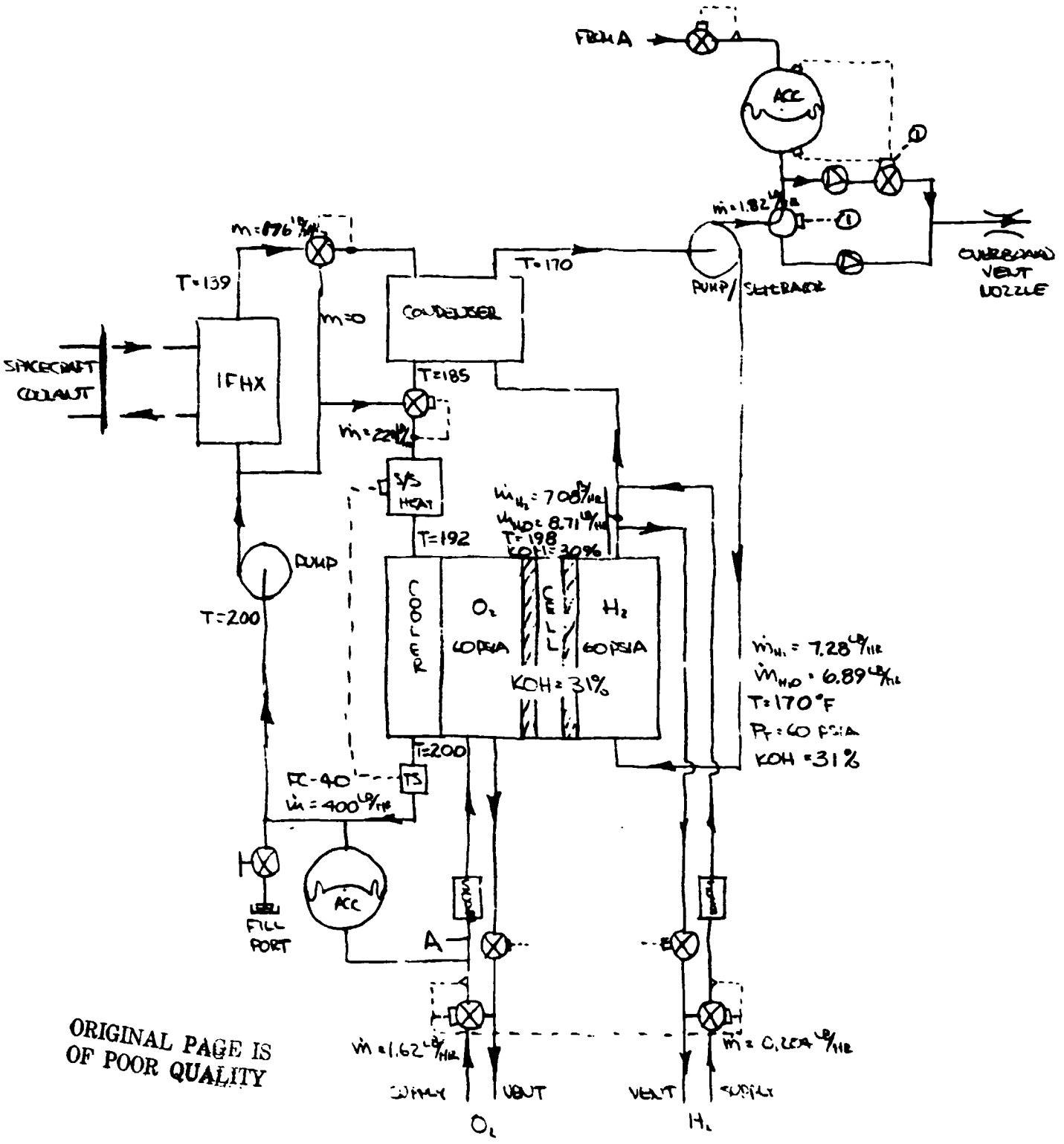

ORIGINAL PAGE IS
OF POOR QUALITY

Figure 61 – Option 6 (Water Removal in Recirculated Hydrogen)
Net Power Output (dc) = 2000 Watts

Phase III Option 7 – This option, shown in Figure 62, maintains the essential features of the Phase I EMS stack design; i.e., passive water removal and evaporative cooling. The system arrangement is changed to separate the water removal and heat removal subsystems and to utilize an electric-driven, rather than gas-driven, water coolant pump. The subsystems operate similar to Option 1 described previously, except that this option, like the Phase I EMS, has no heater for startup or low load operation.

Comparison of Configuration Options

The first area of comparison is ancillary power. The Phase I EMS is designed in such a way as to require essentially no continuous ancillary power. All the above options require power for pumps. It is assumed in all cases that the powerplants are insulated well enough to require no guard heaters to maintain end-cell temperatures and no sustaining heater to maintain powerplant temperature at low load. A preliminary estimate of the ancillary power for the various options is shown below. The coolant loop in Options 1 through 6 is assumed to be single phase. Two-phase cooling would reduce the flow requirements and hence the coolant loop pump power.

	Phase I	Phase III Options						
	EMS	1	2	3	4	5	6	7
Coolant Loop Pump (watts)	---------	45	50	45	50	30	32	25
Product Water Loop Pump (watts)	---------	----	----	30	30	----	50	----

The Phase I EMS and Options 1, 2, 5 and 7 are the most advantageous from the standpoint of ancillary power. However, the power required varies only by 57 watts from the lowest to the highest option.

Operating pressure is another important area of comparison. Option 6 has a performance advantage because it operates at a higher pressure level than the other options. The other options would require an increase in the pressure differential which could be sustained across the water transport plate before higher pressure operation could be considered.

This leads to another area of comparison; stack cooler configuration. The coolers employed in all options except the Phase I EMS are of relatively simple configuration. The Phase I EMS relies on a coolant phase change and vapor separation within the cell stack, and therefore requires a more complicated and heavier cooler with provisions for maintaining phase interface control in zero-gravity. The advantage of such an evaporative cooling arrangement is a low coolant flow requirement and consequently lower pump power. As mentioned previously, the same effect can be achieved by using a circulating two-phase coolant with vapor separation outside the stack.

A fourth difference between options is the type of condenser used. In the Phase I EMS and Options 1, 2, 6 and 7, a static condenser/separator is used. The other portions depend on a jet condenser. The advantages of a static condenser are that it is fairly conventional in design and requires no additional flow either in the main coolant loop or an auxiliary coolant loop.

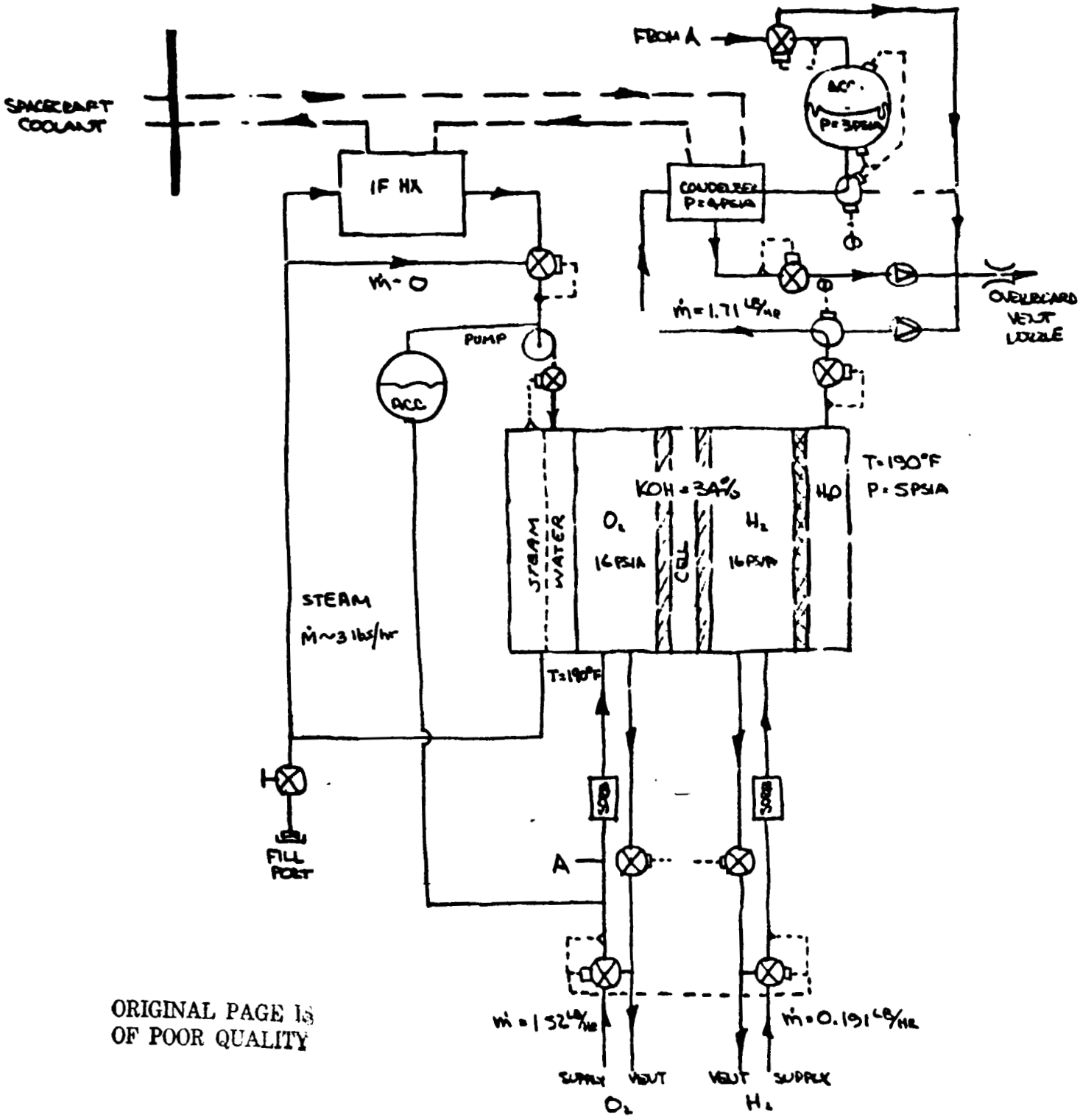

ORIGINAL PAGE IS
OF POOR QUALITY

Figure 62 – Option 7 (Non-Integrated Static Condenser/Separator-Evaporative Cooling Schematic)
Net Power Output (dc) = 2000 Watts

Its disadvantages are in the problems of maintaining gas-liquid interface control, but these are considered to be relatively small. The advantages of a jet condenser lie in the absence of a need to control gas-liquid interfaces and the fact that the heat exchangers involved are simple liquid-to-liquid. The main disadvantage is the need for a separate coolant loop, as in Options 3 and 4, or a much more complicated main coolant loop as in Option 5. There is also no simple method of separating hydrogen carryover from the product water vapor. For these reasons, a static condenser/separator is preferred over a jet condenser.

The cooling loop arrangement is the next point of comparison. The cooling loop differences are the extent to which the condenser/separator is integrated into the stack cooling loop. In Options 2, 4, 5, and 6, the condensers are integrated; in Options 1, 3 and 7 they are not. Because the temperature levels of these loops must be maintained well over 100°F (37.8°C) at the outlet of the interface heat exchanger in order to prevent rejecting too much heat at low load, the size of the condenser or condenser loop heat exchanger must necessarily be larger if it is integrated with the stack cooling than if it is independent and receives coolant at a colder temperature. The interface heat exchanger size will also be smaller because it does not have to reject the condenser heat load. The non-integrated condenser arrangement offers lower weight.

It must be observed that the Phase I EMS seems to have a distinct advantage in that the low coolant flow associated with evaporative cooling allows the use of a reactant gas powered pump requiring no power. High coolant flows are obtainable from a gas-driven pump if reactant supply pressure is sufficiently high. However, early development experience with this type of pump (under contract NAS9-11034) indicated significant problems associated with maintaining adequate flow over the full power range and excessive flow/pressure fluctuations. More development effort would be necessary to make this device suitable for a powerplant. At low reactant supply pressure, its practicality is tied to the use of evaporative cooling.

Based on these studies it was recommended that the EMS Schematic be modified in the following ways for the Tug application:

(1) Simplify the cell stack by substituting a pumped liquid cooling loop for the baseline EMS evaporative cooling system with internal steam separation.

(2) Incorporate a static condenser/separator to condense product water vapor and remove it for storage.

Options 1 and 2 both contain these features. The final choice can be made when the vehicle cooling system is better defined.

C. Alternative Stack Design

The purpose of the alternative stack design study was to; (1) review the present baseline EMS stack and plaque design and recommend changes to the design in view of the lower power and voltage requirements of the Space Tug, and (2) to factor the results of the experimental program to date into the stack design.

EMS Plaque Design

The EMS plaque was designed with a higher power output and higher voltage requirement than that of Tug. The baseline plaque is an integral assembly containing six cells, intercell seals, and manifolds molded into a plastic edge frame. A plan view of the plaque is shown in Figure 63. Each cell is 12 inches (30.4 cm) long and 1.375 inches (3.49 cm) wide and contains 16.5 in^2 (106.4 cm^2) of active area. Total active area per plaque is 0.69 ft^2 (638 cm^2). The six cells are electrically connected in series by connecting the anode of one cell to the cathode of the adjacent cell through the intercell seal. These seals are 0.25 inches (0.64 cm) wide and insulate adjacent cells from each other, physically support the various cell elements, and isolate the reactant gases from each other at the cell edges. The 0.50-inch (1.27-cm) wide edge frame assembly is molded around the cells and fluid manifolds to provide a unitized plaque assembly.

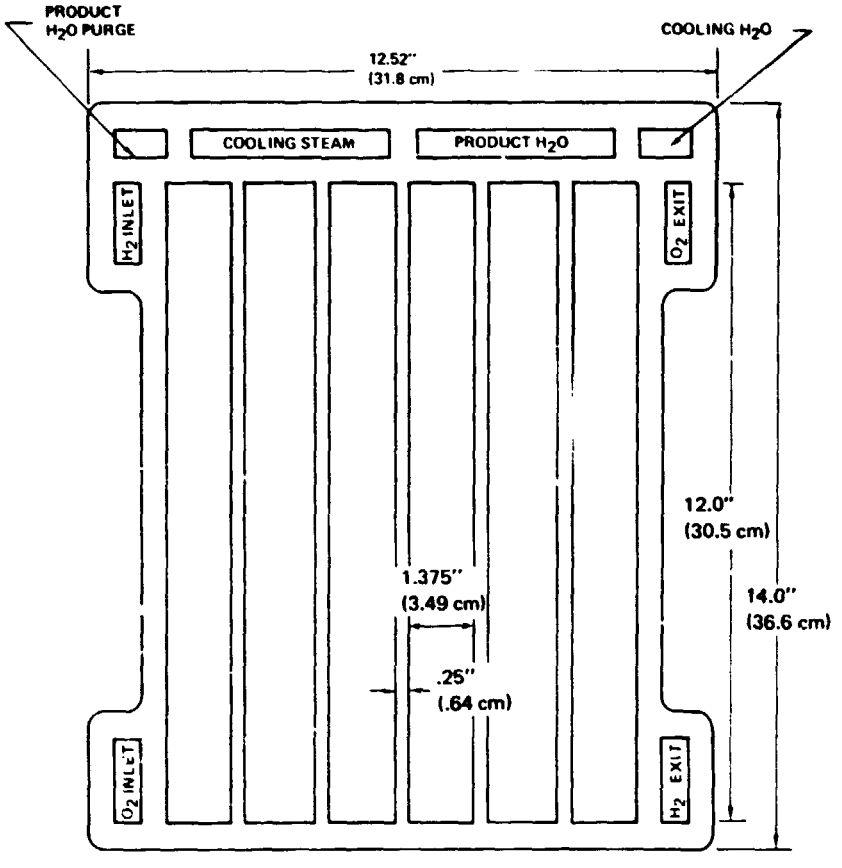

Figure 63– EMS Baseline Plaque Planform

Fluid distribution is handled in two steps: manifolds and ports. Manifolds are fluid flow passages perpendicular to the plaque plane; they provide flow to or from the ports. They are formed when the openings in the edge frames of adjacent stack components are aligned

during final stack assembly. As shown by the plaque plan form, there are eight manifolds within the EMS stack; two for reactant gas inlet, two for reactant gas purge, one for cooling water inlet, one for cooling water vapor exit, one for product water vapor exit, and one for product water vapor purge.

Ports are fluid flow passages parallel to the plaque plane. They provide the flow path between the manifolds and cells. Manifolds and ports are sized to provide low pressure drops consistent with uniform plaque-to-plaque flow distribution. The reactant purge manifolds are larger than required by flow considerations and were chosen to make the plaque planform symmetrical.

Tug Stack Design

Analysis of the Tug power requirements indicated a fuel cell active area of 0.1 to 0.3 ft^2 (92.9 cm^2 to 278.7 cm^2) was sufficient to meet the specified power and voltage regulation. Consequently, four stack designs with cell areas in this range were examined. The cell areas were either single cell plaques of the baseline configuration with an active cell area of 0.1146 ft^2 (106.4 cm^2) or twice this area, 0.229 ft^2 (212.8 cm^2), or a two-cell plaque configuration of 0.1146 ft^2 (106.4 cm^2) per cell. The performance levels and degradation rate used for the studies were those exhibited by single Cell No. 30.

Stack weights were based on a liquid cooling system with passive water removal. The power output-voltage output characteristics of these stacks are shown in Figures 64 through 67. The weights and dimensions of these stacks are presented in Figure 68.

The plaque configuration recommended for the Tug application is a two-cell plaque with each cell having a area of 0.1146 ft^2 (106.4 cm^2). This configuration was selected because:

- It can be arranged as a 17-plaque stack to deliver 1.5 kw or a 34-plaque stack to deliver 3.0 kw.
- Seventeen two-cell plaques weigh slightly less than 34 single-cell (0.1146 ft^2) plaques for the 1.5 kw requirement.
- Thirty-four two-cell plaques weigh only slightly more than 34 single-cell (0.229 ft^2) plaques for the 3.0 kw requirement.
- Use of the two-cell plaque keeps the multicell plaque option open for future higher power, higher voltage requirements.
- Present cell processing and tooling can continue to be used.

The preliminary planform for this plaque is presented in Figure 69.

The estimated weight of 17 pounds for a complete 3-kw cell stack (34 plaques with coolers and end plates) is consistent with a Tug powerplant minimum weight of 33 pounds, assuming water recovery is not required. However, additional components resulting from requirements defined by vehicle or interface studies may add weight to the powerplant.

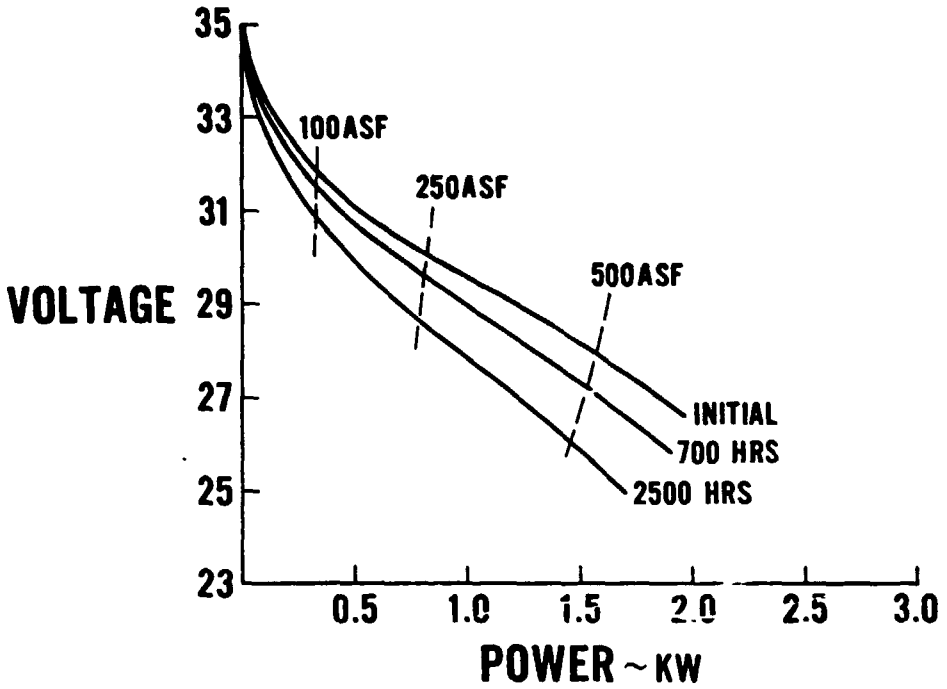

Figure 64 – Powerplant Performance (34 plaques, one cell/plaque-0.1146 ft^2 (106.4 cm^2)/cell)

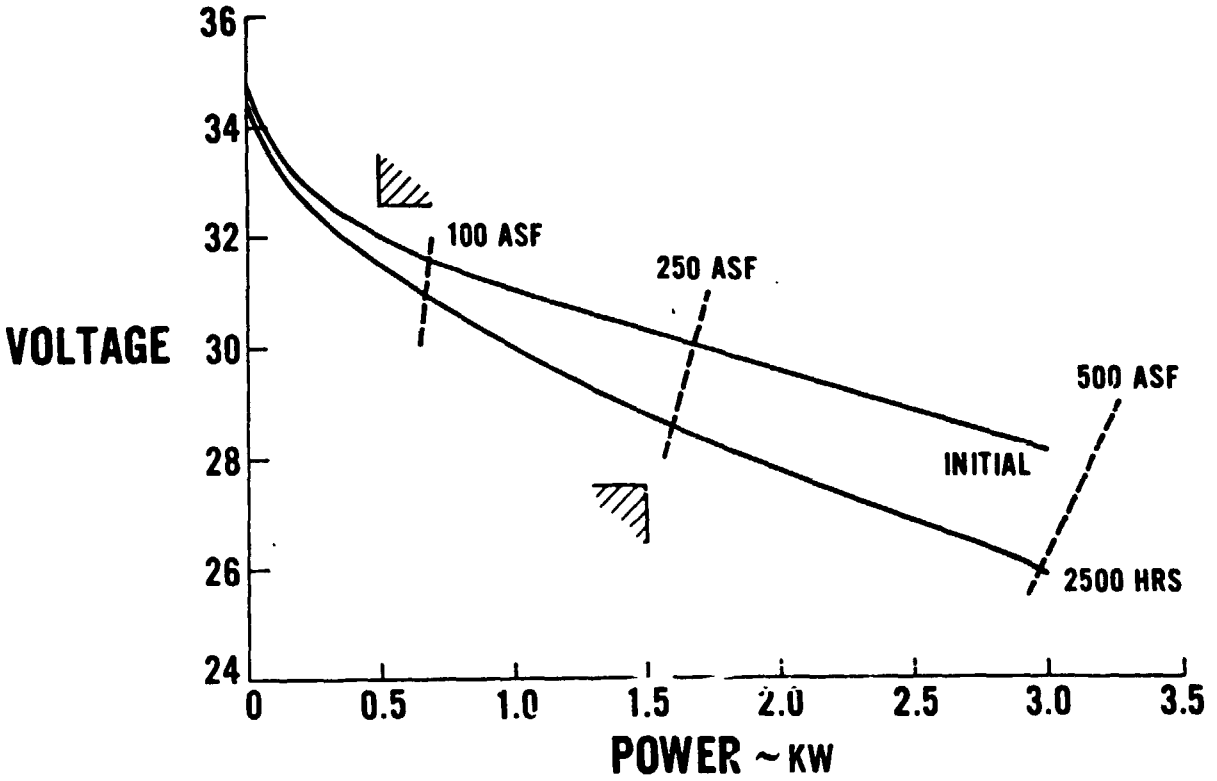

Figure 65 – Powerplant Perfc nance (34 plaques, one cell/plaque - 0.229 ft^2 (212.8 cm^2)/cell)

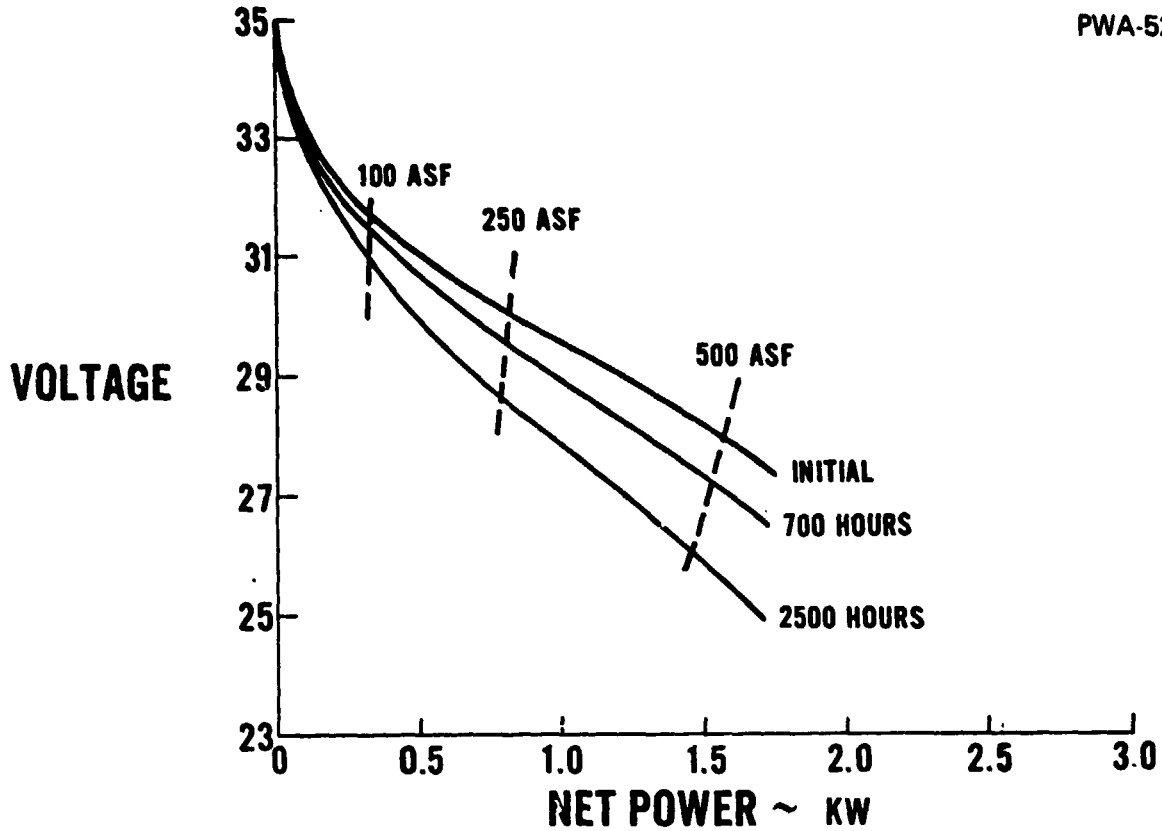

Figure 66 — Powerplant Performance (17 plaques, two cells/plaque - 0.1146 ft^2 (106.4 cm^2)/cell)

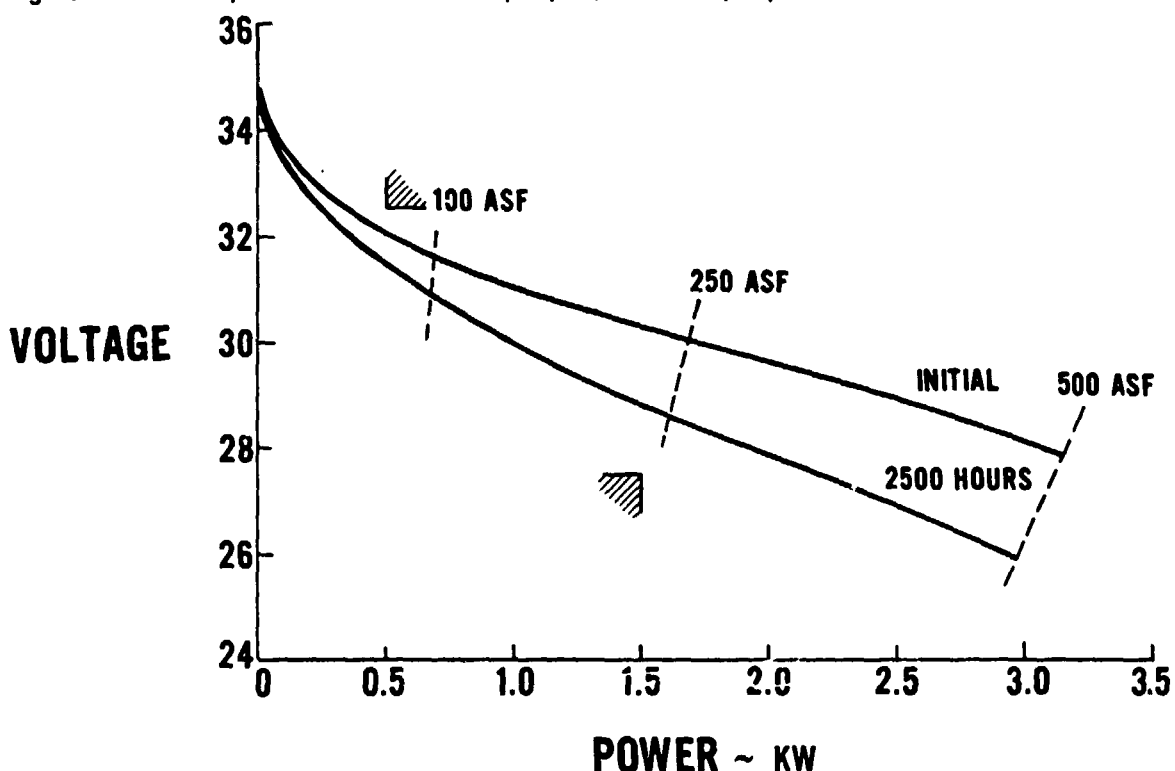

Figure 67 — Powerplant Performance (34 plaques, two cells/plaque - 0.1146 ft^2 (106.4 cm^2)/cell)

	1.5 KW MAX		3.0 KW MAX	
CELL AREA~FT^2	0.1146	0.1146	0.1146	0.229
NO. OF CELLS/PLAQUE	1	2	2	1
NO. OF PLAQUES/STACK	34	17	34	34
WEIGHTS ~ LBS				
PLAQUES	3.7	3.5	7.0	5.9
PWR ASSEMBLIES	3.3	2.7	5.4	5.2
COOLERS	1.4	1.1	2.2	2.2
END PLATES	1.5	2.4	2.4	2.2
TOTAL	9.9	9.7	17.0	15.5
DIMENSIONS~INCHES				
LENGTH	14.5	14.5	14.5	14.5
WIDTH	3.2	5.6	5.6	3.2
HEIGHT (WITH END PLATES)	7.2	5.1	7.2	7.2

Figure 68 – Weight Estimates of Candidate Stacks

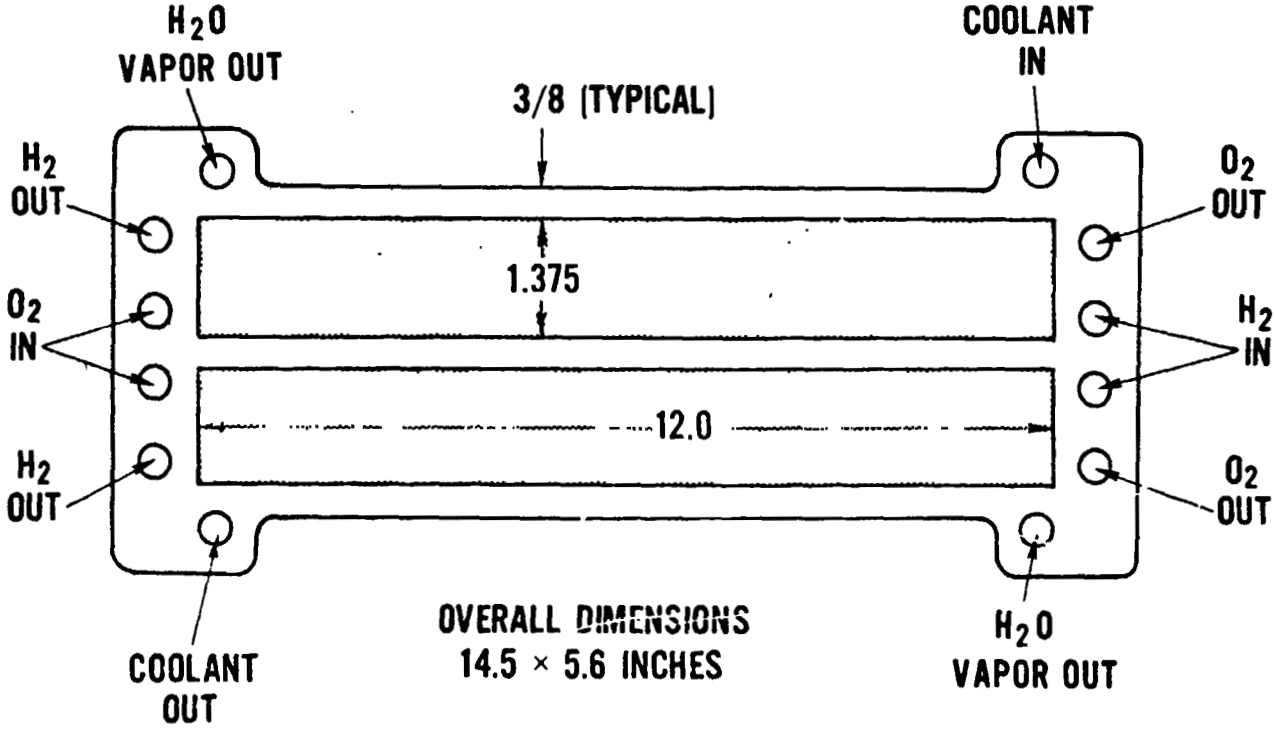

Figure 69 – Preliminary Planform of Two-Cell Plaque

APPENDIX

ANALYTICAL CONSIDERATIONS FOR DEVELOPING A HIGH BUBBLE PRESSURE MATRIX

APPENDIX

ANALYTICAL CONSIDERATIONS FOR DEVELOPING A HIGH BUBBLE PRESSURE MATRIX

Summary

This appendix reports the results of an analytical study conducted to support the NASA LeRC base fuel cell program NAS3-15339. Phase III of this contract included a small program to investigate the potential of a high bubble pressure matrix for use at 250°F or higher. It was found that the high bubble pressures measured with reconstituted asbestos matrix (RAM) could be related to the structure's mean pore size, but screen printed Teflon - bonded-Fybex potassium titanate did not show the same relationship. It was also found that high (30 pounds per square inch) bubble pressure Teflon-bonded-Fybex matrix structures could be produced by direct filtration onto an electrode. In addition, the 30 psi structures contained only one-half the material in comparison to standard RAM.

Program

The approach used in this study was to consider pore structure in a matrix to be a regular arrangement of small capillaries; where the capillary force, which would equal the expulsion force or bubble pressure, can be calculated. Relationships between the forces pulling a fluid up a capillary and the size of that capillary are well known. These forces are depicted in the diagrams shown in Figure 1.

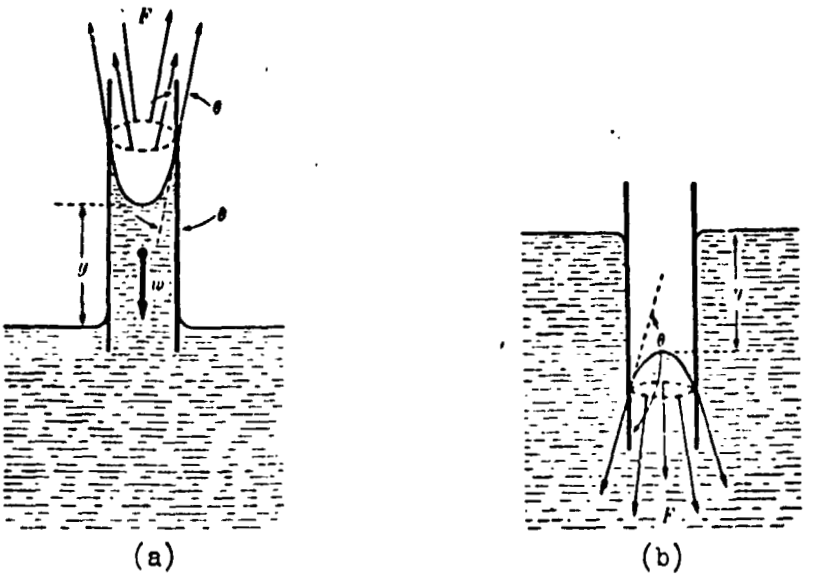

Fig. 1. Surface Tension Forces on a Liquid in a Capillary Tube. The Liquid Rises (a) if $\theta < 90^{\circ}$ and is Depressed (b) if $\theta > 90^{\circ}$.

The total upward force is

$$F = 2\pi r S_{sl}$$

Where: F= force,

r=radius of capillary,
S_{sl}= solid-liquid surface tension

when a cylinder of liquid of height y and radius r is isolated. This equation can in turn be related to the liquid-vapor surface tension by the relationship

$$S_{sl} = S_{lv} \cos \theta$$

where: S_{lv} = liquid-vapor surface tension,
θ = contact angle between a liquid and a solid (as shown in Fig. 2)

Fig. 2 Contact Angles Showing Nonwetting (a) and Wetting (b) Liquids

Thus the capillary force equation becomes

$$F = 2\pi r S_{lv} \cos \theta$$

The downward force is the weight of the liquid within the cylinder.

It was felt that the capillary tube could be considered as being formed by a wall of particles or fibers in a matrix and that the pore size of the matrix is the size of this capillary. The forces which must be overcome to permit gas flow through the capillary would be the capillary forces, and bubble pressure would be a measure of the expulsive force (pressure). Thus the capillary force equation can be further modified:

$$P = F/A = \frac{2\pi r S_{lv} \cos \theta}{\pi r^2} = \frac{2 S_{lv} \cos \theta}{r}$$

Where P = pressure,
A = area against which pressure is being applied (end of capillary)

The equation can be still further modified to relate to the mean pore size of a matrix which is the diameter (d) of that pore.

$$P = \frac{4 S_{lv} \cos \theta}{2r} = \frac{4 S_{lv} \cos \theta}{d}$$

It can be seen that maximum bubble pressures will be achieved when the matrix material is very wettable, that is, when $\theta = 0^o$ so $\cos \theta = 1$. Any other value of θ between 90 and 180^o produces values of $\cos\theta$ that vary from zero to minus one. Wetting is affected by changes in surface free energy (SFE) between a liquid and a solid as the solid is wetted. The total increase or decrease of SFE of the system determines whether or not a solid is wetted by a liquid. The SFE of a solid is directly proportional to its hardness and melting point, and metals and ceramics

generally have surface free energies several times greater than most liquids. The liquid-solid interfacial energy will be lower than the SFE of the solid when a liquid drop is in contact with a high energy surface. A maximal decrease in SFE of the system is realized when as much of the high SFE surface is wetted as is allowed by the energy balance. The energy released by wetting of the high SFE solid will exceed the energy consumed by the increase of the liquid surface as the drop spreads, and liquids will spontaneously tend to wet the solid. Thus, it was felt that the inorganic particulate and fiber materials used in many current matrix structures could be considered completely wetted by water and aqueous electrolytes.

It was also found that lower wetting angles are measured with water, and potassium hydroxide and phosphoric acid solutions as contact time between the liquids and Teflon is increased. Also, receding contact angles are generally lower than advancing angles. Thus, longer soak times should result in higher bubble pressures.

Calculations and experiments showed the following results (see Table):

1. Calculated and measured bubble pressures agree reasonably well for filtered RAM structures.

2. Bubble pressures of screen printed Fybex/Teflon compositions are lower than calculated, thought to be due to either nonuniformity of the structure and/or nonwetting caused by the Teflon bonding material.

3. Bubble pressures of filtered Fybex/Teflon approach analytically calculated values.

4. Bubble pressures of screen printed silicon carbide/Teflon structures are lower than calculated.

TABLE

Calculated and Experimental Bubble Pressures

Material	Prepared	Mean (a) Pore Size	(b) θ	Bubble Pressure (c) Calculated	Experimental
RAM	Filtered	0.7μ	0°	60psi	60psi
96 w/o Fybex/4 Teflon	Screen Printed	1	0	42	7-10
96 Fybex/4 Teflon	Screen Printed	1	85.5	4	7-10
96 Fybex/4 Teflon	Filtered	1(d)	0	42	30-33
96 SiC/4 Teflon	Screen Printed	2	0	21	2
96 SiC/4 Teflon	Screen Printed	2	85.5	2	2

Notes:
(a) Measured
(b) Calculated or assumed
(c) Measured with water
(d) Not measured but expected to be approximately the same as measured with a screen printed structure.

Another consideration was to relate the particle size required to yield a certain pore size. The particles were assumed to be spherically shaped and packed with maximum packing density. The re was again considered to be a capillary; thus the mean pore size could be c ulated from the two dimensional model shown in Fig. 3

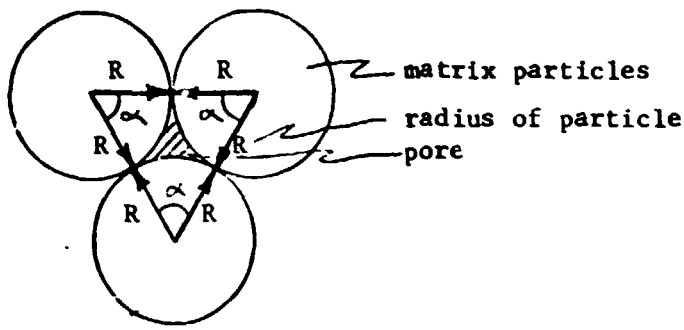

Fig.3 Model Showing Close-Packed Particles and Internal Pore

It can be shown that the area of the pore is $A=2R^2 \cos\alpha/2 - \frac{\pi}{2}R^2$

It can also be shown that the hydraulic diameter (d_h), or mean pore size, for this area is:

$$M.P.S.=d_h = \frac{4A}{p} = \frac{4(2R^2 \cos\alpha/2 - \frac{\pi}{2}R^2)}{\pi R} = 0.2R=0.1D$$

where p is the perimeter of the pore.

II. Conclusions

The following conclusions were drawn from the experiments and calculations described above:

1. High (30 psi) bubble pressure 96 w/o Fybex/4 Teflon 3170 matrix structures can be produced by filtering a water suspension of the material directly on a base cell electrode, followed by drying and sintering of the matrix. Bubble pressures between 30 and 33 psi were achieved with 1.6 mils of solids, half on each electrode. This is approximately half the solids content that is present in a standard 10 mil thick, 70 percent porous RAM matrix. The Fybex material has potential for long term use at 250°F. It lost essentially no weight; while RAM lost approximately 30 percent after corrosion testing 1000 hours at 250°F in 42 percent potassium hydroxide.

2. Greater bubble pressures can be achieved with a filtered than with a screen printed matrix. This is reasonable, as a filtered structure should be more uniform due to material always being deposited within the largest pore in the matrix during filtration.

3. Bubble pressure may be related to mean pore size in a very uniform (filtered), completely wettable matrix by the following equation:

$$B.P.\ (psi) \approx \frac{42}{M.P.S.\ (\mu)}$$

The presence of small amounts of Teflon bonding the structure may cause decreased wettability and bubble pressure.

4. The particle size required to yield a certain pore size in a matrix is on the order of:

$$M.P.S.\ (\mu) \approx 0.103D\ (\mu)$$

assuming the structure is densely packed uniform size spheres.

5. Also, the particle size required to yield a certain bubble pressure is:

$$B.\ P.(psi) \approx \frac{410}{D\ (\mu)}$$

again assuming the structure is densely packed uniform spheres.

III. Future Program

Future programs to develop better high bubble base matrix structures and to better understand the relationships between matrix structures and bubble pressures should include:

1. Cell tests to evaluate the high bubble pressure Fibex/Teflon matrix structures.
2. Evaluation of other filtered structures including a more regularly-shaped particle base cell material such as zirconia and the silicon carbide acid matrix material.
3. Evaluation of the curtain coater to deposit more uniform structures.
4. Evaluation of more wettable polymer bonding materials than Teflon; perhaps initial trials should be with polysulfone.

Bibliography

The following resources were used in preparation of the study conducted:

1. Discussions with R. Sawyer (many thanks, Dick).
2. College Physics, F. W. Sears and M. W. Zemansky, 1957.
3. "Wetting Properties of Aqueous KOH-Solutions," P. C. No. 30 G. M. Kohlmayr, November 25, 1964.
4. "Wetting of TFE Teflon and Platinum by Phosphoric Acid", MDL Lab. No. B-18543, A.J. Scarpellino, November 19, 1969.